République Algérienne Démocratique et Populaire
Ministère de l'Enseignement Supérieur et de la Recherche Scientifique
Université A.MIRA-BEJAIA

جامعة بجاية
Tasdawit n Bgayet
Université de Béjaïa

Faculté des Sciences Exactes
Département de Physique
Laboratoire de Physique Théorique (LPT)

THÈSE

EN VUE DE L'OBTENTION DU DIPLOME DE DOCTORAT

Domaine : Sciences de la Matière **Filière : Physique**

Spécialité : Sciences des Matériaux

Présentée par
LASMI Mustapha

Thème

Propriétés structurales, électroniques, magnétiques et optiques des structures bidimensionnelles et tridimensionnelles des semi-conducteurs et de métaux de transition

Soutenue le : 28/07/2021 **Devant le Jury composé de :**

Nom et Prénom	**Grade**		
Mr AIT AMOKHTAR Hakim	**Prof**	Univ. de Bejaia	Président
Mr MAHTOUT Sofiane	**Prof**	Univ. de Bejaia	Rapporteur
Mr RABILLOUD Franck	**MC, HDR**	Univ. de Lyon	Co-Rapporteur
Mr BELABBAS Imad	**Prof**	Univ. de Bejaia	Examinateur
Mr BOUZAR Hamid	**Prof**	Univ. de Tizi-Ouzou	Examinateur
Mr REZOUALI Karim	**MCA**	Univ. de Bejaia	Examinateur

Année Universitaire : 2020-2021.

Thesis

Presented for obtain the degree of

Doctor from the University of Bejaia

OPTION: Materials Sciences

By

Lasmi Mustapha

Structural, electronic, magnetic and optical properties of two and three-dimensional structures of semiconductors and transition metals

Supervisor Sofiane Mahtout

University of Bejaia, Algeria

Supervisor Franck Rabilloud

University of Lyon 01, France

Contents

Contents

List of Tables

List of Tables

List of Figures

List of Figures

Acknowledgements

”و من لا يشكر الناس لا يشكر الله“

(رواه البيهقي و حسنه الشيخ الألباني في صحيح الجامع رقم ٣٠١٤)

“Et celui qui ne remercie pas les gens ne remercie pas Allah”. **Sahih Al Jami n°3014**

“And he who does not thank people does not thank Allah”. **Sahih Al Jami n ° 3014**

Acknowledgements

I would like to thank people and institutions that made writing this thesis possible.

And like any period, there are people who accompany it. These people have allowed me to surpass myself, beyond the supposed possible. These are the people I want to thank.

But first of all I thank first of all my God 'ALLAH' the almighty one who enlightened me on the right path and granted me the power, the will and the health to complete this work.

I especially thank my supervisors, Prof. Sofiane Mahtout who proposed, supervised and followed me during this thesis. It is my pleasure to thank him very much thanks, and I would like to underline the good working conditions and my admiration for his human qualities and his kindness. His availability, the clarity of his explanations, his patience, his determination and the self-controlling of my time and the resources using them for the work was very important to build my self-assurance and go forward in the realisation of this manuscript. In addition to bringing me into contact with the world of research, this work has been extremely rewarding for me in many ways. I would like to thank Dr Franck RABILLOUD; from Claude Bernard University (France) very much for the honor he did for me to be my co-thesis director and for being accepting to examine this work. I also extend my heartfelt thanks and gratitude to him for all the help and his considerable contribution in the realization of this thesis.

I really appreciate their support and guidance. Discussions that we carried out enabled me to improve the understanding of the topic and stimulated me in the scientific research. Their enthusiasm and passion was contagious and motivated me to overcome the difficulties. I am particularly grateful for the constructive remarks and guidance during the preparation of the manuscript.

I also express warm thanks to the president of the jury, Professor AIT AMOKHTAR Hakim, from the University of Béjaia, for the honor he does me by accepting to chair the jury for my defense.

I would like to thank Professors BELABBAS Imad, from the University of Béjaia, BOUZAR Hamid, Professors from the University of Tizi-Ouzou, and REZOUALI Karim, Professors from the University of Béjaia for their interest. Kindly carry to this job and to have agreed to be part of the jury with the thankless task of examiners.

I would also like to thank all the people I have come to meet over the past four years for their sympathy, their generosity and their good humor. They all contributed in their own way to the smooth running of this thesis work. All my sympathy goes to my nearest friend, Wahib Aggoune, Fares Benissad, Foudil Zaabar, Fayssal Mahrouche, Mohamed Akli Roumili, Fateh Messouaf, and Nadjim Yahiaoui. May all those I might have forgotten to mention find here the expression of my sincere friendship.

I also express my gratitude to Madani Samah, Badis, lyes, Mourad, Chaouki and Sofiane for their encouraging and advices.

I will not forget all my family and loved ones for their patience, endurance and support in my educational journey, May Allah reward you (جزاكم الله خيرا). I specially named nana Tata, my father Hassane, my mother Saliha, my brothers, Mohammed, Abdellah, Yanis and Sofiane and my sister Siham. I will not forget my uncles and aunts.

Finally, I address my thanks to all others who, in various forms, helped me along the way. Many, many thanks.

Introduction

Introduction

General idea and motivation

Nanotechnology is considered a transversal technology. Nano-clusters represent an exciting newer class of nanoparticles that are being used in application from drug delivery to catalysis. Towards developing a better understanding of their structural, electronic, magnetic, and optical properties and stability we have to expand our knowledge in investigating them in different combinations and under a wide range of well-chosen initial conditions using the right tools for making new patterns which predict and guess a specific use for a given configuration in purposes of full exploitation. Note that atomic clusters are the ultimate nanoparticles where structure−property relationships can be studied at this scale of atom and electron at a time and, hence, can answer fundamental questions [1]. The application areas included Clean and Sustainable Energy: Production, Storage, Conversion, and Efficiency (solar, hydrogen, energy storage such as batteries and photo thermal energy conversion) and Medicine (bioactive, bio responsive and biomimetic materials, nanotoxicity, bio engineering and regenerative medicine, diagnostic devices such as sensors and image enhancement, therapeutic devices such as drug design and delivery, and noninvasive cancer treatment)[1]. Crosscutting areas included nanocatalysis (e.g., new developments in core−shell catalysts), properties (electronic, optical, and magnetic), hybrid nanoparticles, carbon nanostructures, polymer nanoparticles, and nanoparticles Ferro fluids [1]. Such domains and application zones make from clusters one of rewarding economic investment in the actual high-tech revolution.

Semiconducting nano-crystalline materials like quantum dots (QDs) demonstrating on a size ranging from 2 up to 10 nm can produce distinctive colors determined by the size of the particles are resulting of the quantum confinement and hence different Band Gaps [2]. Besides that, their properties are not determined only by the size but also by the shape, composition and the structure, is it solid or hollow. As the character of being with such unique physical properties the QDs can be at the core of the next generation displays and other much instrument. Compared to organic luminescent materials used in organic light emitting diodes, QD based materials have purer color, longer lifetime, lower manufacturing cost and lower power consumption. Single electronic transistor, optical application like TV displays and solar cell, information storage, imaging medicine and even censoring there are among the areas that apply strongly this set of nanomaterials. For biological and chemical application QDs are currently under investigation to unveil important medical application, including potential cancer treatment. Their big advantage is that they can be targeted at single organ, such as the lever, much more precisely than conventional drugs. QDs are also being used in place of organic dyes in biological research, for example, they can be used like nanoscopic light bulbs to light up and color specific cells that need to be studied under microscope [2].

To meet this challenge, in order to create materials with enhanced physical and chemical properties, a degree of control and understanding of the individual building blocks is required. The bottom-up self-assembly in clusters design will be the answer of the challenge of the significant demand for the minimisation of devices with many area among them the nanoworld.

Such a metalloid as germanium,which is estimated to be one of the most futuristic elements, as the silicon, Ge is a semiconductor, with anarrow band gap (0.67 eV), high carrier mobilities (μ_e=3900 $cm^2 V^{-1} s^{-1}$, μ_h=1900 $cm^2 V^{-1} s^{-1}$), large absorption coefficient (ca. 2×10^5 cm^{-1}) and large exciton Bohr radius (24 nm), so germanium is a particularly amazing material for charge storage and infrared optical and optoelectronic [3-4]. The use of germanium as precursor is widely recognized, as an example germanium chloride ($GeCl_4$) [5], is uncolored liquid it is used to product Ge semiconducting quality and production of optical fiber, which helps to immediately transfer information over thousands of kilometers, creating the modern Internet. It is used in a transversal industry as 1960's to make transistors [6], such as their use to make solar cells. Another form of germanium is the germanium oxide (GeO_2), which is used to make high quality optical resolo-dispersion rate devices [7]. GeO_2 has another peculiarity, which is been absolutely transparent [8] in infrared light which is used in laser devices. Germanium can reflect visible light but laterite light pass through. Beside of the reaction of Ge with O_2, Ge also reacts with alcolite, which it is used to extract Bismuth Germinate and in radiation detectors asscintillators. However, the numerous application of germanium compounds as already mentioned is very diverse in modern technology. In the following, a comparison between some selected semiconductors and their properties presented in table (I).

Table (I): Properties of selected semiconductors

	Si	Ge	GaAs
Crystal structure	Diamond	Diamond	Zinc blende
Band gap energy (eV)	1.12	0.66	1.42
Lattice constant (A°)	5.43095	5.6579	5.6533
Intrinsic carrier concentration (cm^{-3})	$1x10^{10}$	$2x10^{13}$	$2x10^{6}$
Electronic mobility (cm^2 / Vs)	1500	3900	8500
Hole mobility (cm^2 / Vs)	450	1900	400
Minority carrier lifetime (s)	10^{-6}	10^{-6}	10^{-6}
Thermal extension of the mesh (10^{-6} / K)	2.6	5.9	5.73

3d-transition metals such as Pt [9], Pd [10] and Ir [11] have been as possible catalysts for the electrochemical oxygen reduction. Beyond, in catalysis and electro-catalysis the relationship between specific configuration (size, shape, composition) and the catalytic properties is that the major issue is to identify the active sites in the given structure. In peculiar, due to the differences of chemical and topological environment, catalytic properties are closely related to the modifications of the local electronic structure on various sites. And as a fact, fossil fuel burning in our daily uses causes' environmental pollution by toxic emissions, such as CO, which the need to be oxidized, than the necessity of finding a cheaper catalyst made of earth-abundant elements with the same characteristic as rare one's, and to be able of tuning their performance by electronic structure engineering [12].

The physics and chemistry of atomic aggregates and nanoparticles constitute a significant promising field. The domain is growing with a very immense rate, as certified by such amount of publications, conferences and workshops. In the development of new technologies, there is an inevitable trend towards miniaturization in micro and nanoelectronics. Our goal is to master technologically the most sophisticate devices of such small dimensions that their specific quantum properties are the most important.

The theoretical study of small aggregates makes it possible to interpret and understand the existing experimental results obtained from the manipulation of the different matters at this scale. It also makes it possible to study useful properties even though, the known as difficult to be reached experimentally. For example, the geometric structure, which is an essential data for the interpretation and analysis of the results, remains very difficult to be determined experimentally, and can only be investigated indirectly using theoretical studies combining quantum chemistry methods for energy calculation and geometry optimization. However, because of the existence of several low electronic energy ground states and several isomers, the systematic search for the most stable geometry by ab-initio calculations produce difficulties for aggregates larger than ten atoms. Moreover, it would normally scan the entire hyper-surface potential of the ground state, which is not simple. From a tentative opinion, clusters in sizes between three and one hundred atoms are too large for spectroscopic techniques and too small for macroscopic methods such as electron microscopy or diffraction. For simple metals, spectroscopy techniques allow us to deduce information on the geometries, while for transition metals the situation is much more complicated because of their d orbital characterized by a high density of states. The most widely used technique is based on chemical reactions of reactivity to an atom or a probe molecule.

From the methodological point of view a simply parameterized description of the electronic structure is often necessary for studies of complex transition-metal compounds involving intricate surface, structural and chemical effects. A wide variety of currently available ab-initio Density Functional Theory (DFT) band structure codes are available. Up to now these codes are still applicable to relatively simple structures, and in general, cannot be used in systematic studies of thermally activated structural transformations.

At this time, the race is in heat to understanding the influence of doping metal atoms on germanium clusters and the comparative study of the different physical properties of each doped clusters. Although, to have the agreement between what the calculations predict and the experimental results are not always so simple. To increase the chances of matching theory and experience, it is necessary to always use very precise numerical techniques.

In an attempt to produce germanium clusters, S.Bals and co-author [13] have successfully synthesized small clusters, and characterized them using transmission electron microscopy in combination with ab-initio calculations and identified as possible building blocks, the seven-membered rings, trigonal prisms and some others smaller subunits. Different methods of synthesizing clusters are known by the scientific community, can be used in making such materials, (ion-sputtering, molecular beam epitaxy, redox transmetalation, gas phase cluster deposition, biochemical synthesis of protein - encapsulated grains, reduction of super-hydrides or carbonyls at a high temperature, using the reverse micelles technique and other techniques [14-15-16-17]. Depending on the method used one can obtain structures of different structural and physicochemical properties.

Encapsulating one or more atoms of a transition metal inside the semiconductor cluster can saturate dangling bonds and improve cluster stability. A wide range of elements and transition metals are the subject of doped pure germanium clusters with the intention of seeking and discover the deferent improvement or modification which can be carried by the substitution of one of the atoms of a pure structure by a given doping atom, on structure, stability, cohesion energy, chemical hardness and optical properties. The main reason of making such huge number of calculation and providing a time to investigate all the data created, flow in the attention of sweeping away all the possible cases that may be present in our study and be as close as possible to the reality.

Because of the aforementioned reasons we have carried out a systematic theoretical study of the clusters of germanium doped with different metals (Pd, Pt and Ir), to find their most stable structures and to characterize them from an energetic point of view. One of our goals in this investigation is to compare doped aggregates with pure aggregates and with other's already studied in the literature [56-113]. In doped systems, one would expect a transfer of electronic charges from doping atoms to germanium atoms, which should result in physical properties different from those of pure one's. Therefore, we seek to understand and characterize the stability and growth behavior of our clusters. We calculated their physical properties (structural, electronic and optical) based on the size n = 1-20 and the nature of the doping atom. Our work is a part of a big computational science area which investigates physical and/or chemical properties of the most stable structures of pure and doped clusters by different metals. For this, we have adopted first principles calculations implemented in the SIESTA [18]. This code is an ab-initio program, based on DFT which uses the pseudo-potential method. More details on this code will be presented in the coming chapters of this thesis.

In the beginning, the stable structures of pure and doped germanium clusters are identified by comparing the binding energies of the different possible arrangements of atoms corresponding to each considered size. In fact, the molecular dynamics method makes it

possible to do this work since, during the relaxation step, the program makes it possible to explore the entire configuration space and to identify the best structure according to the convergence conditions imposed in the calculation and, of course, it all depends on the initial atomic configuration in the cluster to be relaxed. For a given size, the number of possible structures is all the greater as the number of initial configurations (i.e. the number of relaxations) is large. The best structures are those with the lowest total energies. In general, for a cluster of a given size, when we obtain the same minimum energy balance structure from two or more different initial configurations, we consider the structure having the lowest binding energy may be the most stable configuration for this cluster. Several parameters which can be compared with other existing calculations are calculated: the symmetry group, the binding energy, the HOMO-LUMO gap, the vertical ionization potential, the electron affinity, chemical hardness, average bond length, second energy differences, and layered electronic structures.

Our thesis is organized as follows:

In chapter 1 we will give a description of the density functional theory (DFT), the theory on which all our calculations are based. We will show in particular how it makes it possible to obtain the total energy of a given system. After having recalled the basis of pseudo-potentials, we will present the way in which they are generated, tested and then used in a calculation practice. The third part of the chapter is devoted to ab-initio molecular dynamics. This has a great flexibility of implementation, so that it is possible, using a single code, to determine the electronic ground state of a system, its structural minima, as well as the stability of a particular geometry.

In chapter 2 we present the SIESTA calculation code. The focus is on its basic principles, its potency, and the various physical properties it can give us. We also give the values chosen for the simulation parameters for the conjugate gradient method.

Chapters 3 and 4 are devoted to the presentation, analysis and discussion of the results obtained. In chapter 3 we present the results of our study on the structure, stability and electronic and optical properties of pure germanium aggregates and doped with Pd and Pt. In the last chapter (Chapter 4) we present the results of calculations on germanium structures doped with Ir metal and we will discuss their structural, electronic and optical properties.

In conclusion the results obtained in the doped clusters will be summarized and a number of improvements along with the future perspectives will be briefly discussed.

Chapter 1

Methodology

Chapter 1

Methodology

1.1 First principles approach

1.1.1Quantum-Mechanical Methods

Quantum mechanics is one of the most successful scientific theories ever created over the last century. Its creation is due to the fact that the other sciences such as Newtonian mechanics, Maxwell's electromagnetic theory and even the Boltzmann's statistics "therefore classical physics in general" could not explain all the physical phenomena encountered at this time in atomic and subatomic behaviors of matter which cannot be neglected. As one of the application of quantum mechanics on behalf the electronic behavior to mimic the true electronic system in simple way, we use Density Functional Theory. DFT was started in 1920's by Thomas [19] and Fermi [20] in purpose to resolve the "many body problem" which is considered the most fundamental difficulty in condensed matter theory.

1.1.2Ab-Initio Methods

Using nothing but the Schrodinger equation equipped by a self-consistent field procedure one can calculate a various models molecular structures like for example Hartree-Fock and Post Hartree-Fock methods. Such a method is used commonly for systems requiring electronic transition and needing a particular fairness. Since for any methods, they have advantages and imperfections. For example they are useful for a broad range of systems, do not depend on experimental data, and allow determining accurate forces and stresses via Hellman-Feynman theorem and permit to determine accurate total energies and energy differences. On the opposite side, they are computationally expensive and are only useful for small systems.

1.1.3Electronic Structure Methods

The physical properties of materials are rarely accurately described due to the complexity of these multi-particle systems. Indeed, the resolution of these so-called "N-body" problems must inevitably have recourse to approximations, not only to simplify the calculations but also for a good representation of this very complicated system.

1.1.4Schrödinger equation

The Schrödinger equation is a fundamental equation in quantum mechanics. It describes the evolution over time of interacting electrons. It brings us to the understanding of

the different physical and chemical properties of materials. However, the astronomical number of variables involved makes it impossible to solve this equation directly, hence the need to introduce approximations to overcome this problem. We are trying to model a set of interacting nuclei and electrons. Classical mechanics remains insufficient and it is necessary to call upon quantum mechanics whose basis is the resolution of the Schrödinger equation. We know that any stationary state of a quantum system is described by a wave function ψ, which is a proper function of the Schrödinger equation independent of time [21]:

$$H\,\Psi = E\,\Psi \qquad (1.1)$$

Where H is the Hamiltonian operator of the system {N nuclei + n electrons} and is written:

$$H = T_e + U_{ee} + U_{eN} + T_N + U_{NN}$$

Where,

T_e: Kinetic energy of electrons

U_{ee}: Electron-electron interaction energy

U_{eN}: Electron-nucleus interaction energy

T_N : Kinetic energy of the nuclei

U_{NN}: Energy of nuclei-nuclei interaction

By developing each term, we will have:

$$H= -\frac{\hbar^2}{2m_i}\sum_i \nabla_i^2 - \frac{\hbar^2}{2M_\alpha}\sum_\alpha \nabla_\alpha^2 + \frac{1}{2}\sum_{i\neq j}\frac{e^2}{|r_i-r_j|} - \sum_{i,\alpha}\frac{e^2 Z_\alpha}{|r_i-R_\alpha|} + \frac{1}{2}\sum_{\alpha\neq\beta}\frac{e^2 Z_\alpha Z_\beta}{|R_\alpha-R_\beta|} \qquad (1.2)$$

m_i: The mass of the electron i

M_α: The mass of the nucleus α

Z_α: The atomic number of the nucleus α

r_i : The position of the electron i

R_α: The position of the nucleus α

An exact solution to equation (1.2) is impossible in the case of poly-electronic systems. It is therefore necessary to implement simplifying procedures associated with a few mathematical tricks in order to make it possible to obtain an exact or approximate solution.

1.2 Fundamental approximation

1.2.1 Born-Oppenheimer approximation (BOA)

Born-Oppenheimer Approximation (BOA) [22], is adopted as a first level of approach to problems with several bodies by highlighting the large gap between the mass of the electrons of the system (lighter, therefore with greater mobility) and that of the nuclei (relatively heavier M ≈ 1800 × m, therefore reduced mobility). In other words, this approximation is based on the idea of considering the nuclei as having sufficiently slow movements, relative to those of the electrons, so as to neglect them without great error, so we will have a purely electronic Hamiltonian. The Hamiltonian will be written in this case in the following form:

$$He = T_e + U_{ee} + U_{eN} \tag{1.3}$$

The wave equation for the system is then written:

$$\left[-\frac{1}{2}\sum_i \nabla_i^2 + \frac{1}{2}\sum_{i\neq j}\frac{1}{|r_i - r_j|} - \sum_{i,\alpha}\frac{Z_\alpha}{|r_i - R_\alpha|}\right]\psi_e = E_e\,\psi_e \tag{1.4}$$

The Born-Oppenheimer approximation is only valid when the couplings of electronic and nuclear movements are negligible, that is to say when the wave functionψ_e does not undergo sudden variations when the nuclei vary. It reaches its limits when we deal, for example, with collision problems or problems of crossing potential energy surfaces. Unfortunately, the number of variables in equation (1.4) remains important and therefore direct resolution is impossible. We still have to go through approximations which should be as reasonable as possible.

1.2.2 Hartree approximation

Despite the simplifications that the Born-Oppenheimer approximation brings, we are faced with a problem with N bodies because of the electron-electron interaction term. The Schrödinger equation cannot be solved exactly for more than one electron. Douglas Hartree (1927) [23], proposed a method for calculating the wave functions and the approximate energies of ions and atoms. The basic idea of this approximation is to consider that the electrons move independently of each other, their movement is uncorrelated. Thus, if we consider two electrons 1 and 2, the probability of the presence of the electron of coordinate's r_1 in the orbital 1 is independent of that of the electron of coordinate's r_2 in the orbital 2. The Hamiltonian of such a system is written:

$$H = \sum_{i=1}^{N_e} h(i) \tag{1.5}$$

Where$h(i)$ is the monoelectronic Hamiltonian.

The wave function with N electrons ϕ (r_1, r_2,...,r_N) is represented as the product of wave

functions at a one particle:

$$\Psi\ (r_i,\ldots\ldots\ r_N) = \prod_{i=1}^{N_e} \phi(r_i) \qquad (1.6)$$

Equation (1.6) is called Hartree Product (HP) [24].

The resolution of Schrödinger's equation goes from a problem of Ne electrons to that of a single electron:

$$\left[-\frac{1}{2}\sum_i \Delta_i{}^2 + V_{ext}r + V_H^i(r)\right]\phi_i(\mathrm{r}) = \varepsilon_i\phi_i(\mathrm{r}) \qquad (1.7)$$

Where

- ✓ $V_{ext}r = \sum_{a=1}^{N_n} \frac{Z_a}{|r_i - R_a|}$
- ✓ $V_H^i(r) = \int \frac{\rho(r')}{|r_i - \boldsymbol{r}'|} dr'$

$V_{ext}r$ is the external potential of the nucleus and $V_H^i(r)$is the Hartree potential, it describes the mean field of the other electrons. N_n and $\rho(r')$ represents the number of nucleus and electron density, respectively.

The great merit of this approach is to have proposed a self-coherent solution to the problem of the electronic system [25]. It has four important consequences:

- ✓ The total Coulomb repulsion $V_{e\text{-}e}$ of the electronic system is over estimated.
- ✓ Simple to solve, but does not give good results.
- ✓ Each electron feels its own charge.
- ✓ The Pauli Exclusion Principle is not taken into account.

A reasonable wave function must be asymmetric when exchanging two electrons [26].This last consequence being crippling, the approximation had to be improved [27] to take into account the spin in the resolution of the Schrödinger equation.

1.2.3 Hartree-Fock approximation

One of the interactions that are not taken into account in the Hartree approximation is the exchange. It is expressed by the asymmetry of the wave function with respect to the exchange of the coordinates of two electrons. The system with N bodies (electrons) can then be described by the following equality:

$$\Psi\ (\mathrm{r}_1, \ldots, \mathrm{r}_a, \ldots, \mathrm{r}_b, \ldots, \mathrm{r}_N) = -\ \Psi\ (\mathrm{r}_1, \ldots, \mathrm{r}_b, \ldots, \mathrm{r}_a, \ldots, \mathrm{r}_N) \qquad (1.8)$$

In which the positions of “a” and “b” have been reversed. Ψ (r1, ...,rb, ..., ra, ..., rN) is the wave function of the N body system resulting from the product of mono-electronic functions.

This is due to the fact that the electrons are Fermions (spin$\frac{1}{2}$) and obey a Fermi-Dirac distribution [28].

V. Fock proposed to replace Hartree's wave-functions with a Slater determinant. We define the Slater determinant as an order N determinant formed on N distinct spin-orbitals which are mono-electronic functions of the space and spin variables [27].

Slater's determinant is written as follows

$$\Psi\left(\mathrm{r}_1\sigma_1,\ldots\ldots\ \mathrm{r}_\mathrm{N}\sigma_N\right)=\frac{1}{\sqrt{N!}}\begin{vmatrix}\psi_1(\mathrm{r}_1\sigma_1)\psi_1(\mathrm{r}_2\sigma_2) & .. & \psi_1(\mathrm{r}_\mathrm{N}\sigma_N)\\ \psi_2(\mathrm{r}_1\sigma_1)\psi_2(\mathrm{r}_2\sigma_2) & .. & \psi_2(\mathrm{r}_\mathrm{N}\sigma_N)\\ \ldots & .. & \ldots\\ \psi_\mathrm{N}(\mathrm{r}_1\sigma_1)\psi_\mathrm{N}(\mathrm{r}_2\sigma_2) & .. & \psi_\mathrm{N}(\mathrm{r}_\mathrm{N}\sigma_N)\end{vmatrix} \tag{1.9}$$

$\mathrm{r_i}$: Space variable.

σ_i : Spin variable.

We thus obtain the Hartree-Fock equations:

$$\left[-\frac{1}{2}\sum_i \Delta_i \quad + V_{ext}r + V_H^i(r) + V_x(r)\right]\phi_i(\mathrm{r}) = \varepsilon_i\phi_i(\mathrm{r}) \tag{1.10}$$

Where $$V_x(r)\phi_i(r) = -\sum_{j\neq i}\delta_{\sigma_\mathrm{i}\sigma_\mathrm{j}}\,\phi_j(r)\int\frac{\phi_{j^*}(r')\phi_i(r)}{|\boldsymbol{r}-\boldsymbol{r}'|}dr' \tag{1.11}$$

$V_x(r)$is the term added by Fock. It is non-linear. It is not only proportional to ϕ_i but also to ϕ_j (i≠j), which has led to calling it, exchange potential. It is also a non-local operator since it implies integration.

It should also be noted that, in the Hartree-Fock method, the electrons are considered to be independent of each other, and each, move in a mean potential created by all of the nuclei and the other electrons. There is therefore no instantaneous electron-electron interaction, hence the development of certain methods to try to remedy this problem of lack of correlation.

1.2.4 Hartree-Fock-Slater approximation

In order to solve the Hartree-Fock equation, Slater [29] gives a more suitable form for the exchange potential $V_x(r)$ for a homogeneous electron gas with density$\rho(r)$:

$$V_x(r)= -6\alpha\left[\frac{3\rho(r)}{8\pi}\right]^{1/3} \tag{1.12}$$

The resulting method is called the method X_α.

At this stage of the approximation, the results are far from satisfactory. In reality, the complexity of interactions between electrons means that this method ignores electronic relationships.

1.2.5 Density Functional Theory

The detailed study of the electronic properties of a molecular system requires taking into account the effects of electronic correlation [30]. This is why, over the past thirty years, the Functional Density Theory or DFT has been used extensively for the study of physical or chemical systems. Initially designed and applied to solid state problems, several reasons contributed to its popularity for physical or chemical applications [30]:

- ✓ This theory includes in its formalism a large part of electronic correlation.
- ✓ The method can be applied to any type of system: covalent, ionic or metallic.
- ✓ The IT tools (Informatics resources) required are lower, making studies of larger molecular systems accessible.
- ✓ The mono-determinative aspect allows a physical or chemical interpretation of the wave function resulting from this type of formalism.

A bit of history

The DFT has its origins in the model developed by Llewellyn Thomas [19] (1927) and Enrico Fermi [20] (1927, 1928) who proposed an alternative method of solving the Schrödinger equation based on electronic density only. It is based on the assumption that the movements of the electrons are decorrelated and that the kinetic energy can be described by a local approximation based on the results for free electrons. Dirac [31] proposed that the exchange effects can be taken into account by incorporating a term coming from the density of exchange energy in a homogeneous electron gas. The thing that made this new approach go further is the fact that the term electronic correlation is missing. It was not until the sixties that the contributions of Pierre Hohenberg, Walter Kohn [32] and Lu Sham helped establish the theoretical formalism on which the current method is based.

1.2.6 Hohenberg-Kohn theorems and equations

Theorem 1: The electronic density ρ(r) is the only function necessary to obtain all the electronic properties of any system [32]. In other words, there is a one-to-one correspondence

between the electronic density of the ground state $\boldsymbol{\rho_0(r)}$and the external potential (r) and therefore between $\boldsymbol{\rho_0(r)}$and the wave function of the ground state ψ_0.

The Hamiltonian of the electronic system will be written:

$$\mathrm{H} = -\frac{1}{2}\sum_i^n \Delta_i + \sum_{i\neq j}^{Ne} \frac{1}{2r_{ij}} + \sum_i^{Nn} V\mathrm{ext}(r_i) \tag{1.13}$$

$V\mathrm{ext}(r_i)$ is the external potential, it has the following form:

$$V\mathrm{ext}(r_i) = -\sum_k^{Nn} \frac{Z_a}{|R_k - r_i|} \tag{1.14}$$

By integrating the electronic density $\rho_0(r)$ we obtain:

$$\int \rho_0(\mathrm{r})\mathrm{dr} = \mathrm{n} \tag{1.15}$$

The energy functional will be written as:

$$E[\rho_0] = T[\rho_0] + U_{N_e}[\rho_0] + U_{ee}[\rho_0] \tag{1.16}$$

With $$U_{eN}[\rho_0] = \int \rho_0(r) v_{eN}(r) dr \tag{1.17}$$

$T[\rho_0]$: Kinetic energy of the non-interacting electrons

$U_{ee}[\rho_0]$: Classical Coulomb Interaction (Hartree energy)

$v_{eN}(r)$: Nuclear-electron potential

The energy functional can also be written in the form:

$$E[\rho_0] = F[\rho_0] + \int \rho_0(r) v_{eN}(r) dr \tag{1.18}$$

With $$F[\rho_0] = T[\rho_0] + U_{ee}[\rho_0] \tag{1.19}$$

The functional $[\rho_0]$are unknown.

Theorem 2: the energy $E[\rho]$ associated with any test density, satisfying the necessary boundary conditions $\rho(\mathrm{r}) \geq 0$ and $\int \rho(\mathrm{r})\mathrm{dr} = \mathrm{n}$ and associated with an external potential $V\mathrm{ext}(r_i)$, is greater than or equal to the energy associated with the electron density of the ground state $E[\rho_0]$.

$$E[\rho_0] = \mathrm{Min}\, E[\rho] \tag{1.20}$$

This theorem is nothing other than the variational principle expressed for functional energies of a density, $E[\rho]$and not of a wave-function, E[Ψ] [33-34].

$$E_0 \leq \mathrm{E}[\rho(r)] = U_{eN}[\rho_0] + T[\rho(r)] + U_{ee}[\rho(r)] \tag{1.21}$$

In summary: all the properties of a system defined by an external potential V_{ext} (r) can be determined from the electronic density of the ground state. The energy of the system $E[\rho]$reaches its minimum value if and only if the electron density is that of the ground state. The use of this variational approach is limited to the search for the energy of the ground state, and to be more precise, this reasoning is limited to the ground state for a given symmetry [30].

1.2.7 Kohn-Sham equations

To better exploit the theorems of Hohenberg and Kohn, W. Kohn and L. J. Sham [35] proposed in 1965 to use a fictitious system of electrons without interaction of the same density ρ (r) as the system of electrons in interaction. Based on this reference system, it is then possible to give an exact expression to the kinetic energy of a non-interacting system of N electrons as a functional of the density ρ (r).

The Hamiltonian of the fictitious system is written:

$$H_s = \sum_{i=1}^{Ne}\left[-\frac{1}{2}\sum_i \nabla_i^2 + V_{eff}(r_i)\right] = \sum_{i=1}^{Ne} h_i^{ks} \qquad (1.22)$$

Where

$V_{eff}(r) = V_{ext} + \int \frac{\rho(r')}{|r-r'|} dr' + V_{xc}$, is the effective potential.

$V_{xc} = \frac{\delta E_{xc}[\rho(r)]}{\delta \rho(r)}$, is the potential for exchange and correlation which is given by the derived functional.

$\rho(r) = \sum_{i=1}^{Ne} |\varphi_i(r)|^2$ is the density which is given by a sum of all the occupied orbitals φ_i.

$\int \frac{\rho(r')}{|r-r'|} dr' = V_H$, is the Hartree potential of the electrons.

The Schrodinger equation to be solved in the framework of Kohn and Sham's approach is of the following form:

$$\left[-\frac{1}{2}\nabla_i^2 + v_{KS}(r)\right]\varphi_i(r) = \varepsilon_i \varphi_i(r) \ , \ i = 1, \ldots\ldots, N \qquad (1.23)$$

In terms of the energy functional:

$$\begin{aligned} E[\rho] &= T_{KS}[\rho] + \underbrace{\int v_{KS}(r)\rho(r)dr}_{\hat{U}_{KS}[\rho]} \\ &= T_{KS}[\rho] + \end{aligned} \qquad (1.24)$$

We develop the term of energy in the equation (1.24) like that of an electron gas without interaction, and subjected to the action of external potentials (nuclei) and exchange-correlation, we will then have:

$$E[\rho] = T_{KS}[\rho] + \underbrace{\int v_H(r)\rho(r)dr}_{U_H[\rho]} + \underbrace{\int v_{ext}(r)\rho(r)dr}_{U_{ext}[\rho]} + E_{XC}[\rho]$$

$$= T_{KS}[\rho] + U_H[\rho] + U_{ext}[\rho] + E_{XC}[\rho] \quad (1.25)$$

In the following a Self-consistent algorithm for solution of Kohn-Sham equations is presented in Figure 1.1.

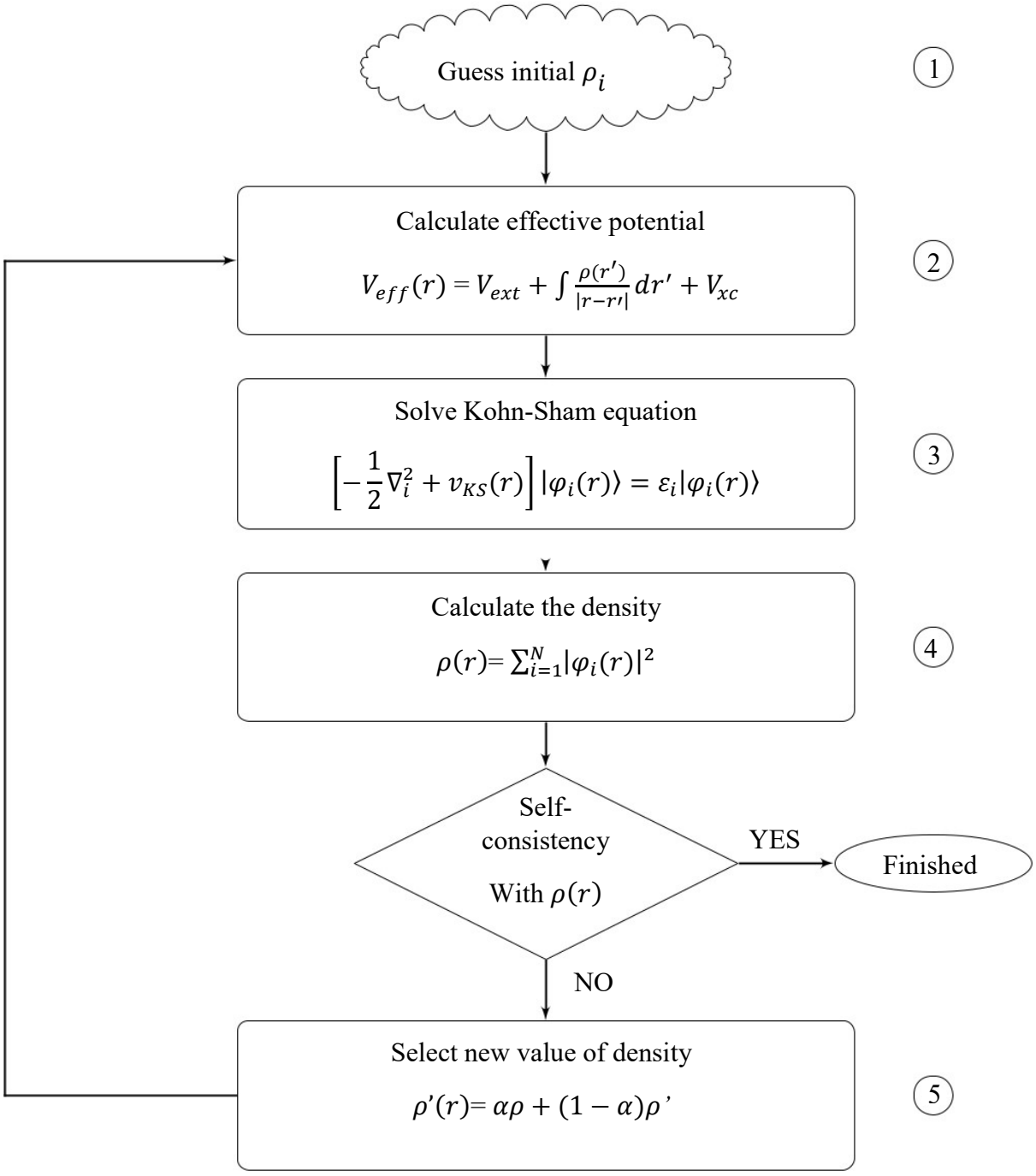

Fig (1.1): Self-consistent algorithm for solution of Kohn-Sham equations [36].

In this expression $E_{XC}[\rho]$ is the energy of exchange-correlation, which gathers everything that is not known in the system, namely the effects of correlations due to the quantum nature of the electrons.

$$E_{XC}[\rho] = (T[\rho] - T_{KS}[\rho]) + (E_{ee}[\rho] - \hat{U}_{KS}[\rho]) \quad (1.26)$$

These equations must be solved in a self-consistent way in order to find the density of the ground state (figure1.1). All DFT type calculations are based on the iterative resolution of these equations. Note that for DFT, only total energy, Fermi energy and electron densities have a physical meaning. The states and energies of Kohn-Sham are only intermediaries of calculation. However, they are used in many scientific works to calculate certain quantities such as band structures.

1.2.8 Approximation of the Local Density (LDA)

To approximate the functional of the exchange-correlation energy $E_{XC}[\rho]$Kohn and Sham proposed in 1965 the local density approximation (LDA) [35]. The principle of this approximation is based on the assumption that we can replace the functional of $E_{XC}[\rho]$by that of a homogeneous gas with density $\rho(r)$that varies slowly around a point, in other words, it is considered locally uniform. The term $E_{XC}[\rho]$will be written:

$$E_{XC}^{LDA}[\rho(r)] = \int \rho(r)\varepsilon_{XC}[\rho(r)]dr \quad (1.27)$$

The term $\varepsilon_{XC}[\rho(r)]$ is particle exchange-correlation energy density of electron gas. In addition, $\varepsilon_{XC}[\rho(r)]$ is considered as the sum of an exchange and correlation contribution:

$$\varepsilon_{XC}[\rho(r)] = \varepsilon_X[\rho(r)] + \varepsilon_C[\rho(r)] \quad (1.28)$$

The term exchange$\varepsilon_X[\rho(r)]$, called "Dirac exchange" [37] is written as follows:

$$\varepsilon_X[\rho(r)] = -\frac{3}{4}\left(\frac{3\rho(r)}{\pi}\right)^{\frac{1}{3}} \quad (1.29)$$

The correlation part $\varepsilon_C[\rho(r)]$cannot be expressed exactly. The approximation of this term established by Vosko, Wilk and Nussair (VWN) [38] has been the most successful. It is based on an interpolation of the results of very precise quantum Monte-Carlo calculations on the uniform gas of electrons carried out by Ceperley and Alder [39].

In general, the LDA approximation gives good results when it comes to describing the structural properties, i.e. it allows to determine the energy variations with the crystal structure although it overestimates the cohesive energy. It also makes it possible to determine the parameter of mesh for the majority of solids and gives good values for the elastic constants like the modulus of isotropic compressibility. But this model is inappropriate for inhomogeneous systems.

1.2.9 Generalized Gradient Approximation (GGA)

At the molecular level, the inhomogeneities of the density can prove to be consequent from where the need to introduce these effects in the functional of exchange-correlation. The approximation implementing this type of correction is called Generalized Gradient Approximation (GGA) [40]. This approximation of the GGA has as main base the introduction of the non-homogeneity characterizing the charge densities of the real poly-electronic systems through a substitution of the energy density E_{XC} of the LDA, $\varepsilon_{XC}^{LDA}[\rho(r)]$by an energy density GGA, $\varepsilon_{XC}^{GGA}[\rho, |\nabla\rho|]$, dependent not only of the charge density but also of the gradient of this density.

The mathematical form of energy is as follows:

$$E_{XC}^{GGA}[\rho, \nabla\rho] = \int \varepsilon_{XC}^{GGA}[\rho(r), |\nabla\rho(r)|]dr \tag{1.30}$$

These contributions are often developed separately:

$$E_{XC}^{GGA}[\rho, \nabla\rho] = E_{X}^{GGA}[\rho, \nabla\rho] + E_{C}^{GGA}[\rho, \nabla\rho] \tag{1.31}$$

The exchange part is generally the functional of Becke (B), the correlation part that of Lee, Yang and Parr (LYP) or that of Perdew-Wang (PW) and Ernzerhof (E) with variants 86 and 91 , hence the keywords PBE, BLYP, BPW86 and BPW91 [41].

1.2.10 Success and limits of the DFT

Density functional theory has emerged as a tool for solving quantum problems constituted by physical systems of different nature (atoms, molecules or solids). Several quantities are targeted, either to explain them or to obtain them because they are inaccessible by experience. The DFT methods allow a good estimate of the structure of the systems studied. The total energy is rendered with fairly good precision. The errors are, however, quite substantial for spin states. The exchange coupling, the electronic, magnetic and optical properties are accessible by a DFT calculation. However, the DFT method still suffers from several shortcomings, including the lack of real criteria which allow improving the functional and molecular properties [42].

1.3 Molecular modeling

1.3.1 Pseudo-potentials

In order to further simplify the resolution of the N electron problem, an idea based on the distinction between two types of electrons is highlighted: core electrons and valence electrons. Heart orbitals are the lowest in energy. They are located near the nucleus, very little sensitive to the environment and do not participate in chemical bonds. In addition, they are difficult to represent on the basis of plane waves because they generally have strong oscillations around the nuclei. On the other hand, the valence orbitals are not very localized

and therefore extend far from the nucleus. They are the ones that determine physicochemical properties in the first order. From this separation, the following model is established: the core electrons and the nucleus form an effective potential, acting on the valence electrons. It is the pseudo-potential which includes all the interactions between the nucleus and the valence electrons as well as between the core electrons and the valence electrons. This idea, first expressed by Fermi in 1934, made it possible to reduce the number of equations to be solved, and therefore to get rid of the most localized results. Hellmann proposed in 1935 pseudo-potential for potassium of the form [43-44]:

$$w(r) = -\frac{1}{r} + \frac{2.74}{r} e^{-1.16\, r} \tag{1.32}$$

The pseudo-potentials are potentials which lead, for an electronic reference configuration of the isolated atom, to exact Eigen-values and to Eigen-functions as regular as possible in agreement with the atomic wave functions beyond a certain radiusr_c chosen, called the cut-off radius. These Eigen-functions, called pseudo-functions, have the same diffusion properties (the same logarithmic derivatives) as the real wave functions. They are asked to have the greatest possible transferability, which means that they can be used in the greatest possible number of systems, meaning that they can be used in different thermodynamic environments [45].

There are several types of pseudo-potentials, each of which has its advantages and disadvantages:

- ✓ The pseudo-potentials with conserved norm introduced by Hamman et al [46]
- ✓ The ultra-soft pseudo-potential introduced by Vanderbilt [47]
- ✓ The "dual-space Gaussian" pseudo-potentials introduced by Goedecker et al [48-49]

We have chosen to use conserved norm pseudo-potentials for their conceptual simplicity of use and digital implementation.

1.3.2 The ab-initio pseudo-potentials

Currently, physicists uses ab-initio pseudo-potentials which means "from first principles", that is to say without adjusted parameters which are from experience. The ab-initio norm-preserving pseudo- potentials are pseudo-potentials that have been adjusted by keeping the charge density of the core electrons [44-50].

The family of preserved standard pseudo-potentials meets the following conditions:

- ✓ Equality of pseudo (PS) and real (AE) Eigen-values for a given configuration

$$\varepsilon_{n,l}^{AE} = \varepsilon_{n,l}^{PS} \tag{1.33}$$

- ✓ The real and pseudo wave functions are equal beyond the chosen cut-off radius r_c

$$R_{n,l}^{AE}(r) = R_{n,l}^{PS}(r) \text{For} \quad r > r_c \tag{1.34}$$

- ✓ The pseudo-wave function has no nodes.
- ✓ The integrals of the real and pseudo charge densities agree for each valence state (conservation of the norm)

$$\int_0^{r_c} \left|R_{n,l}^{AE}(r)\right|^2 r^2 dr = \int_0^{r_c} \left|R_{n,l}^{PS}(r)\right|^2 r^2 dr \; r < r_c \qquad (1.35)$$

$R_{n,l}$ Is the radial part of the wave function.

From this condition follows the fact that the logarithmic derivatives of the real and pseudo wave functions and their first derivatives with respect to energy agree for $r > r_c$.

The interest of this pseudo-potential lies in the fact that it gives smooth wave pseudo-functions, not subject to numerous breaks. This is not without importance as to the quality of the pseudo- potential, especially its transferability, the relativistic effect, and its effectiveness. In the following, schematic representation of the pseudo-potential and valence pseudo wave-function versus all electron potential and true wave-function is presented in figure 1.2.

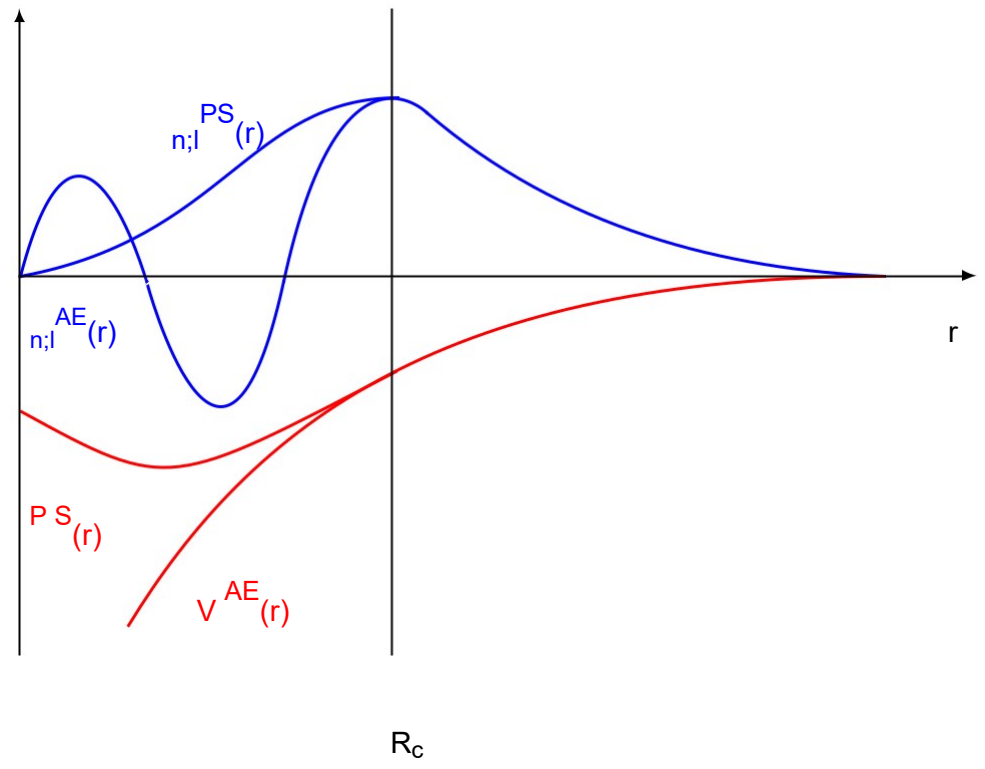

Fig (1.2): Schematic representation of the pseudo-potential and valence pseudo wave-function versus all electron potential and true wave-function.

1.3.3LCAO approximation method

The linear combination of atomic orbitals was established by Lennard-Jones in 1929 [51]. Because of the impossibility of analytically calculating the electronic function of molecules, many quantum methods use the LCAO approximation. A molecular wave function ψ is then written according to the n orbitals ϕ_i of the atoms that the molecule contains:

$$\psi = \sum_{i=1}^{n} C_i \phi_i \tag{1.36}$$

The product $C_i\phi_i$ represents the percentage of atomic orbitals in each molecular orbital and C_i the corresponding coefficient. The solution of Schrödinger's equation in the LCAO approximation requires the calculation of a large number of integrals, of the order of n^4, n: being the number of atomic orbitals in the system.

1.4 Different Optimization Algorithms

1.4.1 Steepest descent method

The ’steepest descent’ ’method is the first program developed for minimizing and optimizing geometry. Proposed by Wiberg [52], its principle is simple, after having calculated the energy corresponding to an initial geometry, we move each atom according to the three spatial coordinates and we recalculate their energy for each displacement. This amounts to calculating the first derivative only. Then one moves all the atoms on a distance which depends on the derivative according to the Cartesian coordinates, and then one carries out again the same operations. The "steepest descent" method consists in finding the direction of greatest slope during which the objective function F_{X_γ}decreases more quickly. The direction followed will be that indicated by the direction of the greatest slope of the energy function, which is the direction in which energy decreases the fastest, at least locally. The problem with this method is that it is random and very long in most cases. Towards the end of each minimization cycle, convergence becomes very slow beyond the first cycles (oscillating phenomena, rising energy).

1.4.2 Conjugated gradient method

The principle is the same as the steepest descent method. For a quadratic energy surface, a function of 3N variables converges in 3N steps [53]. This method retains good efficiency, but is slower than the steepest descent method. The step is adjusted with each cycle to obtain the best reduction in energy. The interest of this algorithm is to avoid an oscillatory behavior around the minimum and to accelerate convergence.

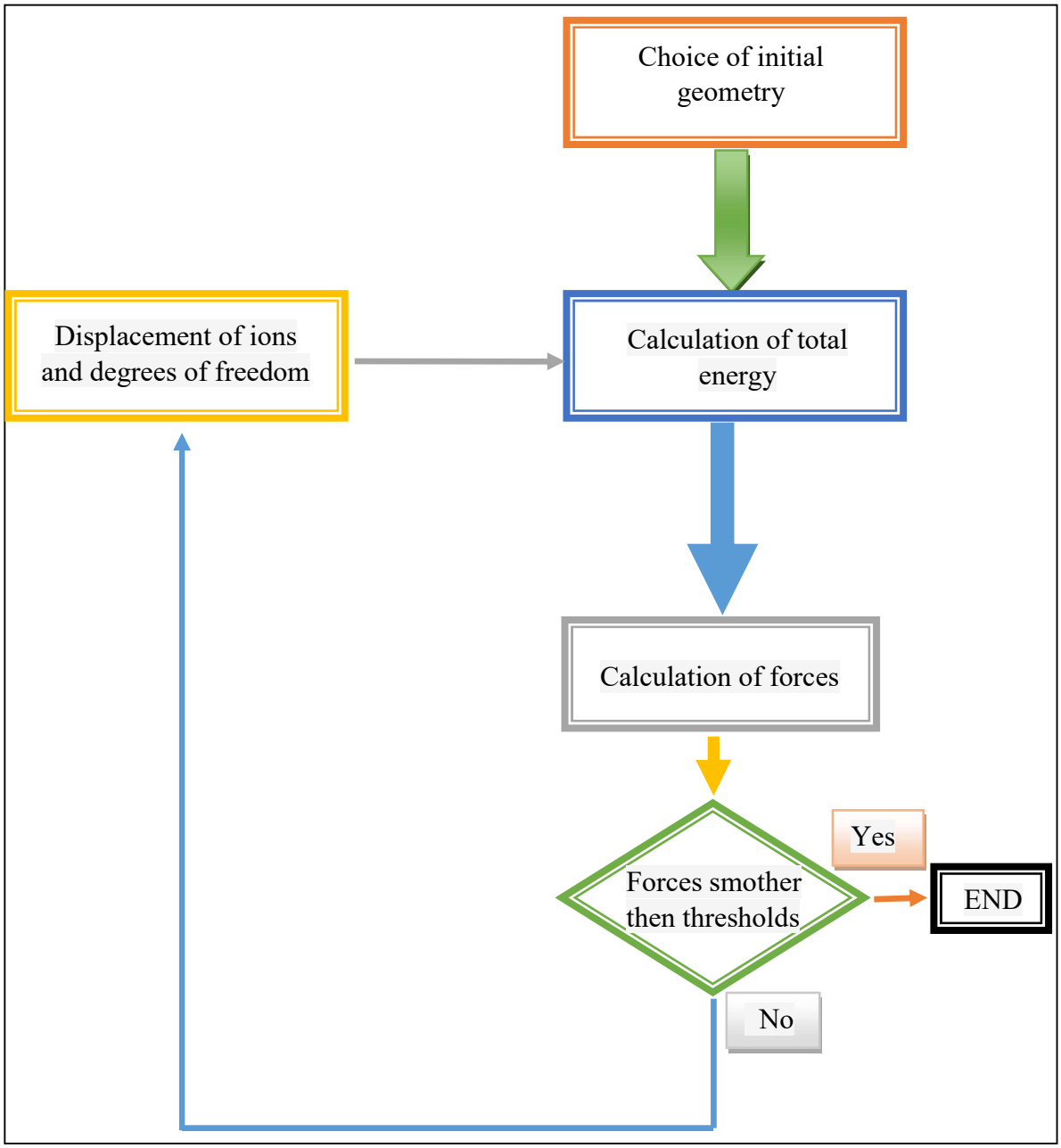

Fig (1.3): Schematic diagram of the determination of the most stable state of equilibrium using molecular dynamics.

Chapter 2

Calculation methods

Chapter 2

Calculation methods

The calculation code (SIESTA)

Siesta (Spanish Initiative for Electronic Simulations with Thousands of Atoms) is computer code that performs electronic structure calculations and ab initio molecular dynamics simulations of molecules and solids using density functional theory (DFT) [18].

2.1 Basics

SIESTA belongs to the category of methods with basic sets centered on the atom (localized atomic orbital). The advantage of using this kind of functions is to have a reduced bases set and a relatively fast convergence, contrary to the other codes using a much larger base and which would make computations heavy, even impossible in certain cases.

Its main features are:

✓ It uses the Kohn-Sham density functional method in the local density approximation (LDA-LSD) and the generalized gradient approximation (GGA), as well as in a non-local form including Van interactions der Waals (VDW-DF).

✓ It uses pseudo-potentials with norm preserved in their nonlocal form (Kleinman-Bylander).

✓ It projects the functions and densities of electronic waves on a grid of real space in order to calculate the Hartree and exchange-correlation potentials.

✓ It allows the use of linear combinations of occupied localized orbitals (functions of the valence link or of Wannier type), which makes the dependence of the memory and time scale of the linear computer with the number of atoms. Simulations with several hundred atoms are possible with modest workstations.

✓ It is written in FORTRAN 95 language and memory is allocated dynamically.

✓ It can be compiled for serial or parallel execution.

Siesta provides us with:

✓ Total and partial energies.

✓ Atomic forces, stress tensors.

✓ The electric dipole moment.

✓ Atomic and orbital populations and electronic density.

✓ Geometric relaxation in a fixed or variable cell.

✓ Molecular dynamics at constant temperature.

✓ Polarized spin calculations.

✓ Sampling of the Brillouin zone.

✓ Projected local and orbital state density

✓ Dielectric polarization, Vibrations (phonons) and Band structure.

2.2 Program execution

The SIESTA program has several application examples. To launch a calculation, three files are essential:

✓ The input file with the extension ".fdf" which contains all the information relating to the simulation work.

✓ The pseudo-potential which is an unformatted file with a functionally equivalent "vps" or ASCII file**,** but the latter is easier to transport and to consult.

The executable of the SIESTA program obtained after its compilation.

After compilation of the program, several files are created in the directory:

✓ The **Fdf.log** file (contains all the data used, explicit or chosen by default).

✓ The **.ion** file (complete information on the base and KB projectors).

✓ The **.XV** file (contains positions and speeds).

✓ The **.STRUCT_OUT** file (contains the vectors of the final cells and the positions in the crystallographic format).

✓ The **.DM** file (contains the density matrix to allow a restart of the calculation).

✓ The **.ANI** file (contains the coordinates of each step for moving atoms).

✓ The **.FA** file (contains the forces exerted on the atoms).

✓ The file **.EIG** (contains the Eigen-values of the Kohn-Sham Hamiltonian).

✓ The **.out** file (contains all the results).

2.3 Input data file

FLEXIBLE DATA FORMAT (FDF)

The main input file contains all the physical data of the system and the parameters of the simulation to be performed. This file is written in a special format called FDF, developed by Alberto Garcia and José M. Soler. Data can be entered in any order and even omitted in favor of default values.

✓ The FDF syntax is a “data label” followed by its value. Values that are not specified in the data file are given a default value.

✓ All text proceeded by the character # is taken as a comment.

✓ Logical values can be specified as follows: T, true, .true, Yes, F, false, .false. A space ("a blank") is also equivalent to "true".

✓ Character strings must not be enclosed in single quotes.

✓ The actual values which represent a physical quantity must be followed by their unit.

✓ It is important to include a decimal point in a real number to distinguish it from a whole number, in order to avoid ambiguities when mixing types on the same input line.

✓ Complex data structures are called blocks and are placed between ‘’% block label ‘’ and’% end block label ’’ (without the quotes).

✓ If the same label is specified twice, the first takes precedence.

✓ If a label is misspelled, it will not be recognized (there is no internal list of “accepted” tags in the program). You can check the actual value used by siesta by looking for the label in the fdf.log output file.

2.4 Detailed description of Program options

Here is a description of the variables that can be defined in the Siesta input file, with their data type and their default value.

✓ **SystemName (string):** a string of one or more words containing a descriptive name of the system (maximum 150 characters).

Default value: empty.

✓ **SystemLabel (string):** a single word (max. 20 characters without blanks) containing a System nickname, used to name the output files.

Default value: siesta

✓ **NumberOfSpecies (integer):** Number of different atomic species in the simulation. Atoms of thesame species, but with a different set of pseudo-potentials or bases, are counted as different species. Default value: there is no default value. This variable must be specified.

✓ **NumberOfAtoms (integer):** Number of atoms in the simulation. Default value: there is no default value. This variable must be provided.

✓ **ChemicalSpeciesLabel (data block):** it specifies the different chemical species that are present, assigning them a number for later identification. Siesta recognizes the different atoms by the given atomic number.

✓ **AtomicMass (data block):** it allows the user to enter the atomic masses of the different species used in the calculation, which is very useful in the dynamics of isotopes for example. If the species index is not found in the block, Siesta assigns natural mass to the corresponding atomic number. If the block is absent, all the masses are natural. Each species is characterized by a line containing, an index of the species

(integer), and the desired mass (real). The order is not important. If there is no integer or real numbers in the line, the line is ignored.

- ✓ **Net charge (real):** specifies the net load of the system (in unit e). For charged systems, energy slowly converges with the size of the cell. For molecules and atoms, a Madelung corrective term is applied to energy to facilitate convergence with cell size (this only applies to CS, CC and CFC cells). For other cells or for periodic systems, this correction term does not apply and the user is warned by the program [54, 55].

2.5 Pseudo-potentials

Siesta uses pseudo-potentials to represent the electron-ion interaction (as most plane wave codes do and unlike so-called "all electron" programs). In particular, the pseudo-potentials are of the "conservative of standards" type and can be generated by the Atom program. It should be noted that all pseudo-potentials must be thoroughly tested before using them. A number of other codes (such as APE) can generate pseudo-potentials that Siesta can use directly (usually in .psf format).

The pseudo-potentials will be read by Siesta from different files, one for each defined species (species defined in the Chemical Species Label block). The file names can be: Chemical label.vps (unformatted) or Chemical label.psf (ASCII),where the chemical label corresponds to that defined in the ChemicalSpeciesLabel block.

Table (II):Ionic charge, electronic configuration and cut-off radii of each orbital, for the different atoms used.

Atom	Z ion	Configuration	r_c(Bohr)			
			r_s	r_p	r_d	r_f
Ge, Z=32	4	$4s^2 4p^2 4d^0 4f^0$	2.06	2.85	2.58	2.58
Pd, Z=46	10	$5s^1 5p^0 4d^9 4f^0$	2.58	2.71	2.45	2.45
Ir, Z=77	9	$6s^1 6p^0 5d^8 5f^0$	2.63	2.77	2.63	2.63
Pt, Z=78	10	$6s^1 6p^0 5d^9 5f^0$	2.6	2.73	2.6	2.6

By using these pseudo-potentials, only valence electrons are treated explicitly in the calculations. The pseudo-potentials are adjusted to the wave functions of these atoms in their electronic configurations (see tableII). These pseudo-potentials are selected in our work after finding energetic and structural properties that are well comparable with other experimental and theoretical work. In general, the use of pseudo-potentials is closely related to the basis of wave functions.

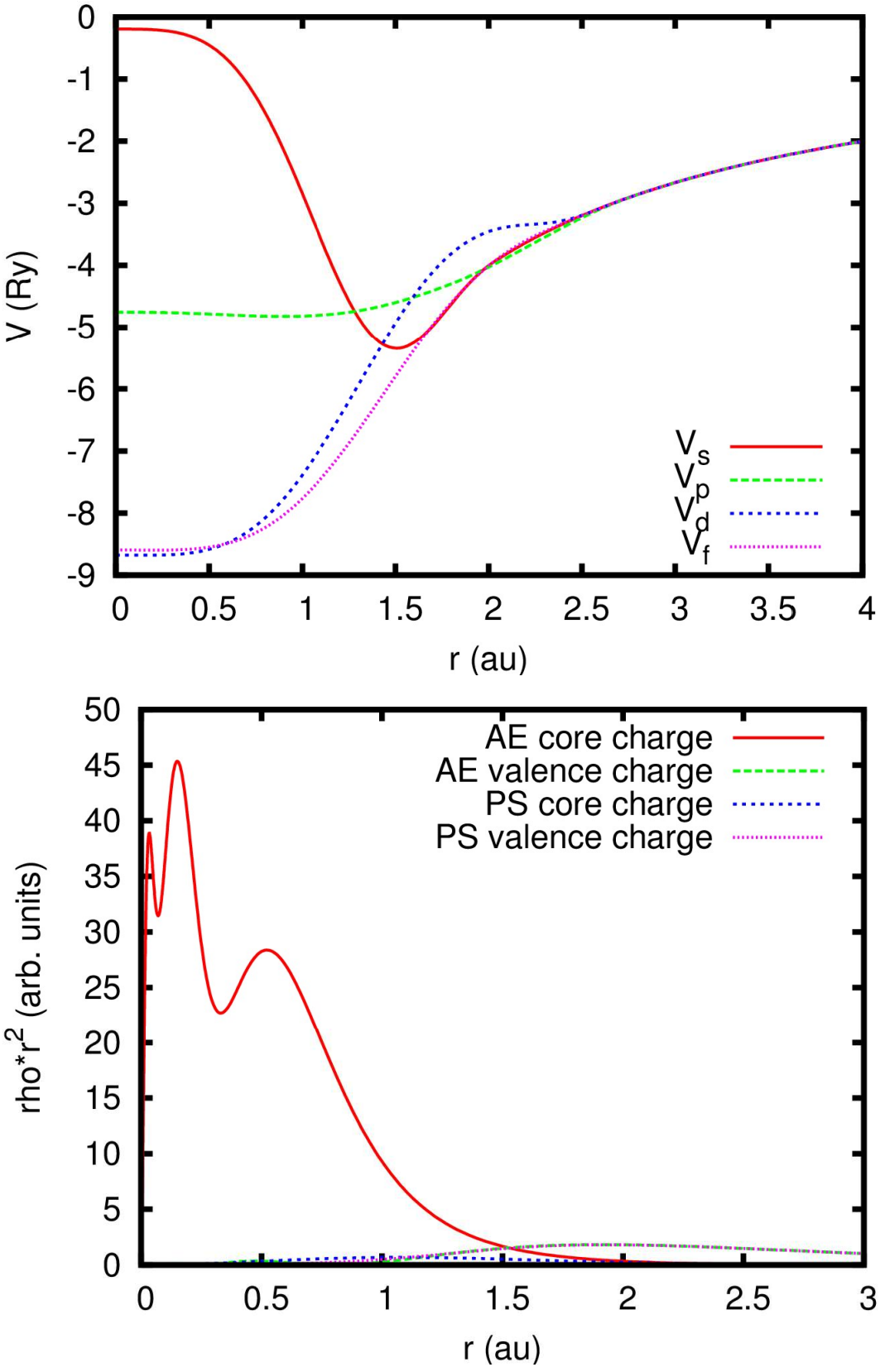

Fig (2.1): Pseudo-potentials and charge densities of the Ge atom

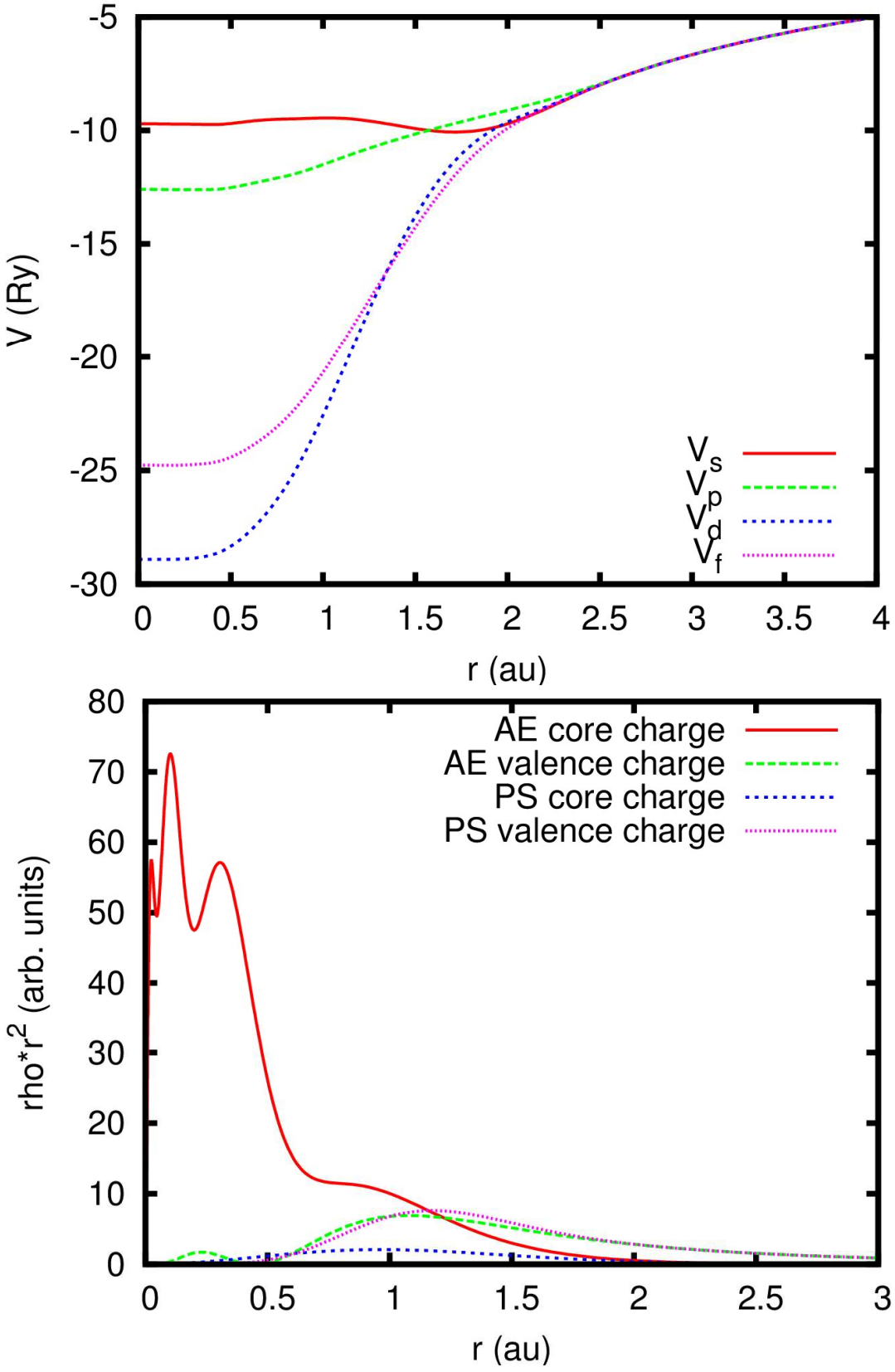

Fig (2.2): Pseudo-potentials and charge densities of the Pd atom

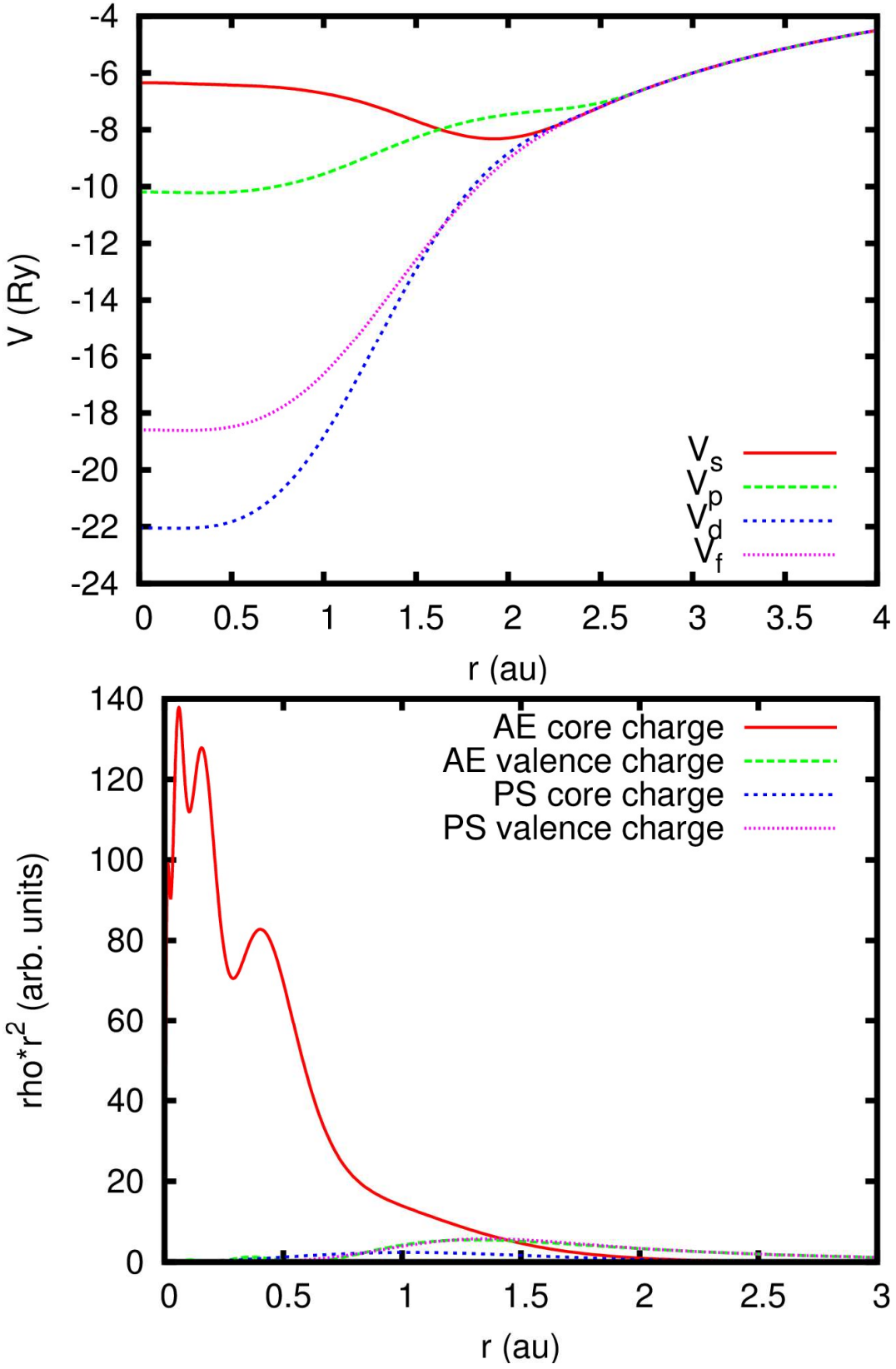

Fig (2.3): Pseudo-potentials and charge densities of the Ir atom

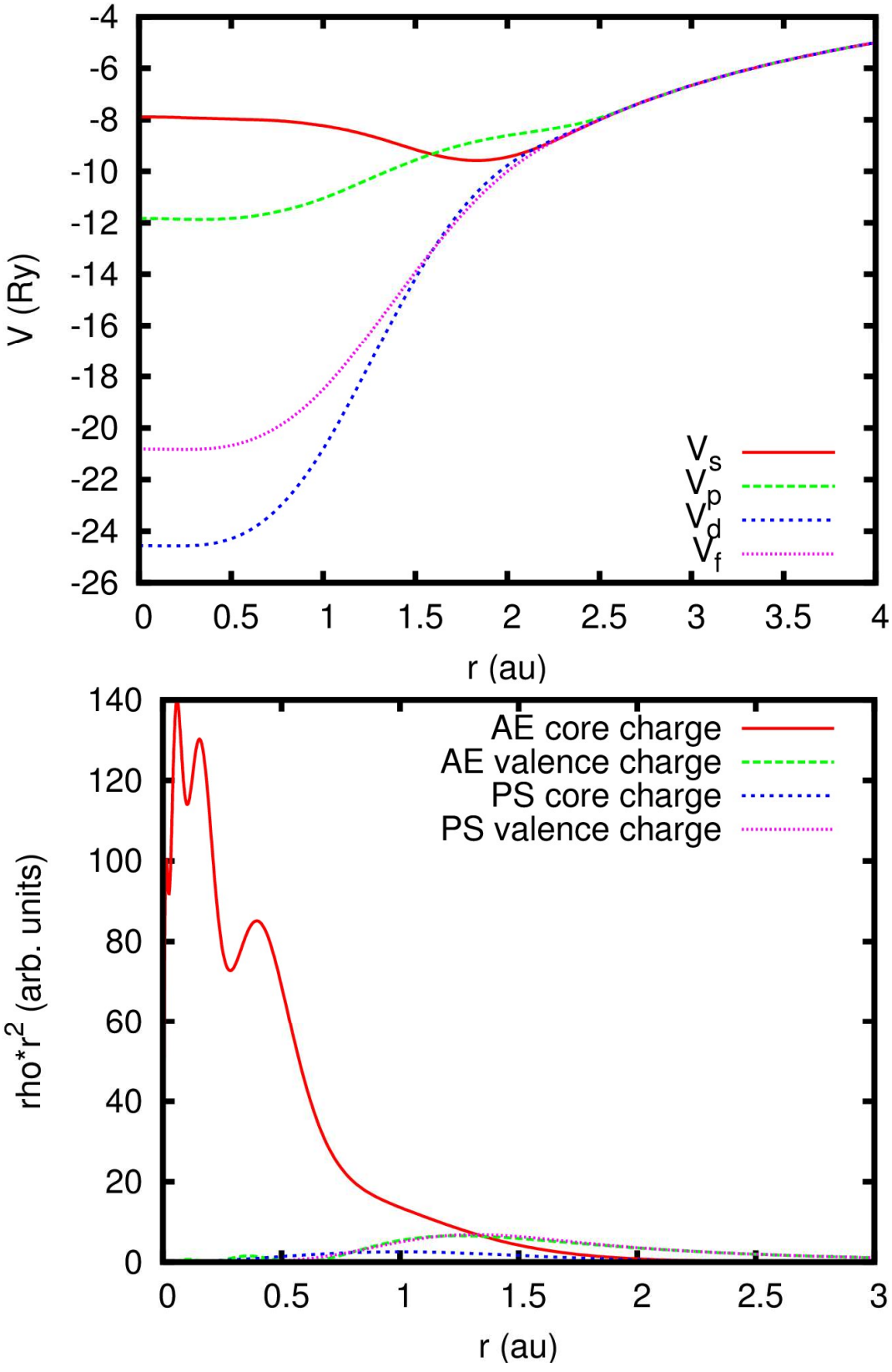

Fig (2.4): Pseudo-potentials and charge densities of the Pt atom

2.6 Definition of the bases

- ✓ **PAO.BasisSize (string):** it defines the usual basic sizes. This only has an effect if there is no PAO.Basis block. The possible bases are:
- ✓ **SZ or MINIMAL:** minimum or simple zeta base.
- ✓ DZ: double zeta base, in the scheme defined by PAO.BasisType.
- ✓ SZP: single-zeta polarization orbital base.

DZP or STANDARD: Like DZ with polarization orbitals. The polarization orbitals are constructedfrom the theory of disturbances. They are defined with a minimum angular moment so that there can be no orbitals occupied with the same in the valence band of the atomic configuration in the ground state. Default value: DZP.

- ✓ **PAO.EnergyShift (real energy):** a standard for the radii of containment of the orbital. It is the excitation energy of the PAO due to confinement. It offers a general procedure for defining the confinement radii of the original PAOs (first-zeta) for all species, thus guaranteeing the compensation of the base. This only has an effect when the PAO block. Basis is not present or when the radii specified in this block are zero for the first zeta.

Use: it must be positive. Default value: 0.02 R.

- ✓ **LatticeConstant (real length):** used to define the scale of the vectors of the crystal lattice. Default value: Minimum size to include the system (assumed to be a molecule) without intercellular interactions.
- ✓ **LatticeParameters (data block):** crystallographic way of specifying the vectors of the network, giving six real numbers: the three vector modules, a, b and c and the three angles (Angle between b and c). The three modules are given in LatticeConstant units; the three angles are in degrees.

Default values: 1.0 1.0 1.0 90. 90. 90.

- ✓ **LatticeVectors (data block):** cell vectors are read in units of the network constant. They are read as a CELL matrix (ixyz, ivector), each vector being a line.

Default value:

1.0 0.0 0.0

0.0 1.0 0.0

0.0 0.0 1.0

If the LatticeConstant parameter is used, the default value of LatticeVectors is always diagonal but not necessarily cubic.

- ✓ **SuperCell (data block):** Entire 3x3 matrixes defining a super cell in terms of unit cells.
- ✓ **Spinpolarized (logical):** logical variable which allows the choice between the polarized spin calculation ‘’ True ’’ or none polarized ‘’ False’**.**

Default value: False.

Chapter 3

Theoretical investigation of $PdGe_n$ and $PtGe_n$ Clusters

Chapter 3

Theoretical investigation of $PdGe_n$ and $PtGe_n$ Clusters

3.1 Introduction

During the last decade, many efforts have been devoted to investigate the properties of pure or metal-doped germanium clusters due to their potential uses as assembled nanomaterials in the field of semiconductor materials and nanoelectronics. The scientific community basing on the uniqueness properties of this new category at this scale of matter have invested a big amount of effort to understand their riddles and knowing the perfect way to be used for. Great ideas were studied and others were established in different fields, for example: phototherapy of cancer cells, bio-imaging, catalysis and biosensors and even superconductivity and magnetism effects. The opportunities that will be created by the mastery of these new materials are outstanding, at the same time, properties are related to the size, the shape and the composition of every cluster which in turn the number of possible isomers become very important, so that searching for the lowest isomer is a very challenging task.

Physical and chemical properties of pure and doped germanium clusters are widely investigated theoretically and experimentally, it is often working, before any practical applications can be developed, the chemical, electronic and optical properties of the clusters have to be established in purpose to avoid an over-expenditure of time and financial resources.

Several studies were encountered during the bibliographic research in the literature in attention to provide an update on the different approaches implemented in the analysis and investigation of the pure germanium clusters [56-71]. The low-lying neutral germanium clusters Ge_n in the size range of ($21 \leq n \leq 29$) had performed by Yoo and Zeng [56], it can be seen that the binding energies per atom increase rather smoothly with the increase of cluster size n. Among the generic motifs examined, they found that two motifs stand out in producing most low-lying clusters, namely, the six/nine motif, a puckered-hexagonal-ring Ge_6 unit attached to a tricapped trigonal prism Ge_9 , and the six/ten motif, a puckered-hexagonal-ring Ge_6 unit attached to a bicapped antiprism Ge_{10} . The low-lying clusters obtained are all prolate in shape and their energies are appreciably lower than the near-spherical low-energy clusters. This result is consistent with the ion-mobility measurement in that medium-sized germanium clusters detected are all prolate in shape until the size n ~ 65. Wang and Zhao [57] have elucidated that when cluster size increases the super cluster architectures become less distinct for all Ge_n (n = 30 – 39) clusters and prefer the motif of super-cluster structures stacked by several stable subunits such as Ge_{10} and Ge_6, connecting via a few bridging atoms, whereas the computed binding energies for all Ge_n clusters studied are not size sensitive. Wielgus et al [58] deduct that the bonding analyses revealed that the trimers and tetramers are stabilized through multicenter π bonding. In pentamers, this stabilizing factor is eliminated due to the

further cluster growth. The ionization of clusters does not change their geometrical characteristics. King et al [59] have published a Ge_8^z (z = −6,−4, −2, 0, +2, +4) study of the effects of electron count on cluster geometry and revealed that the choice of germanium as the vertex atom for this study of eight-vertex clusters minimizes the maximum charge required for the range of 22 to 10 skeletal electrons in eight-vertex clusters with bare vertex atoms. As well, in a past work [60] they study the nine-atom germanium clusters effect of electron count on cluster geometry of Ge_9^z clusters (z=−6, −4, −3, −2, 0, +2, and +4) and found that accord with Wade's rules for a 2n+2 skeletal electron structure global minimum for the germanium cluster Ge_9^{2-} is a tricapped trigonal prism and for Ge_9^{4-} the global minimum is the elongated tricapped trigonal prism. In the case of Wade's rules for a 2n+4 skeletal electron structures for the capped square anti-prism is only 0.21 kcal/mol, above this global minima indicate that these two structures have very similar energies. Thus, the global minimum for the neutral cluster Ge_9 was found to be a bicapped pentagonal bipyramid.

Zhao and co-authors [61] on a comparison of the growth pattern of Si_n and Ge_n clusters (n=25-33) they estimate that both of these clusters display a large deviation in that size range, and especially for n=29 that reveal a remarkable stabilities. they also noted that when small clusters serve as building blocks of bigger clusters, their surfaces tend to show puckered rhombuses which might be favorable interfaces for clusters' aggregation and can also lead to bulk-motif linking with other blocks. Islam and Ray [62] have deducted that Ge_2 is found to have triplet ground state at both the self consistent field (SCF) and MP4 levels. For germanium trimers, the most favoured structure at the SCF level is found to be Ge isosceles, and for germanium tetramers, at the SCF level, the most favoured structure is rhombus Ge. Deutsch et al [63] in a comparative study of electron affinities of Ge_n^- (n= 2-5) clusters, the G_2 electron affinities of the germanium cluster anions are very similar to those of the corresponding silicon anions, and for (n=2-4) are in good agreement with experiment values. As well in former work [64] they found that binding energies of Ge_n (n = 2-5) using G2 theory was in reasonable agreement with the experimental values, and the Ge_n fragmentation energies parallel as a function of cluster size.

In a case of an experimental study Bals and co-workers [13] in atomic scale dynamics of ultra-small germanium clusters stated that using quantitative scanning transmission electron microscopy in combination with ab initio calculations (see Fig3.1), they was able to characterize the transition between different equilibrium geometries of a germanium cluster consisting of less than 25 atoms. Seven-membered rings, trigonal prisms and some smaller subunits are identified as possible building blocks that stabilize the structure and in view of this configuration, the cluster was found to break up into smaller fragments consisting of 3–7 atoms. Zhao et al [65] revealed in a study of the fragmentation behaviour that the lowest-energy structures of the Ge_n clusters with n=17–33 can be viewed as an assembly of small stable subunits of a Ge_6 or Ge_9 linkage attaching to several small clusters. According to the large fragmentation energies conclude that the germanium clusters with $11 < n \leq 33$ can be easily dissociated into small stable germanium clusters, and they noted that the thermodynamic stability of Ge_n clusters have an oscillation character. Luo and co-authors [66] in a density functional theory study of germanium Ge_{11} clusters have found that clusters derived from bi-capped square anti-prism structure have the lowest total energies in general

and thus is an important core unit in Ge_{11} model design, and that frequency analysis indicated that some of the formerly reported Ge_{11} cluster structures are likely to be unstable.

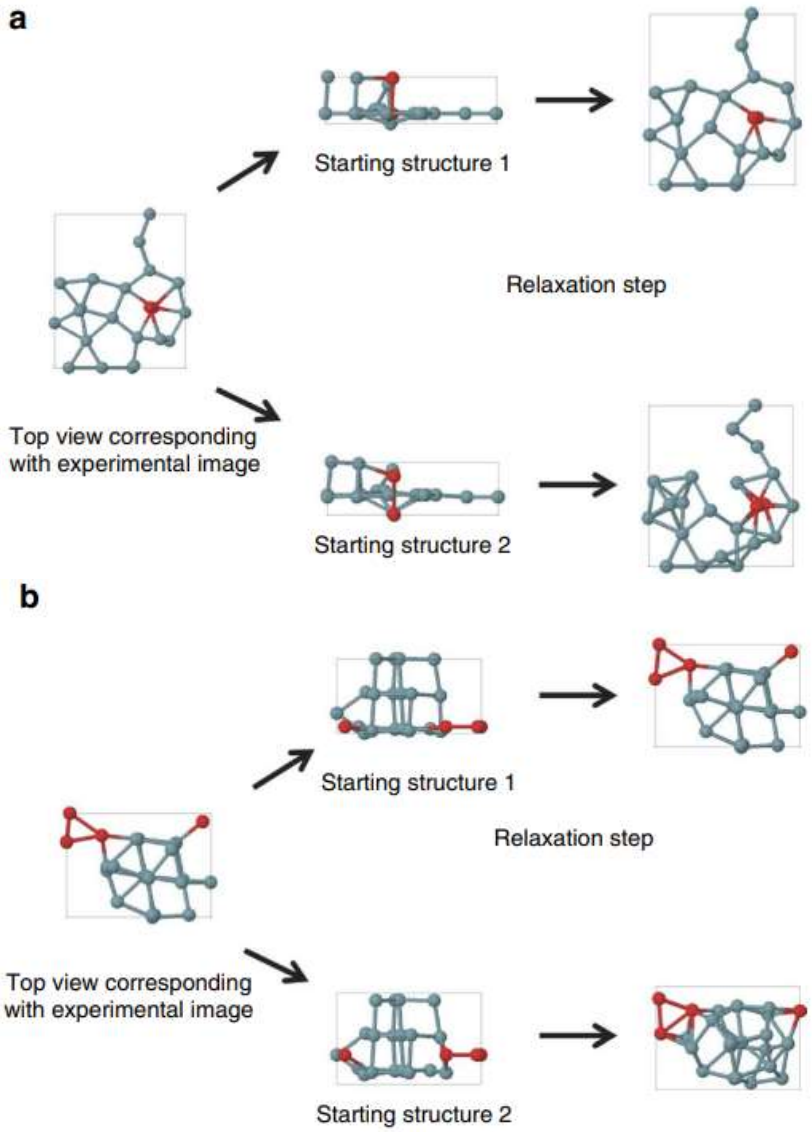

Fig (3.1): Two examples of slightly varying starting configurations resulting in significantly altered relaxed structures. (a,b) The left panels represent the top view of a model that corresponds to the experimental picture. The panels in the middle give two different configurations that are indistinguishable if viewed from the top. After relaxation with density functional theory (panels on the right), only one of the two possibilities is still compatible with the experimental image [13].

In a study of stable structures of neutral and ionic Ge_n (n=11–19) clusters, Li et al [67] have summarized that most of the ground state structures for the neutral and cationic Ge clusters have similar configurations, but different for the anionic Ge clusters. Most of the lowest energy structures for the neutral and ionic Ge_n (n=11–19) clusters are obviously different from those of the corresponding Si_n clusters although the geometrical configurations of the small clusters (n<10) are basically the same. Their results also show that all the lowest

energy structures of the cationic Ge_n (n=11–19) clusters have the similar geometrical configurations to those of the corresponding neutral Ge_n (n=11–19) clusters except for n=11. However, for the anionic Ge_n (n=11–19) clusters, the conclusion is almost the reverse. In another work King and co-workers [68] studied the 11-atom bare germanium clusters using DFT. This work shows that the lowest energy structures for a given stoichiometry need not always be symmetrical and the low energy low symmetry isomers are all found to obey the Wade-Mingos rules. Li and co-workers [69] in an investigation of Ge_n^- and Ge_n^+ (n = 5–10) clusters in comparison with corresponding Si_n ions have shown that the ground state structures of some Ge cluster ions are different from those of their corresponding neutral Ge clusters. Furthermore, the positive Ge ions have more severe structural distortion than the negative Ge ions due to Jahn–Teller distortion. In addition, there are differences between the ground state structures of Ge ions and Si ions, although most of the Ge ions have similar geometrical configurations to their corresponding Si ions.

In the case of stable structures of Ge_n (n = 21–25) clusters, Liang and Li [70] show that all the lowest energy structures are the stacked prolate structures including a tricapped trigonal prism (TTP) subunit at least and that the structural characteristic is similar to that of the ground-state structures for Si clusters and specially in the range of 21–25 the most stable structures for Ge and Si clusters are obviously different. Habib ur Rehman and co-workers [71] studied the properties of Si_n, Ge_n, and Si_nGe_n Clusters with 2-44 atoms. For the mixed clusters, the lower energy of Ge-Ge bonds leads to the occurrence of only few such bonds, whereas Si-Si and Ge-Si bonds are dominating. In the case of Si_n clusters for which a transition from oblate to prolate shapes is found for clusters with slightly more than 30 atoms. Although, for the strongest bonds, in our case the Si-Si, show a tendency for the Si atoms to occupy the internal parts and for the Ge atoms to be found in the external parts. Finally, the overall decrease in the HOMO-LUMO gap as a function of increasing size can be observed.

A wide interest of doping pure germanium clusters by metal transition atoms have being successfully carrying out [72-111]. Mahtout et al [72] have found that Cu doping Ge_n (n=1-19) clusters enhances the stability of the corresponding germanium frame, although in the case of Ag and Au the binding energies are always lower than those of pure germanium clusters, and in same time the metal atom is encapsulated inside a germanium cage from n=10 for Cu and from n = 12 for Ag and Au. Siouani et al [73] they noticed that the endohedral structures in which the vanadium atom is encapsulated inside a Ge_n cage are predicted to be favoured for $n \geq 10$. The dopant V atom in the Ge_n clusters has not an immediate effect on the stability of small germanium clusters ($n < 6$), but it largely contributes to strengthen the stability for $n \geq 7$. Remarkable stability of the VGe_{14} cage-like geometry and a peculiar electronic structure had concluded.

An investigation of electronic and magnetic properties of medium-sized $CrGe_n$ ($15 \leq n \leq 29$) clusters had made by Mahtout and Tariket [74], their result show that encapsulation of Cr atoms within Ge_n clusters leads to stable clusters, the binding energies generally increase while HOMO–LUMO gaps decrease with the increasing of cluster size. Moreover, Cr atom in the clusters's size and shape led the magnetic property. Djaadi et al [75] had investigate Ge_{n+1} and $SnGe_n^{(0,\pm1)}$ (n = 1 – 17) and found that they adopt compact structures when the cluster size is increasing, further the Sn atom occupied a peripheral position for $SnGe_n$ clusters when

n < 12 and occupied a core position for n > 12. Bulusu et al [76] have performed an unbiased search for the global minimum geometries of small-to-medium sized germanium clusters Ge_n ($12 \leq n \leq 18$) as well as a biased search (using seeding method) for Ge_n ($17 \leq n \leq 20$). All the low-lying clusters in the size range of ($12 \leq n \leq 20$) contain the tri-caped trigonal prism motif and are all prolate in geometry, which is in agreement with the experiment. Wang and Han [77] after studding geometries, stabilities, and electronic properties of Ge_n and $CuGe_n$ (n = 2 – 13) clusters, they have found that the relative stabilities of $CuGe_{10}$ and Ge_{10} are the strongest among all different sized $CuGe_n$ and Ge_n clusters, respectively. Besides that when the size of clusters increases the HOMO-LUMO gaps are decreasing when Cu is doped into the Ge_n clusters, even charge always transfers from copper to germanium atoms in all different sized clusters contrarily to some TM- doped silicon clusters.

Jing et al [78] have predict that the Ge_nCo (n = 1 – 13) clusters magnetic moment does not quench in which that the previous results with transition-metal-doped Si_n clusters are in contrast with. For the ground state structures they found that the Ge_nCo ($n \leq 9$) clusters adapt a metal-encapsulated Ge_n cages in which the dopant atom occupy the center and enhances the stability of the host Ge_n clusters, whereas among them the most stable one is $Ge_{10}Co$. Deng et al [79] in thier work have investigated theoretical and experimental series of cobalt-doped germanium clusters, $CoGe_n^{-/0}$ (n = 2–11), they found that the transition from exo- to endohedral structures began from n = 9 and this transition is caused by the transfer of electrons from the Ge_n framework to the Co atom and the minimization of the magnetic moments for both anionic and neutral $CoGe_n$ clusters. Kumar et al [80] in their report have shown that in both neutral and anionic series of germanium doped transition metal (TM = Ti, Zr and Hf) the clusters having 20 valence electrons turn out to be relatively more stable and all clusters with size n>9 absorb TM atom endohedrally in the cage of Ge_n pure cluster while all TM- doped clusters beyond n>7, the spin on these last is quenched. Bandyopadhyay [81] in his work of studing chemical and physical properties of Ge_nCu clusters within the size range n=1–20 had approved that the addition of a Cu atom to a Ge cluster is always a favorable action, whatever the cluster size, and that the most stables one's are n=9, 10 and 11 in all of neutral, anionic, and cationic clusters. According to the shell model predictions the study shows an agreement with nearly 20 valence electrons for neutral and charged clusters.

A study of thorium encapsulated by germanium clusters from 16-20 atoms had carried out by Singhet et al [82], they explained that the stability was highly raised and compared to Ge clusters in the same size the binding energy was very higher in which suggests a strong possibility of their experimental realization in large quantities. Also, $Th@Ge_{16}$ has a large highest HOMO-LUMO gap that makes it interesting for optoelectronic applications in visible domain. Wang and Han [83] have studied the behaviours of the $NiGe_n$ (n =1-13) clusters by ab-initio method and concluded that for the small-sized the Ni-convex or substituted Ge_n frames but for the middle or larger-sized, Ni-concaved or encapsulated Ge_n frames and that the Ni-encapsulated Ge_{10} cluster is the most stable species of all different-sized clusters. Whereas, the charge transfer phenomena depend on the sizes of the Ni-doped Ge_n clusters. As well in separate work [84] exactly on tungsten-doped germanium clusters (n =1-17), they found that the charges transfer from the germanium framework to the W atom. Additionally, the WGe_{12} cluster is supposed to be a suitable as a building block of assembly cluster material

comparing it with all others clusters. At the end they conclude that the growth pattern of the $TMGe_n$ depends on the kind of doped TM impurity. Even more, Wang and Han [85] had investigated the bimetallic Mo_2Ge_n (n =9-15) clusters, the calculated fragmentation energies and the obtained relative stabilities demonstrate that the remarkable Mo_2-doped Ge_{12} is the most stable species of all different sized clusters and it enable to be a unit of multiple metal Mo-doped germanium nanotubes. While the vibration mode analyses of Mo_2-Ge_n clusters demonstrate that the Mo-Mo stretching vibrations are sensitive to the geometries of the germanium frame.

Gopakumar et al [86], in a study of the electronic structure of germanium mono-hydrides, Ge_nH, with n ranging from 1 to 3, in the neutral, cationic, and anionic states, for all germanium monohydrides considered, a low-spin electronic ground state is predicted, considering charge, a certain positive net charge on the germanium unit, indicating a considerable charge transfer to the H atom leading to a Ge_n^+Hpolarization, and compared to the result it seems that the Ge_3 cluster could capture a hydrogen atom in whatever charge state, leading to a stable entity. Zdetsis [87] in a study of Bismuth on germanium and silicon clusters show that are characterized by high stability and symmetry and relatively large HOMO-LUMO energy gaps. It is shown that the lower energy structures of these clusters and their bonding and electronic characteristics are fully compatible with very powerful stability rules and structural laws similar to the ones for the corresponding isovalent boranes, carboranes, and bisboranes. Bandyopadhyay and Sen [88] in neutral and cationic pure and Ni doped Ge clusters containing 1-20 Ge atoms are calculated and shown that clusters having 20 valence electrons turn out to be relatively more stable, whereas when n > 9 the Ni atom is absorbed endohedrally in the Ge cage. Shi and co-workers [89] study the aluminium doped germanium clusters Ge_nAl (n = 1–9) and that the clusters up to n = 9 prefer the close-packed configurations and that the small Ge_7 and Ge_5Al isomers are the most stable geometries for Ge_{n+1} and Ge_nAl clusters, respectively. Beside that the atomic magnetic moments (μ_B) brings the decrease as the cluster sizes increase for most of the aluminium doped germanium clusters.

In investigation of Ge_nCr clusters for n=1–13, Kapila and co-workers [90] show the preference of Cr atom to stabilize at the exohedral position, and that the most stable clusters among all other's are for Ge_5Cr and $Ge_{10}Cr$, in addition to that, they suggest donor nature of Cr atoms as there is uniform charge transfer from Cr to Ge atoms. Hernandez and Leyva [91] in a study of small binary Fe_nGe_m ($n+m\leq4$) clusters the magnetic moments at Fe atoms are larger than the bulk magnetization, whereas the magnetic moments at Ge atoms take significant values and also found that the charge transference is from Fe atoms to Ge atoms. Li et al [92] in a study of bimetallic Au–Ge nanoclusters, endohedral cage-like $AuGe_n^-$ clusters was favoured at n = 10, whereas the most stable cluster was found at n=12. The results demonstrated that the induced effects by an additional electron to the neutral clusters can enhance their stabilities. Kapila and co-workers [93] in another work of studying Mn, Co, Ni in Ge_n for (n=1–13) clusters, show that transition metal (TM) atom prefers to occupy surface positions for n<9 and endohedral positions for n≥9, and comparing between the (TM) doped Ge_n clusters the Ni show higher stability as in front of Mn and Co atoms and that the magnetic moment is mainly localized at the TM site and neighbouring Ge atoms. Zhao and

Wang [94] in DFT investigation of $MnGe_n$ (n=2–16) clusters found that doping of one Mn atom contributes to strengthening the stability of the germanium framework and they also found that charge always transfers from manganese to germanium atoms in all sized $MnGe_n$ clusters and the magnetic moment of the Mn atom does not quench when embedded in all sized Ge_n (n = 2–16) clusters.

Hou et al [95] in chromium-doped germanium Clusters $CrGe_n$ (n=1-5) study, show that most of the clusters considered prefer structures with high-spin ground state and large magnetic moments whereas the Cr atom acts as a general electron donor in neutral $CrGe_n$ clusters. Tang and co-workers [96] study using the relativistic all-electron density functional theory, the 3d transition-metal endohedral $Ge_{12}M$ (M = Sc–Ni) clusters, they found that the optical gaps of $Ge_{12}M$ are blue-shifted whereas the magnetic moment of the $M@Ge_{12}$ cluster are mainly comes from the doped transition metal atom (TMA), while the local magnetic moment of the TMA mainly originate from the unpaired electrons of the 3d state, and that the reactions to synthesize them are exothermic and favorable in the energy point. Ju-Guang Han [97] in his paper investigate Ge_nF^- and Ge_nF (n=3–6) clusters, and show that all of the, electron affinities, fragmentation energies and even the populations and geometric parameters are influenced by the extra charge. Lu and Nagase [98] in an investigation of a metal-doped germanium clusters MGe_ns (M=Hf, W, Os, Ni, and Zn) in the sizes of n=12 and 10 prefer irregular structures compared with the MSi_n clusters partially due to the dynamic instability and comparing with others clusters WGe_{12}, $OsGe_{12}$ and $ZnGe_{12}$ turn out to be chemically stable and are maybe the smallest MGe_n building block of cluster-assembled materials. The interaction between the Zn atom and the Ge_n cage is much weaker than that between the W or Os atom and the Ge_n cage owing to a complete occupation of the Zn 3d orbitals.

A study of photoelectron spectroscopy (PES) of germanium- fluorine binary cluster anions had made by Negishi et al [99], they show that compared between the PES of Ge_nF^- and those of the Ge_n^-, it was found that the doped F atom in Ge_nF^- deprives each Ge_n^- cluster of the excess electron without any serious rearrangement of the Ge_n framework. The F doping method estimate the HOMO-LUMO gap of the corresponding neutral Ge_n clusters (n = 4-11). For a diatomic GeF^- cluster, furthermore, the vibrational structures could be resolved to determine its vibrational frequency. Han and co-workers [100] studied Ge_nSn (n=1–4) clusters and show that the natural populations of the most stable Ge_nSn (n=1–4) clusters indicate that charges are transferred from Sn atom to Ge atoms, while enthalpy of reactions at the B3LYP/LanL2DZ level is in good agreement with those of the third law of enthalpy change. In another study of germanium clusters at medium size, Ma and Wang [101] show that from n ≥19, the atoms of the medium size germanium clusters are organized into two shells and the core atoms increase with the cluster size, the ionization potentials and HOMO–LOMO gaps are decreased with the cluster size. And conclude that the structures obtained by the two methods (B3LYP/LANL2DZ) are similar.

As well, in the same field Wang and Han [102] study the growth behaviours of the Zn-doped different sized germanium clusters and reveal that the Zn atom is encapsulated in caged germanium clusters at n = 10 while the icosahedral $ZnGe_{12}$ cluster has stronger relative stability as compared to other sized clusters, and that charges in the Zn-doped Ge_n clusters transfer from the Zn atom to the Ge_n frame, which is different from other clusters that are

being changed at certain size of cluster. In the case of $FeGe_n$ (n = 9–16) clusters, Zhao and Wang [103] have shown that the strongest stability of $FeGe_{14}$ might stem from its highest symmetry (O_h), and that the HOMO–LUMO gaps are obviously reduced when the Fe atom is doped into the Ge_n clusters. They also found that charge always transfers from iron to germanium atoms in all sized $FeGe_n$ clusters and the magnetic moment of the Fe atom does not quench when embedded in large-sized Ge_n clusters. Goswami et al [104] investigated the Ge_xC_y (x+y=2–5) nanoclusters by B3LYP-DFT method and they concluded that the most stable structures are those which contain the maximum number of carbon atoms while the nanoclusters containing even number of carbon atoms have large HOMO–LUMO gap and those containing odd number of carbon atoms have small HOMO–LUMO gap. And comparing to Ge-C bond the C-C bond has important role in stabilizing the clusters. In another work King et al [105] have studied using density functional theory the 10-atom germanium clusters: effect of electron count on cluster geometry and found that the isoelectronic Ge_{10}^{2-} use to be the global minimum by more than 15kcal/mol. The global minima found for electron-rich clusters Ge_{10}^{4-} and Ge_{10}^{6-} are not those known experimentally. While the global minimum for Ge_{10} is the C_{3v}-tetracapped trigonal prism predicted by the Wade−Mingos rules and found experimentally in isoelectronic $Ni@Ga_{10}^{10-}$.

Deng et al [106] on photoelectron spectroscopy and density functional calculations of VGe_n^- (n = 3−12) clusters. For both anionic and neutral VGe_n clusters, with $n \leq 7$, the dominant geometries are exohedral structures whereas at n=8, the $VGe_n^{-/0}$ clusters show half-endohedral boat-shaped structures. Thus, from n = 9 to 11 the additional Ge atoms form Ge_n cage. At n=12, a D 3d distorted hexagonal prism cage structure is formed. The electron transfer from the Ge_n framework to the V atom and the magnetic moments is decreasing to the lowest values at n=8−12, and that both of them are caused by the structural evolution. King and co-authors [107] investigate the Endohedral Nickel, Palladium, and Platinum Atoms in 10-Vertex Germanium Clusters. For the neutral clusters $M@Ge_{10}$ the global minima are singlet bicapped square antiprisms. However, triplet regular pentagonal prismatic structures become increasingly energetically competitive in the series Ni,Pd and Pt. The pentagonal prismatic dianions $M@Ge_{10}^{2-}$ (M=Ni, Pd, Pt) appear to have closed shell structures and are the global minima for palladium and platinum. However, the global minimum for $Ni@Ge_{10}^{2-}$ is the capped square antiprism suggested by the Wade-Mingos rules. In an investigation of experimental detection and theoretical characterization of germanium doped lithium clusters $Li_nGe^{0,+}$(n = 1-7), Ngan et al [108] show that clusters having from 4 to 6 valence electrons prefer high spin states, and low spin ground states are derived for the others because valence electron configurations are formed by filling electrons to the shells 1s/1p/2s/2p based on Pauli's and Hund's rules. Thus, both the 8- and the 10-electron systems are more stable than the others because of the closed electronic shells, while the 8-electron species is more favoured than the 10-electron clusters. And comparing to C, Ge was behaving differently in their doped lithium clusters and that because of the difference in atomic radii. Additionally, Li atoms do not bond to each other but through Ge or pseudo-atoms, and an essentially ionic character can be attributed to the cluster chemical bonds.

Nagendran and co-workers [109] study the reduction of the chloride $[PhC(NtBu)_2]GeCl$ with potassium in THF. The X-ray structure and DFT calculation indicate

that the Ge-Ge bond possesses an unusual gauche-bent geometry. Furthermore, the Ge-Ge bond length is 2.570 Å, which is very close to the single Ge-Ge interaction. In an investigation of neutral and anion $ZrGe_n$ (n = 1–21) clusters, Jaiswal and Kumar [110] found that the strongly magic cluster with high symmetry structure and large HOMO–LUMO gap was for n = 16. As well they have noticed that $ZrGe_n$ anion cluster may also be present in experiments but often the neutral clusters of such anions are found to have the lowest energy. Further, the addition of an electron to the neutral $ZrGe_{11}$ cluster changes its geometrical configuration drastically, while, the Zr atom is encapsulated in a cage-like structure at a size of thirteen or more Ge atoms. Jin et al [111] investigate the Ruthenium-Doped Germanium Clusters, going from the size of n = 2 to n = 12, it is perceived that the cluster growth is directed toward the formation of an endohedral aggregate. For the n= 2-6 they obtained small open-shell geometries, and for n=9-12 the endohedral geometries. The endohedral constructions contain the Ru atoms at their interstitial positions. In the case of positive values of highest occupied molecular orbital energies of global minimum anions depict the electronic instability, while the counter-cation effect is discussed to show the compensation of coulomb repulsion among excess negative charges. The transfer of negative charge from the Ge_n framework to the Ru atom decreases with increasing ionization.

3.2 Computational Methodology

The spin-polarized DFT implemented in the SIESTA package [18] are used in all calculations performed in this work. Under the generalized gradient approximation formulated by Perdew, Burke, and Ernzerhof [112] (PBE), the exchange−correlation energy functional was described. In the case of norm-conserving Troullier−Martins nonlocal pseudo-potentials [45], a flexible basis set of localized numerical-type atomic orbitals were used together and a Mesh Cut-Off of 150 Ry was taken and the Energy-Shift is taken equal to 50 meV. Furthermore, core electrons were replaced by nonlocal, norm-conserving pseudo-potentials factorized in the Kleinman− Bylander form [113]. We used $4d^3$ and $4f^{14}\ 5d^9\ 6s^1$ configurations for Pd and Pt respectively and $4s^2\ 4p^2$ for Ge. In this study the geometries were optimized without any symmetry constraints, and by solving the Kohn−Sham equations [30] the optimization of electronic structure was obtained, using self- consistent with a convergence criterion of 1×10^{-4} a.u. on the energy and electron density. For Brillouin zone sampling we used the k = 0 (Γ) point approximation. We used the double ζ (DZ) basis for Ge atoms and double ζ (DZP) basis with polarization function for Pd and Pt atom. In the optimization process, the volume of the system was kept constant, and a big super-cell of 40 Å was used to avoid interaction between the neighboring clusters. Structural optimizations were performed using conjugate gradient algorithm, and the convergence criterion on the Hellmann−Feynman forces imposed that the residual forces were less than 10^{-2} eV/Å. Several spin multiplicity states were tested. The Mulliken population analyses were done to obtain the atomic charge and the unpaired spin population. In order to find the global minimum structures of MGe_n (M=Pd,Pt) clusters. Firstly, we have used several optimized isomers of pure germanium clusters with size of 2–21 atoms [73]. Moreover, a great number of isomers doped MGe_{n+1} from 1-20 were considered. Supplemental analysis and investigation of the electronic properties and molecular orbitals has been performed with the software Gaussian09 [114]

using PBE and the Gaussian-type basis sets cc-pvtz for Ge and LanL2DZ for Ir. They include the electron population analysis, the plot of density of states, as well as the prediction of optical absorption spectra calculated in the framework of the Time-Dependent DFT (TDDFT).

The stability of Pd- and Pt-doped germanium clusters can be studied by the calculation of the binding energy, HOMO–LUMO gap, and the second-order energy difference. The binding energies per atom of MGen (M = Pd, Pt) are defined by the following formula:

$$E_b(MGe_n)(eV/atom) = (n\,E(Ge) + E(M) - E(MGe_n)) / (n + 1) \quad (3.1)$$

Where E (Ge) is the total energy of free Ge atom, E(M) is the total energy of free M atom and E(MGen) is the total energy of the MGen cluster. The HOMO–LUMO gap is calculated from the energy of the orbitals:

$$\Delta E\,(eV) = E\,(LUMO) - E\,(HOMO) \quad (3.2)$$

The second-order energy difference for the ground-state MGen (M = Pd, Pt) clusters can be calculated by:

$$\Delta_2 E = E\,(MGe_{n+1}) + E\,(MGe_{n-1}) - 2\,E\,(MGe_{n2}) \quad (3.3)$$

where E is the total energy of the most stable structure for each species. At the present level of calculation, the bond lengths of Ge_2 were found to be 2.450 Å, and it is in good agreement with the experimental results of the literature [115]. The binding energy per atom was calculated to be 1.44 eV, which is also in good agreement with both theoretical [77, 90, 95] and experimental (~1.35 eV) [116] data.

3.3 Results and discussion

The ground state isomers of $PdGe_n$ and $PtGe_n$ clusters were established using the earlier described method. In atomistic simulation investigation, the determination of the ground-state of the initial structures is very important tasks which will allow us after that to unveil the other properties by modifying distinguish parameters. As a beginning we looked into the doped germanium clusters and compare them and see the important changes in order to bring the most remarkable improvement and why not to manage a useful way to be indented for.

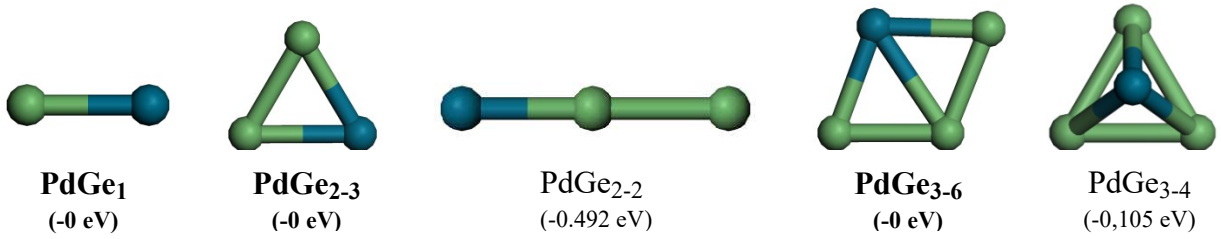

$PdGe_{1}$ **(-0 eV)** | **$PdGe_{2-3}$** **(-0 eV)** | $PdGe_{2-2}$ (-0.492 eV) | **$PdGe_{3-6}$** **(-0 eV)** | $PdGe_{3-4}$ (-0,105 eV)

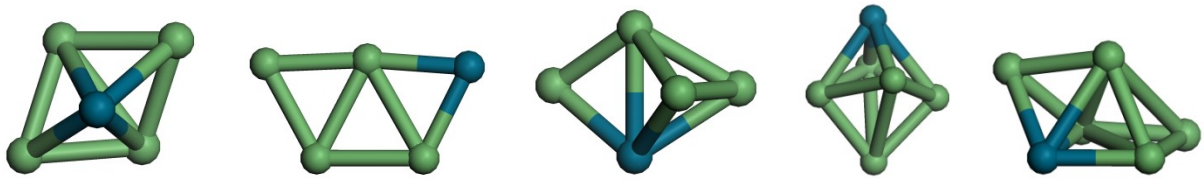

$PdGe_{4-1}$ **(-0 eV)** | $PdGe_{4-14}$ (-0,112 eV) | $PdGe_{4-11}$ (-0.185 eV) | **$PdGe_{5-1}$** **(-0 eV)** | $PdGe_{5-17}$ (-0.055 eV)

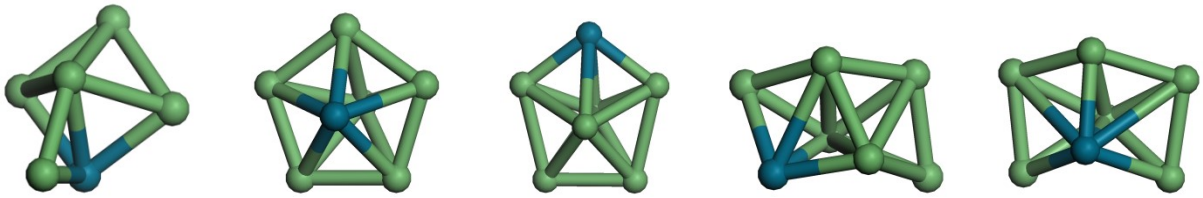

$PdGe_{5-12}$ (-0,125 eV) | **$PdGe_{6-4}$** **(-0 eV)** | $PdGe_{6-25}$ (-0,02 eV) | $PdGe_{6-6}$ (-0,029 eV) | $PdGe_{6-21}$ (-0,076 eV)

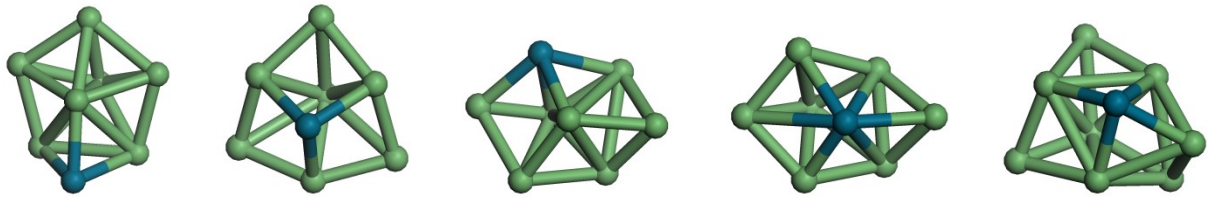

$PdGe_{7-3}$ **(-0 eV)** | $PdGe_{7-7}$ (-0,01 eV) | $PdGe_{7-10}$ (-0,039 eV) | $PdGe_{7-5}$ (-0,042 eV) | **$PdGe_{8-8}$** **(-0 eV)**

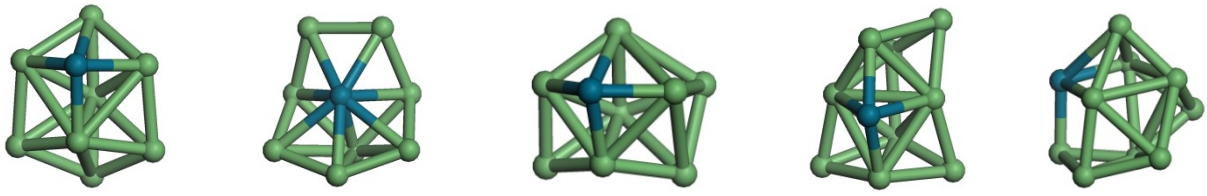

$PdGe_{8-1}$ (-0,003 eV) | $PdGe_{8-9}$ (-0,007 eV) | $PdGe_{8-7}$ (-0,033 eV) | **$PdGe_{9-23}$** **(-0 eV)** | $PdGe_{9-15}$ (-0,009 eV)

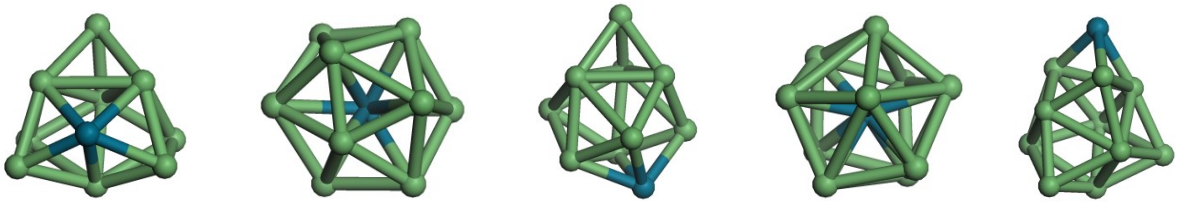

$PdGe_{9-1}$ (-0,017 eV) | $PdGe_{9-25}$ (-0,02 eV) | $PdGe_{9-10}$ (-0,03 eV) | **$PdGe_{10-9}$** **(-0 eV)** | $PdGe_{10-13}$ (-0,005 eV)

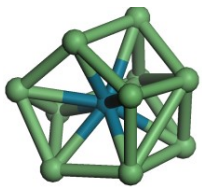

$PdGe_{10\text{-}2}$
(-0,006 eV)

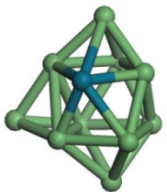

$PdGe_{10\text{-}6}$
(-0,02 eV)

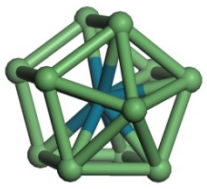

$PdGe_{11\text{-}1}$
(-0 eV)

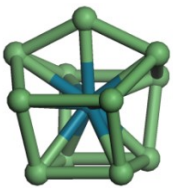

$PdGe_{11\text{-}9}$
(-0,009 eV)

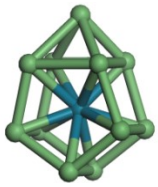

$PdGe_{11\text{-}13}$
(-0,013 eV)

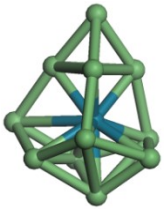

$PdGe_{11\text{-}6}$
(-0,035 eV)

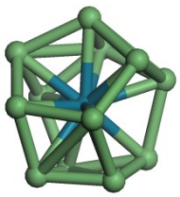

$PdGe_{12\text{-}22}$
(-0 eV)

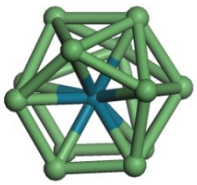

$PdGe_{12\text{-}16}$
(-0,03 eV)

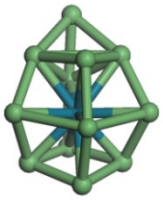

$PdGe_{12\text{-}24}$
(-0,042 eV)

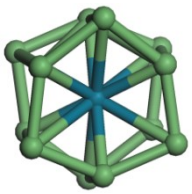

$PdGe_{12\text{-}1}$
(-0,056 eV)

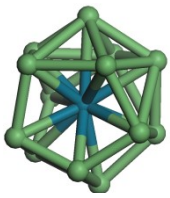

$PdGe_{13\text{-}2}$
(-0 eV)

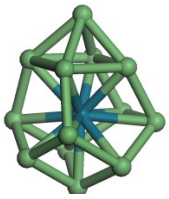

$PdGe_{13\text{-}7}$
(-0,015 eV)

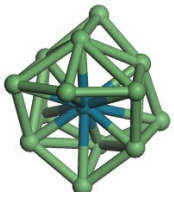

$PdGe_{13\text{-}1}$
(-0,02 eV)

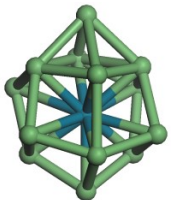

$PdGe_{13\text{-}4}$
(-0,043 eV)

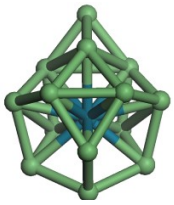

$PdGe_{14\text{-}19}$
(-0 eV)

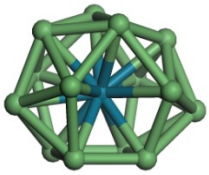

$PdGe_{14\text{-}14}$
(-0,003 eV)

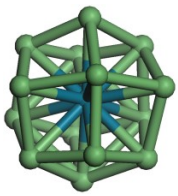

$PdGe_{14\text{-}11}$
(-0,008 eV)

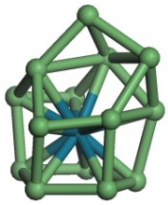

$PdGe_{14\text{-}20}$
(-0,009 eV)

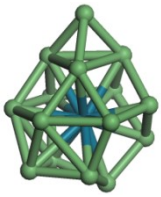

$PdGe_{15\text{-}18}$
(-0 eV)

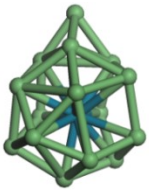

$PdGe_{15\text{-}1}$
(-0,009 eV)

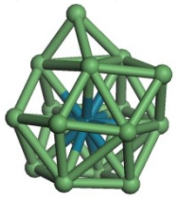

$PdGe_{15\text{-}6}$
(-0,012 eV)

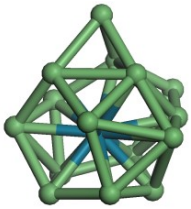

$PdGe_{15\text{-}21}$
(-0,024 eV)

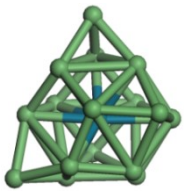

$PdGe_{16\text{-}3}$
(-0 eV)

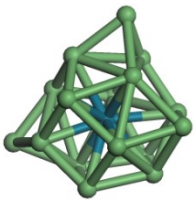

$PdGe_{16\text{-}19}$
(-0,027 eV)

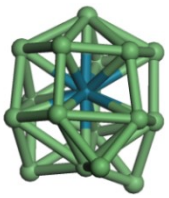

$PdGe_{16\text{-}12}$
(-0,03 eV)

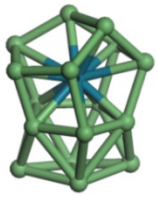

$PdGe_{16\text{-}13}$
(-0,041 eV)

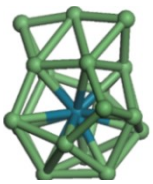

$PdGe_{17\text{-}21}$
(-0 eV)

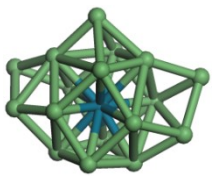

$PdGe_{17\text{-}23}$
(-0,016 eV)

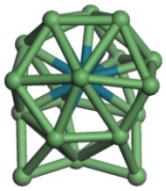

$PdGe_{17\text{-}8}$
(-0,019 eV)

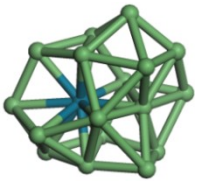

$PdGe_{17\text{-}9}$
(-0,033 eV)

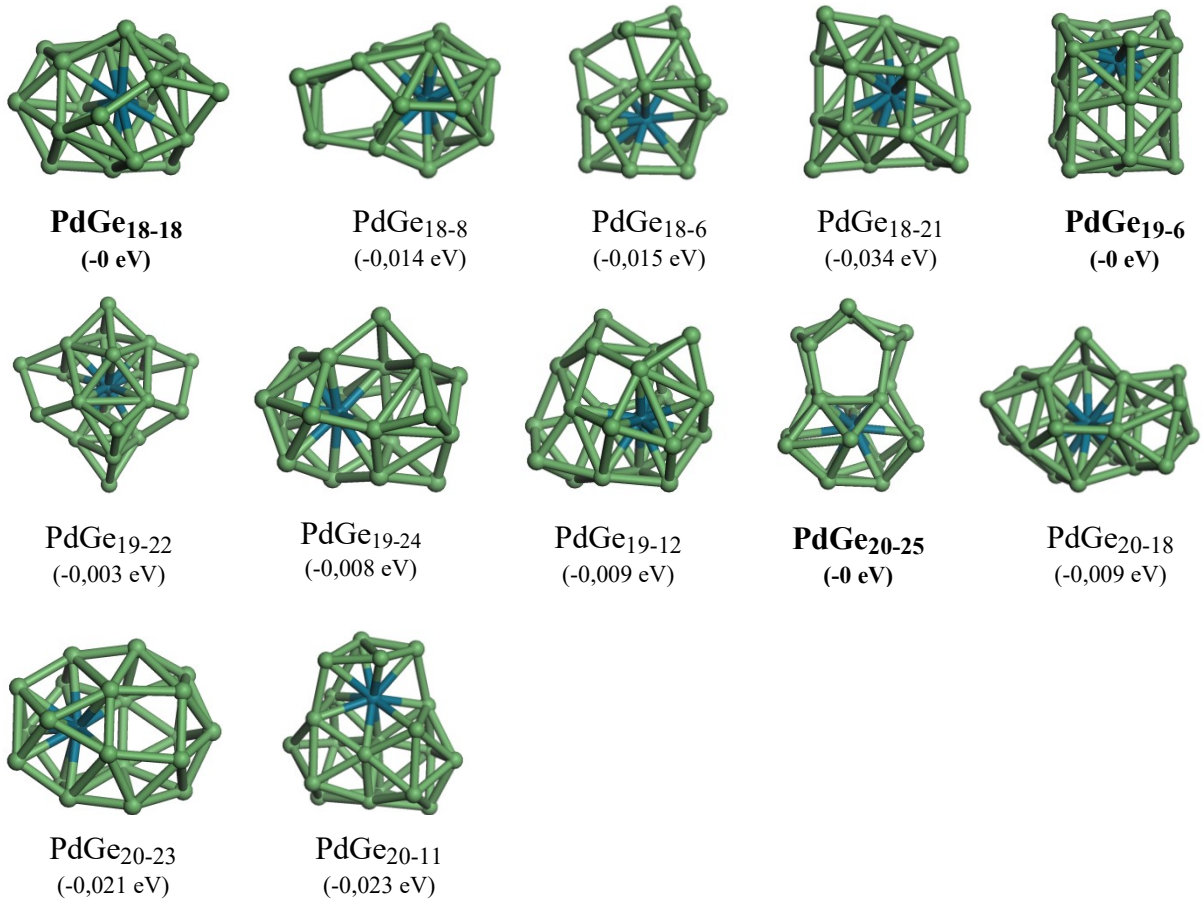

Fig (3.2): Low energy structures and their corresponding isomers for $PdGe_n$ (n=1-20) clusters.

3.3.1 Structural properties

The doped germanium clusters MGe_n (M=Pd,Pt) in our calculations show a growth pattern in which the planar structures only appears in the very small clusters, while the tridimensional structures dominate from n + 1 = 5. Up to n + 1 = 21, prolate type structures compete with nearly spherical structures, and almost all atoms are located in surface. Many of the obtained best structures are in agreement with the previous theoretical studies of the literature. Our lowest-energy isomers are shown in Figure 3.1 and 3.2 for each size, data for most stable isomers are reported in bold character. The symmetry group, binding energy E_b (eV/atom), HOMO–LUMO gap ΔE (eV), the vertical ionization potential VIP (eV), the vertical electron affinity VEA (eV), the chemical hardness η (eV) and the average Ge–Ge and M–Ge bond lengths are summarized in Table 1 and Table 2 for all $PdGe_n$ and $PtGe_n$ clusters, respectively, and as they appear the most stable structures of $PdGe_n$ clusters are generally similar to those of $PtGe_n$ clusters.

First of all, the dimers MGe (M=Pd and Pt) had a bond length of 2.349 and 2.364 Å, respectively. In the case of binding energy (per atom) was 1.292 and 1.201 eV for PdGe and PtGe, respectively. For the trimers $PdGe_2$ and $PtGe_2$ clusters, the bond length was 2.475 and 2.533 Å, respectively and 2.141 and 2.064 eV for the binding energy. The triangular structure with C_{2v} symmetry is found to be the lowest-energy structure. Low laying isomers of $PdGe_3$

and $PtGe_3$ have obtained and their structure had C_{3v} symmetry for both of them with 2.574 and 2.629Å bond length. The binding energy for this lowest-energy structure was 2.530 and 2.477eV respectively. A tri-dimensions structure was assigned to $PdGe_4$ and $PtGe_4$ with a symmetry group of C_{2v}, 2.698 and 2.757 Å was found for the bond length. The analyzing of binding energy per atom had given us 2.738 and 2.703 eV respectively.

The bipyramidal geometry with C_s symmetry is found to be the lowest-energy structure for $PdGe_5$ and $PtGe_5$ with 2.959 and 3.001 Å bond lengths respectively, 2.846 and 2.802 eV for the binding energy per atom. For the $PdGe_6$ and $PtGe_6$ a geometry of a bicapped pentagonal with C_{5v} symmetry were found for both of them with 2.824 and 2.740 Å bond length along of 2.924 and 2.902 eV for the binding energy per atom. In the case of $PdGe_7$ and $PtGe_7$ have had the capped pentagonal bipyramid structure-like with C_s symmetry shown to be the ground state structure. 2.535 and 2.719 Å was their bond length and for the binding energy per atom a 2.992 and 2.9596eV were presented, respectively. The lowest-energy structure of the $PdGe_8$ and $PtGe_8$ clusters was tricapped trigonal prism geometry without any symmetry (C_1). The bond length was respectively 2.596 and 2.656 Å and for their binding energy per atom its 2.987 and 2.9598eV. In the case of $PdGe_9$ and $PtGe_9$ clusters, the lowest-energy structure can be viewed as a pentagonal bipyramid face-capped with C_1 symmetry and bond length of 2.586 and 2.648 Å while the binding energy was 3.041 and 3.014 eV, respectively. The doped germanium clusters from n=10~20 atom show an encapsulated metal atom for the all low-lying isomers structure.

For the $PdGe_{10}$ and $PtGe_{10}$ clusters, we see that the most stable isomer was for $PdGe_{10}$ a partially encapsulated metal atom in an open cage with D_{4d} symmetry. Toward the $PtGe_{10}$ the low-lying structure-like was an open cage with C_1 symmetry where the metal atom localized on the periphery. The bond length was 2.608 and 2.605Å for the stable isomers where their binding energy per atom was 3.096 and 3.064eV. The $PdGe_{11}$ cluster presents a capped pentagonal bipyramid structure with a centered metal atom with C_{5v}symmetry, while the $PtGe_{11}$ cluster shows a bipyramid near hexagonal base geometry of C_s symmetry. The stable isomer bond length was 2.716 and 2.806Å which the binding energy was 3.126 and 3.086eV, respectively. The stable structure for both doped germanium clusters was a capped pentagonal bipyramid for n = 12 size, with a symmetry group of S_4, present a bond length of 2.834 and 2.856Å and a binding energy per atom of 3.184 and 3.169 eV, respectively. A compact near hexagonal geometry was preferred to $PdGe_{13}$ with a lack of symmetry (C_1) where the $PtGe_{13}$ cluster shows a prolate-type structure-like with C_s symmetry. The bond length for stable isomer and the binding energy respectively was 2.880 and 2.888Å as well 3.171 and 3.146 eV. The shape of $PdGe_{14}$ cluster shows a capped pentagonal bipyramid structure with C_s symmetry. However, $PtGe_{14}$ present a compact near capped spherical geometry when the symmetry was absent. The bond length for the stable isomers was 2.925 and 2.947Å when the binding energy for this lowest-energy structure was 3.172 and 3.176eV, respectively. Let's move on the next clusters, which are $PdGe_{15}$ and $PtGe_{15}$, they presents an augmented tridiminished icosahedrons like-structure with an encapsulated metal atom in C_s symmetry. Moving into the bond length for the stable isomer we noticed 2.801 and 2.892 Å, respectively, while the binding energy per atom was 3.196 and 3.189 eV.

For $PdGe_{16}$ and $PtGe_{16}$, a near cage prolate-type geometry was obtained with C_2 and C_1 symmetry, respectively. Concerning the bond length structure and the binding energy per atom we mentioned 2.877 and 2.906Å with 3.204 and 3.188 eV. An irregular cage-like

structure was found for $PdGe_{17}$ and $PtGe_{17}$, when the symmetry was absent (C_1). 2.933 and 2.956Å, respectively, was the bond length for stable isomer, while the respective binding energy was 3.162 and 3.151 eV. Thereafter, comes $PdGe_{18}$ and $PtGe_{18}$, they present a near prolate-like structure with also a lack of a symmetry (C_1). By the same way, the bond length structure was 2.891 and 2.919Å, although the 3.170 and 3.159 eV have been mentioned for the respective binding energy. In the case of $PdGe_{19}$ a near compact hexagonal structure was identified and for $PtGe_{19}$ a compact near cage-like structure was the one reached. The symmetry obtained for each clusters was C_{3v} and C_1, respectively. In the subject of bond length structure and binding energy per atom, 2.917 and 2.971Å with 3.142 and 3.134 eV have been pulled, respectively. Cage-like structures without any symmetry (C_1) was revealed for the last clusters isomers, $PdGe_{20}$ and $PtGe_{20}$. When the bond length for the stable isomers was 2.844 and 2.949 Å while the binding energy has been mentioned 3.155 and 3.143 eV.

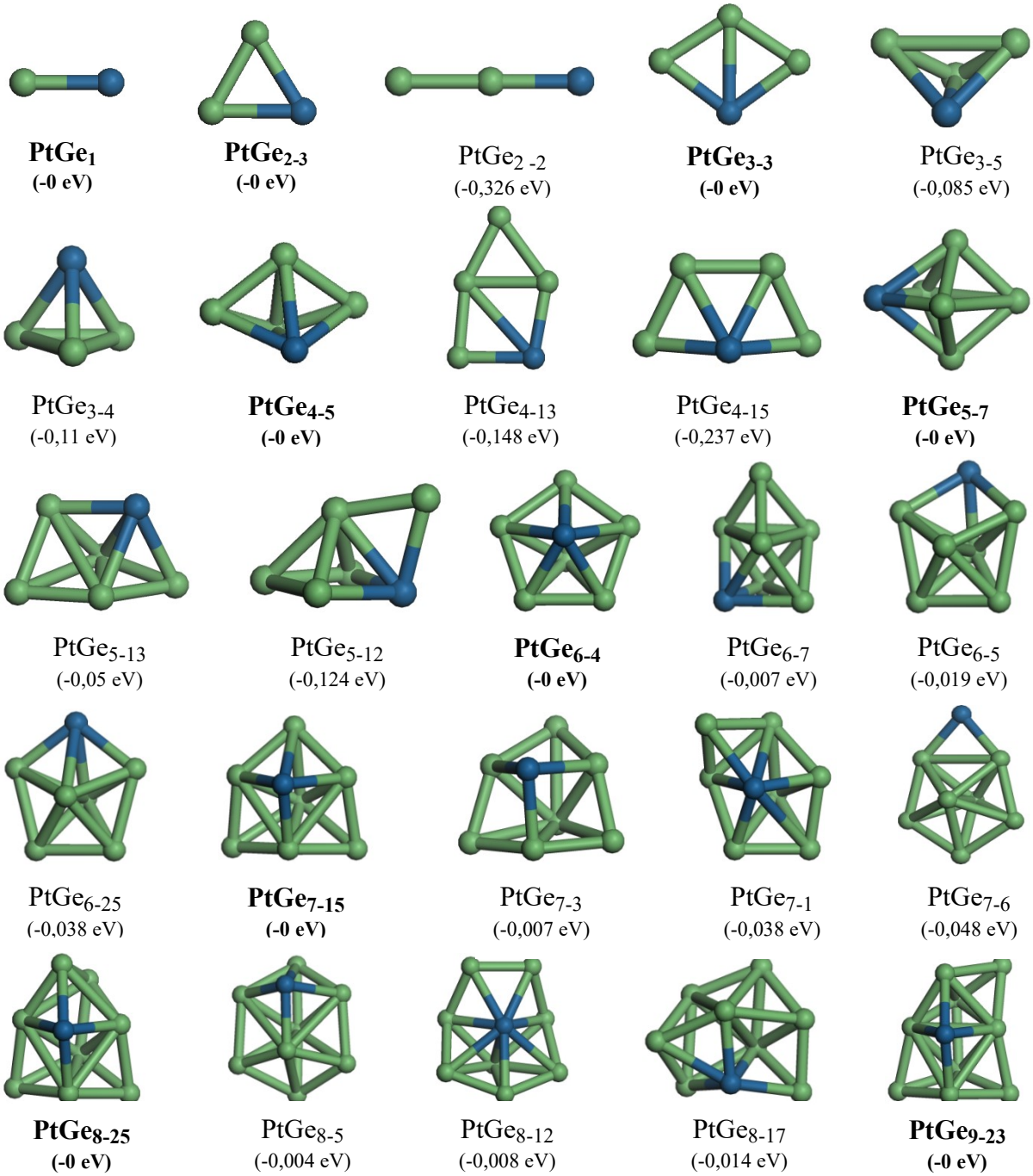

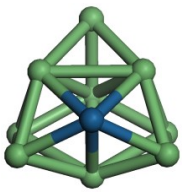

PtGe$_{9\text{-}1}$
(-0,02 eV)

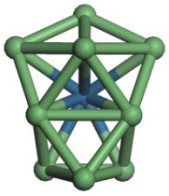

PtGe$_{9\text{-}12}$
(-0,028 eV)

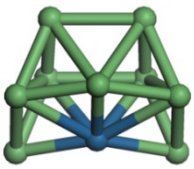

PtGe$_{9\text{-}9}$
(-0,03 eV)

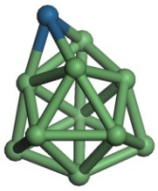

PtGe$_{10\text{-}13}$
(-0 eV)

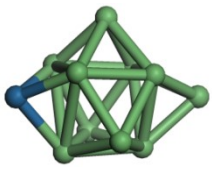

PtGe$_{10\text{-}16}$
(-0,019 eV)

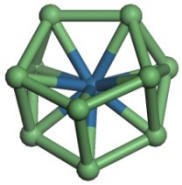

PtGe$_{10\text{-}3}$
(-0,023 eV)

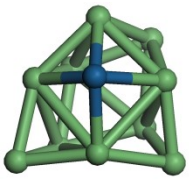

PtGe$_{10\text{-}7}$
(-0,024 eV)

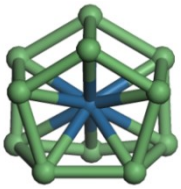

PtGe$_{11\text{-}13}$
(-0 eV)

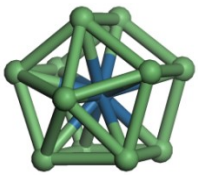

PtGe$_{11\text{-}22}$
(-0,001 eV)

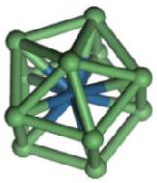

PtGe$_{11\text{-}1}$
(-0,001 eV)

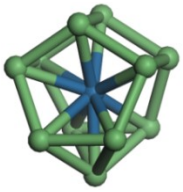

PtGe$_{11\text{-}9}$
(-0,014 eV)

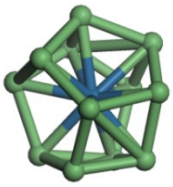

PtGe$_{12\text{-}22}$
(-0 eV)

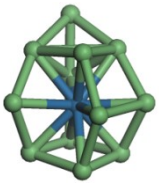

PtGe$_{12\text{-}24}$
(-0,055 eV)

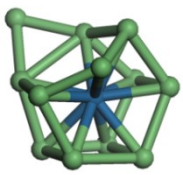

PtGe$_{12\text{-}13}$
(-0,067 eV)

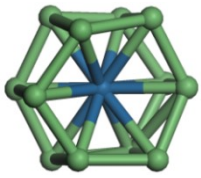

PtGe$_{12\text{-}1}$
(-0,073 eV)

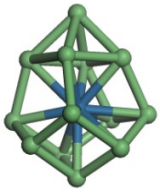

PtGe$_{13\text{-}7}$
(-0 eV)

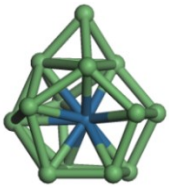

PtGe$_{13\text{-}5}$
(-0,008 eV)

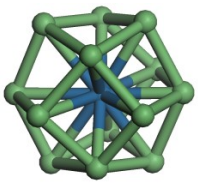

PtGe$_{13\text{-}4}$
(-0,016 eV)

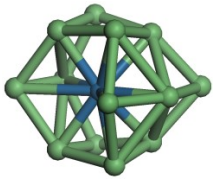

PtGe$_{13\text{-}1}$
(-0,02 eV)

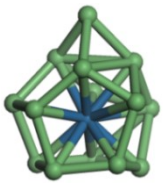

PtGe$_{14\text{-}20}$
(-0 eV)

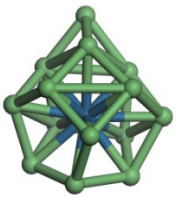

PtGe$_{14\text{-}19}$
(-0,012 eV)

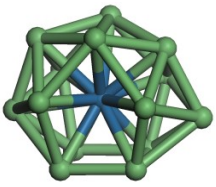

PtGe$_{14\text{-}14}$
(-0,02 eV)

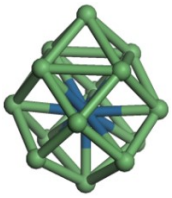

PtGe$_{14\text{-}11}$
(-0,032 eV)

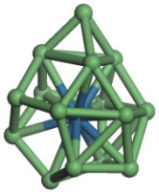

PtGe$_{15\text{-}18}$
(-0 eV)

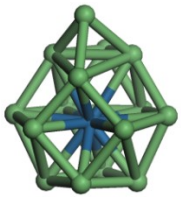

PtGe$_{15\text{-}6}$
(-0,022 eV)

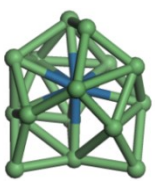

PtGe$_{15\text{-}21}$
(-0,036 eV)

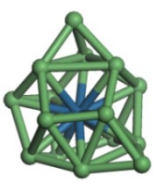

PtGe$_{15\text{-}1}$
(-0,041 eV)

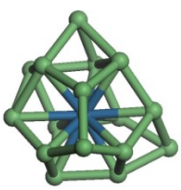

PtGe$_{16\text{-}1}$
(-0 eV)

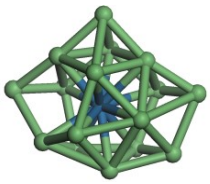

PtGe$_{17\text{-}19}$
(-0,042 eV)

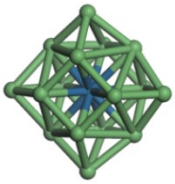

PtGe$_{16\text{-}8}$
(-0,051 eV)

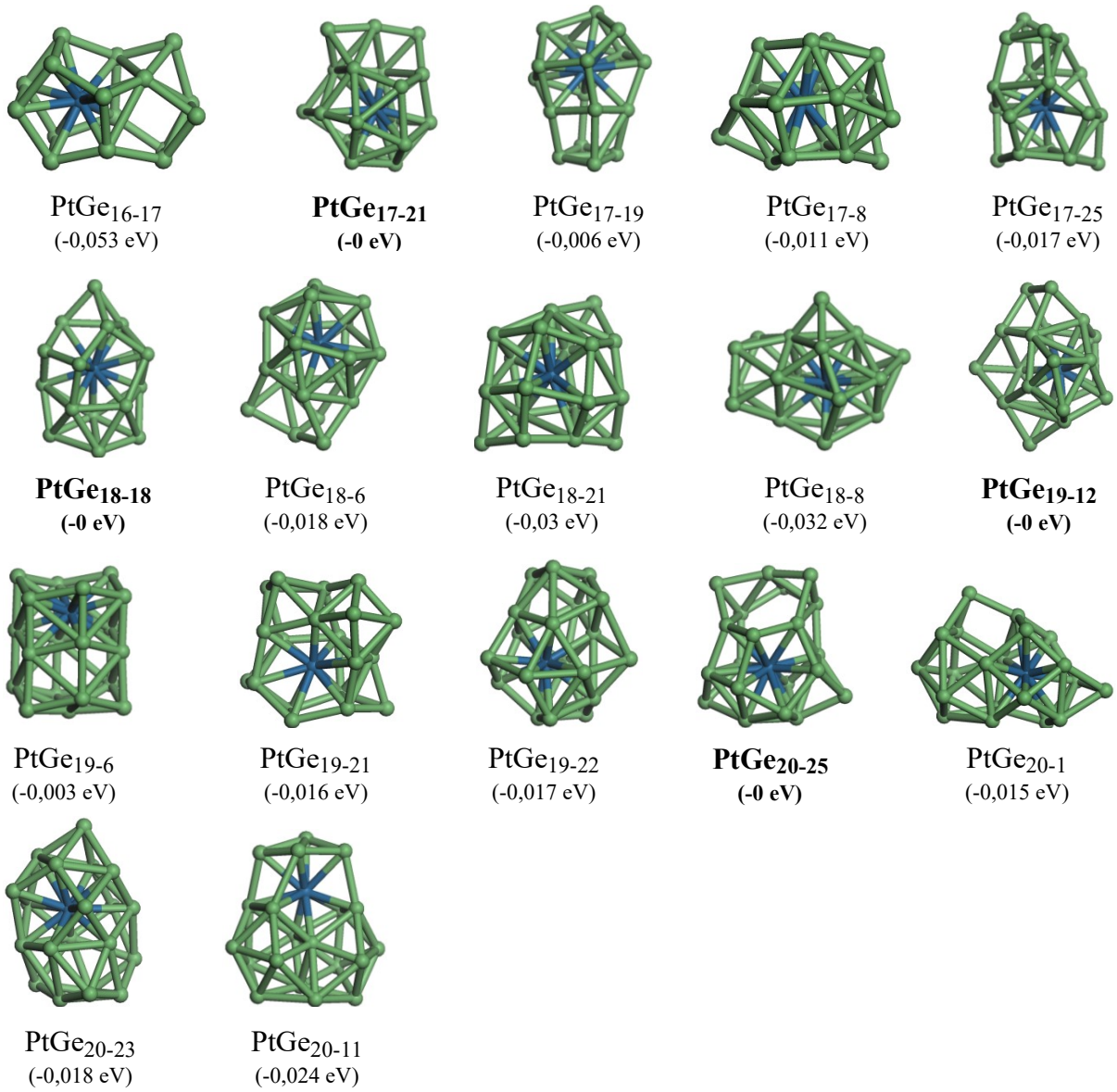

Fig (3.3): Low energy structures and their corresponding isomers for $PtGe_n$ (n=1-20) clusters

Table (III.1): Symmetry group, binding energy E_b(eV/atom), HOMO-LUMO gap ΔE (eV), vertical ionization potential VIP (eV), vertical electron affinity VEA (eV), chemical hardness η (eV) and average bond length $a_{Ge\text{-}Ge}$ (Å) and $a_{Pd\text{-}Ge}$(Å) for $PdGe_n$ clusters.

Size (n)	Sym.	Eb (eV/atom)	ΔE (eV)	VIP (eV)	VEA (eV)	η(eV)	$a_{Ge\text{-}Ge}$(Å)	$a_{Pd\text{-}Ge}$(Å)
PdGe1	**C_∞**	**1.292**	**0.597**	**6.599**	**0.693**	**5.906**	/	**2.349**
PdGe2-3	**C_{2v}**	**2.141**	**0.758**	**7.309**	**1.217**	**6.092**	**2.456**	**2.475**
PdGe2-2	C_∞	1.821	0.410	6.818	1.435	5.384	2.450	2.359
PdGe3-6	**C_{2v}**	**2.530**	**1.331**	**7.338**	**0.999**	**6.340**	**2.420**	**2.574**
PdGe3-4	C_{3v}	2.425	0.601	6.979	1.428	5.551	2.652	2.592
PdGe4-1	**C_{2v}**	**2.738**	**1.328**	**7.450**	**1.259**	**6.191**	**2.610**	**2.698**
PdGe4-14	C_s	2.626	1.009	7.236	1.404	5.832	2.613	2.458
PdGe4-11	C_s	2.553	0.627	6.950	1.452	5.498	2.574	2.663
PdGe5-1	**C_s**	**2.846**	**1.413**	**7.566**	**1.367**	**6.199**	**2.759**	**2.959**
PdGe5-17	C_1	2.791	1.086	7.155	1.466	5.689	2.696	2.667

PdGe5-12	C_s	2.721	0.856	7.054	1.675	5.378	2.631	2.594
PdGe6-4	**C_{5v}**	**2.924**	**1.007**	**7.458**	**2.027**	**5.431**	**2.737**	**2.824**
PdGe6-25	C_{2v}	2.904	1.291	7.215	1.431	5.784	2.774	2.710
PdGe6-6	C_1	2.895	1.224	7.104	1.527	5.578	2.756	2.696
PdGe6-21	C_s	2.848	0.647	6.888	1.944	4.944	2.675	2.597
PdGe7-3	**C_s**	**2.992**	**1.400**	**7.248**	**1.605**	**5.643**	**2.800**	**2.535**
PdGe7-7	C_{3v}	2.982	1.908	7.294	1.195	6.099	2.766	2.512
PdGe7-10	C_1	2.953	1.097	6.977	1.671	5.306	2.759	2.630
PdGe7-5	C_1	2.950	0.788	6.840617	1.893	4.947	2.746	2.695
PdGe8-8	**C_1**	**2.987**	**0.933**	**6.976**	**2.160**	**4.816**	**2.788**	**2.596**
PdGe8-1	C_s	2.984	1.194	6.807	1.758	5.049	2.773	2.630
PdGe8-9	C_s	2.980	1.092	7.148	2.230	4.918	2.679	2.757
PdGe8-7	C_1	2.954	1.026	6.936	2.036	4.810	2.836	2.633
PdGe9-23	**C_1**	**3.041**	**1.401**	**6.964**	**1.842**	**5.122**	**2.784**	**2.586**
PdGe9-15	C_1	3.032	1.610	7.098	1.734	5.364	2.718	2.651
PdGe9-1	C_s	3.024	0.846	6.863	2.256	4.607	2.793	2.628
PdGe9-25	C_s	3.021	0.942	6.970	2.251	4.719	2.824	2.689
PdGe9-10	C_s	3.011	0.964	6.946	2.196	4.750	2.798	2.612
PdGe10-9	**D_{4d}**	**3.096**	**1.282**	**7.504**	**2.463**	**5.041**	**2.823**	**2.608**
PdGe10-13	C_1	3.091	1.737	7.227	1.647	5.581	2.794	2.533
PdGe10-2	C_s	3.090	1.007	7.115	2.332	4.784	2.699	2.678
PdGe10-6	C_s	3.076	1.670	7.051	1.505	5.546	2.784	2.689
PdGe11-1	**C_{5v}**	**3.126**	**1.054**	**6.958**	**2.158**	**4.800**	**2.766**	**2.716**
PdGe11-9	C_{2v}	3.117	0.807	7.103	2.532	4.571	2.664	2.741
PdGe11-13	C_s	3.113	1.071	7.074	2.300	4.774	2.742	2.696
PdGe11-6	C_s	3.091	1.068	6.768	2.038	4.731	2.781	2.656
PdGe12-22	**S_4**	**3.184**	**1.004**	**7.065**	**2.431**	**4.634**	**2.630**	**2.834**
PdGe12-16	C_s	3.154	0.937	6.997	2.372	4.626	2.738	2.809
PdGe12-24	C_s	3.142	1.340	6.864	1.869	4.995	2.718	2.761
PdGe12-1	D_{3d}	3.128	0.968	6.280	2.489	3.791	2.609	2.889
PdGe13-2	**C_1**	**3.171**	**0.959**	**6.739**	**2.236**	**4.503**	**2.727**	**2.880**
PdGe13-7	C_s	3.156	0.934	6.562	2.081	4.481	2.682	2.867
PdGe13-1	C_s	3.151	1.158	6.685	2.005	4.681	2.742	2.787
PdGe13-4	C_s	3.128	0.952	6.550	2.063	4.488	2.736	2.776
PdGe14-19	**C_s**	**3.172**	**0.766**	**6.679**	**2.461**	**4.218**	**2.659**	**2.925**
PdGe14-14	C_s	3.169	0.810	6.667	2.377	4.290	2.785	2.917
PdGe14-11	C_{4v}	3.164	0.747	6.682	2.398	4.284	2.757	2.862
PdGe14-20	C_1	3.163	0.692	6.574	2.449	4.126	2.661	2.860
PdGe15-18	**Cs**	**3.196**	**1.142**	**6.638**	**2.092**	**4.546**	**2.739**	**2.801**
PdGe15-1	C1	3.187	1.211	6.666	2.076	4.589	2.722	2.955
PdGe15-6	Cs	3.184	1.038	6.797	2.345	4.451	2.733	2.879
PdGe15-21	Cs	3.172	0.996	6.596	2.248	4.349	2.767	2.878
PdGe16-3	**C2**	**3.204**	**1.674**	**6.779**	**1.845**	**4.934**	**2.772**	**2.877**
PdGe16-19	C1	3.177	0.892	6.466	2.280	4.185	2.784	2.906
PdGe16-12	C1	3.174	1.132	6.696	2.255	4.441	2.767	2.910
PdGe16-13	C1	3.163	0.944	6.612	2.391	4.220	2.729	2.870
PdGe17-21	**C1**	**3.162**	**1.141**	**6.590**	**2.248**	**4.343**	**2.787**	**2.933**
PdGe17-23	C1	3.146	0.962	6.554	2.383	4.171	2.789	2.876
PdGe17-8	C1	3.143	1.179	6.555	2.128	4.427	2.787	2.936
PdGe17-9	C1	3.129	0.992	6.647	2.430	4.217	2.740	2.845
PdGe18-18	**C1**	**3.170**	**1.206**	**6.618**	**2.262**	**4.356**	**2.765**	**2.891**
PdGe18-8	C1	3.156	1.074	6.656	2.427	4.229	2.776	2.926
PdGe18-6	C1	3.155	0.730	6.576	2.708	3.869	2.660	2.844

PdGe18-21	C1	3.136	1.054	6.429	2.227	4.202	2.742	2.964
PdGe19-6	**C3v**	**3.142**	**1.008**	**6.415**	**2.305**	**4.110**	**2.703**	**2.917**
PdGe19-22	Cs	3.139	0.952	6.408	2.377	4.030	2.750	2.892
PdGe19-24	C1	3.134	0.887	6.484	2.511	3.973	2.770	2.875
PdGe19-12	C1	3.133	0.511	6.352	2.761	3.590	2.769	2.884
PdGe20-25	**C1**	**3.155**	**1.068**	**6.625**	**2.548**	**4.076**	**2.723**	**2.844**
PdGe20-18	C1	3.146	0.976	6.387	2.350	4.037	2.822	2.894
PdGe20-23	Cs	3.134	0.954	6.643	2.631	4.012	2.793	2.911
PdGe20-11	C1	3.132	0.859	6.302	2.420	3.883	2.817	2.787

3.3.2 Electronic properties

3.3.2.1 Binding energy

By using formula (3.1) we calculated the binding energy per atom. In the Figure 3.3, we plotted the evolution of binding energy with cluster size. The binding energy gradually increases with increasing size of clusters, when the curve of doped one is higher than the non-doped at n > 6. This means that doping with Pd and Pt atoms has no immediate effects on enhancing the stability of germanium cluster at small size. An increase in binding energy is observed for the very small size (n < 6), then the binding energy increases more smoothly. We also observe that the binding energies of $PdGe_n$ and $PtGe_n$ clusters from n > 6 are with 3D structure-like and had exactly the same behavior toward the size dependence for both of them. Remarkable peaks were identified on n = 12 and 16 for both of doped clusters, which mean that they are more stable than the neighboring clusters. The great stability is enhanced for the endohedral structures in which Pd and Pt is encapsulated in a quasi-perfect Gen cage. This behavior is due to the absorption of the dangling bonds of the germanium cage by the doping palladium and platinum atoms located in a central position.

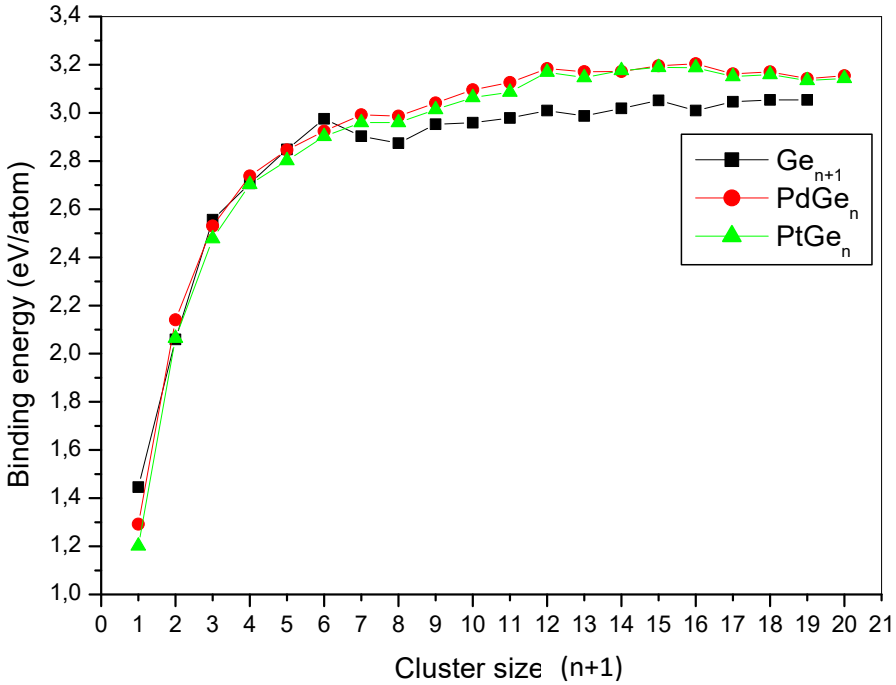

Fig (3.4): Binding energy per atom (Eb) for the ground-sate isomers of Gen [73] and MGen (M=Pd,Pt and n=1-20) clusters

3.3.2.2 Second-order difference

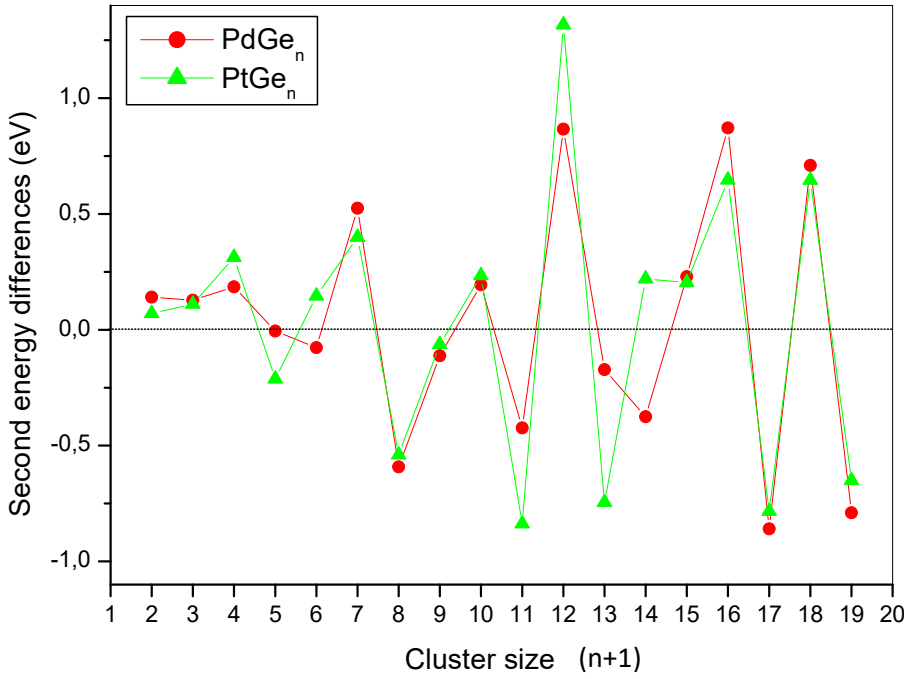

Fig (3.5): Second energy differences (Δ_2E) for the ground-sate isomers of MGe_n (M=Pd,Pt and n=1-20) clusters.

In cluster physics, the second-order difference in energy (Δ_2E) defined by the relation (3.3), can well reflect the relative stabilities of the corresponding clusters.It is generally compared with the relative abundances determined in mass spectroscopy experiments and the lowest-energy isomer second-order of different species studied here are calculated shown in Figure 3.4. We reported that if the values of Δ_2E are positive this means that the dissociation of Pd and Pt atoms is an unfavorable process and the clusters are particularly stable. The pronounced positive values of Δ_2E are observed for Pd-$PtGe_{2,3,4,}$ and Pd-$PtGe_{7,10,12,15,16,18}$, indicating that these clusters may have special stabilities. This suggests these clusters to be more favorable than their neighbors.

3.3.2.3 HOMO–LUMO gaps

In the intention of having more information about the small clusters kinetic stability we investigate the energy difference between highest occupied molecular orbital (HOMO) and the lowest unoccupied molecular orbital (LUMO), which can also characterize the chemical activity of clusters. According to the literature, large HOMO−LUMO gap implies a low chemical activity and a high chemical stability, while the latter decreases as the HOMO−LUMO gap decreases. The corresponding Pd and Pt doped germanium HOMO−LUMO gap was presented in Figure 3.5, using formula (3.2). In contrast to the roughly decreasing tendency of the evolution of HOMO-LUMO gaps for pure Ge_n clusters, an oscillating behavior is observed for Pd- and Pt-Ge_n clusters. As expected, the gap of very

small metal-doped Ge_n is lower than that of the pure germanium clusters, but for n ≥ 10 the presence of the metal generally increases the HOMO-LUMO gap.

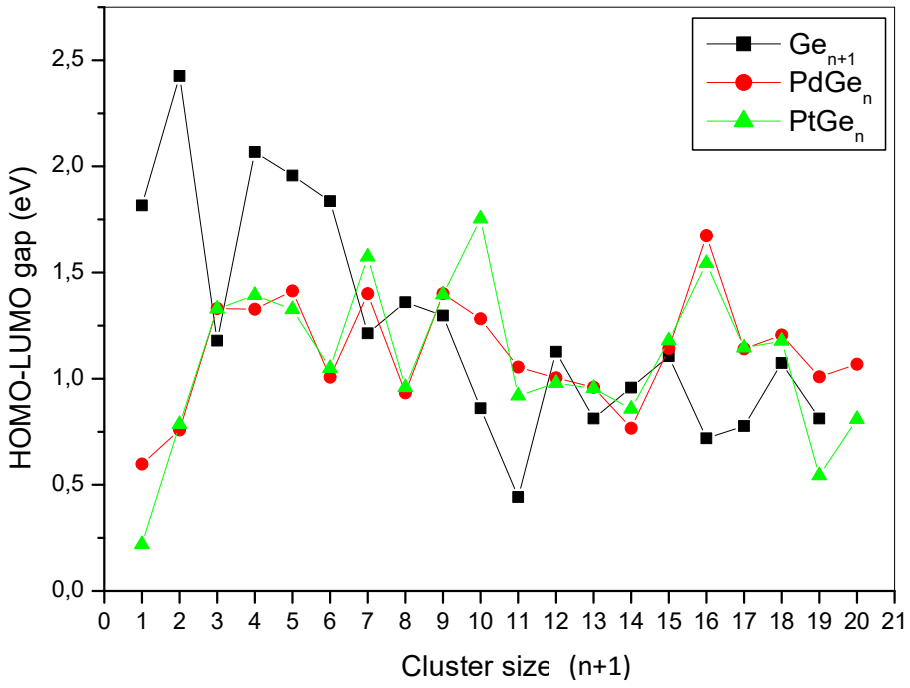

Fig (3.6): HOMO-LUMO gaps (ΔE) for the ground-sate isomers of [73] and MGe_n (M=Pd,Pt and n=1-20) clusters.

This somewhat surprising behavior is due to the encapsulation of the metal into the Ge structure which stabilizes the electronic structure by absorbing the dangling bonds. Values oscillate in the 0.5−2.0 eV range, but the evolution with cluster size shows a non-monotonic behavior. Very noticeable or marked values are introduced, especially for $PdGe_{7,9,16,18}$ and $PtGe_{7,10,16,18}$. Indicate that these clusters may have a relative low reactivity comparing to others. The apparition of the near-metallic behavior was defined for small clusters whereas in the growth process, this characteristic was vanishing except for $PtGe_{19}$.

3.3.2.4 Vertical ionization potential and vertical electron affinity

In the attention of having good perception about small clusters we plotted the size dependence on vertical ionization potential (VIP) and vertical electron affinity (VEA) in Figure 3.6 and 3.7. They are two important parameters that can determine the chemical stability and the behavior of the small clusters. They are defined as following:

$$VIP = E\,(MGe_n)^+ - E\,(MGe_n) \qquad (3.4)$$

$$VEA = E\,(MGe_n) - E\,(MGe_n)^- \qquad (3.5)$$

The VIP is defined by the energy difference between the cationic $E(MGe_n)^+$ and neutral clusters calculated at the equilibrium geometry of the neutral MGe_n cluster, while that the

VEA is the energy difference between the neutral E(MGe_n) and the anionic clusters calculated at the geometry of the neutral cluster. The VIP can give information about the capacity of a cluster to lose a valence electron. We notice an oscillating behavior governing in both curves. Values are in the 6.2-7.6 eV range. For n < 6 the VIP increases with clusters size than for n ≥6 the decreasing process was the apparent except for some pronounced one, for example n = 10, 12, 16 and for both Pd and Pt doped germanium clusters.

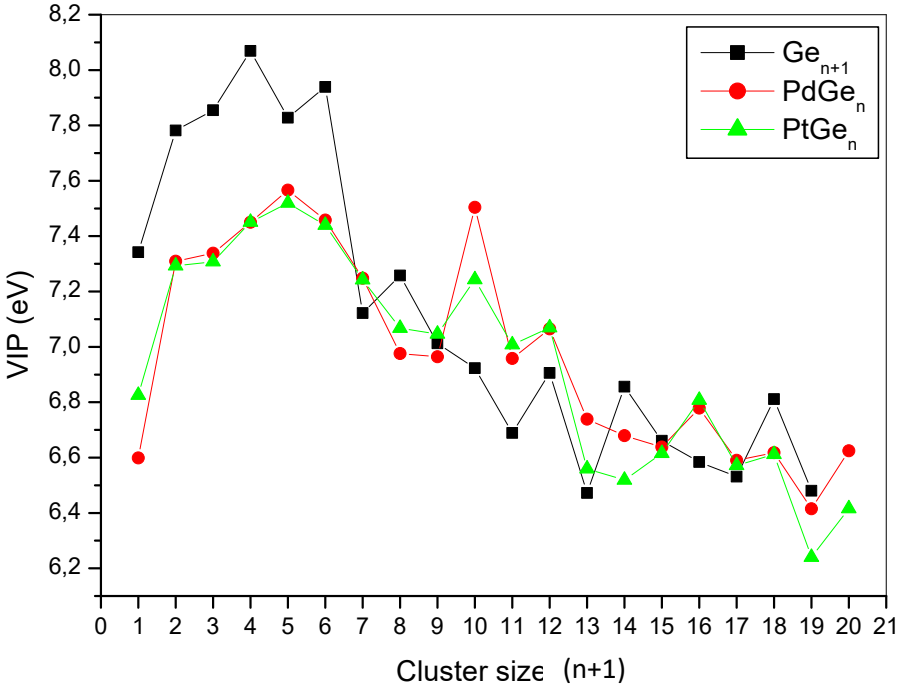

Fig (3.7): Vertical ionization potential (VIP) for the ground-sate isomers of [73] and MGe_n (M=Pd,Pt and n=1-20) clusters

On behalf the VIP becomes smaller; the cluster will be more close to a half-metallic behavior which means these clusters can more easily lose one electron comparatively to other clusters. While for the big values of VIP and for sharp peaks, the loss of one electron is more difficult and then the half-metallic character is less important.

In the case of VEA, which give us information about the capacity of a cluster to get a new valence electron. We distinguish an increasing tendency curve with a dependence on clusters size. This indicates that the clusters with large size will capture an electron more easily. The values of all species increase from 0.6 to 2.6 eV. As we can deduce for n = 7, 9, 13, 15, 16. The VEA had a local minimum for both Pd and Pt doped germanium, further $PtGe_{10, 16}$ and $PdGe_{11, 16}$. This means that they are less able to acquire an electron. As well, we can perceive the behavior of pure germanium for both VIP and VEA figure that show an overall and overlapping curve which states that these doping clusters had a weak feedback towards doped metal atoms.

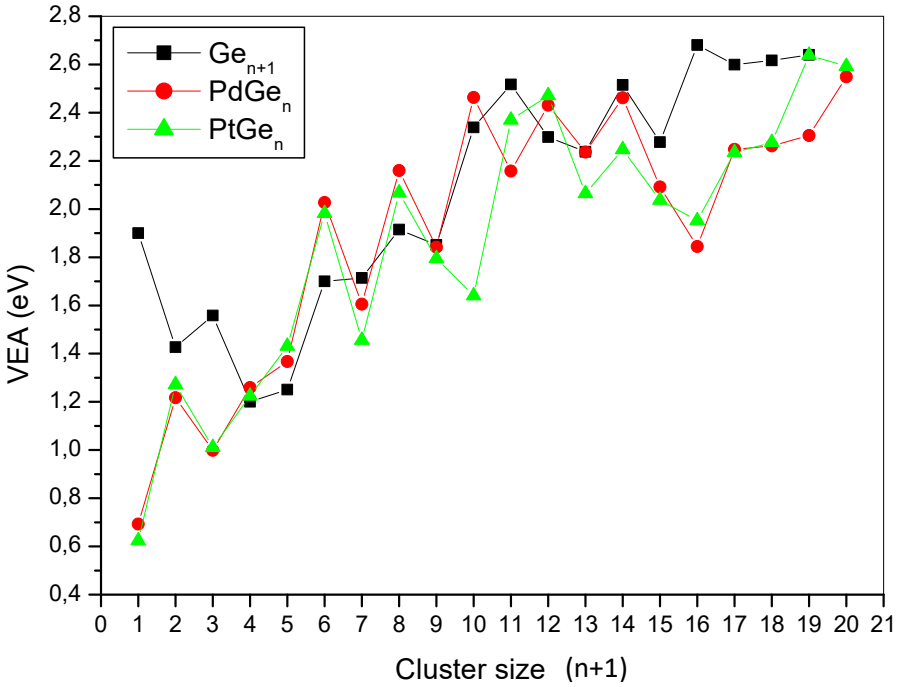

Fig (3.8): Vertical electron affinities (VEA) for the ground-sate isomers of [73] and MGe_n (M=Pd,Pt and n=1-20) clusters.

3.3.2.5 Chemical hardness

Another parameter that can be used to give more information about the relative stability of molecules and small clusters is the chemical hardness defined through the principle of maximum hardness (PMH) of Pearson [117-118] as:

$$\eta = VIP - VEA \qquad (3.6)$$

where VIP and VEA are the vertical ionization potential and electron affinity of the corresponding cluster. It considered as a good parameter to unveil the reactiveness of small clusters where the highest value is viewed to be less reactive cluster. The relationships of η and the size n are shown in Figure 3.9 for both species. The value of η presents a roughly decreasing evolution with increasing size for both $PdGe_n$ and $PtGe_n$ clusters A relative high value is observed for $PdGe_{5,7,16,18}$ and $PtGe_{7,10,16,18}$suggesting that these clusters should be less reactive than their neighbors. Beyond the pure germanium clusters an overlapping behavior was noted.

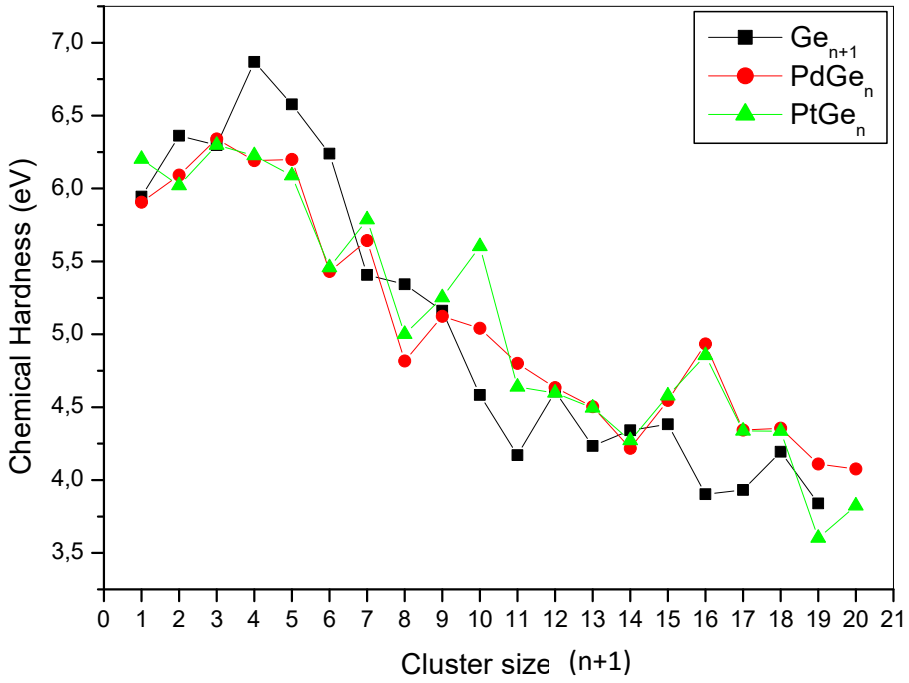

Fig (3.9): Chemical hardness (η) for the ground-sate isomers of [73] and MGe_n (M=Pd,Pt and n=1-20) clusters.

Table (III.2): Symmetry group, binding energy E_b(eV/atom), HOMO-LUMO gap ΔE (eV), vertical ionization potential VIP (eV), vertical electron affinity VEA (eV), chemical hardness η (eV) and average bond length $a_{Ge\text{-}Ge}$ (Å) and $a_{Pt\text{-}Ge}$(Å) for $PtGe_n$ clusters.

Size (n)	Sym.	Eb (eV/atom)	ΔE (eV)	VIP (eV)	VEA (eV)	η (eV)	$a_{Ge\text{-}Ge}$(Å)	$a_{Pt\text{-}Ge}$(Å)
PtGe1	**C_∞**	**1.201**	**0.219**	**6.826**	**0.624**	**6.202**	/	**2.364**
PtGe2-3	**C_{2v}**	**2.064**	**0.785**	**7.293**	**1.272**	**6.021**	**2.468**	**2.533**
PtGe2-2	C_∞	1.738	0.392	6.875	1.537	5.338	2.460	2.411
PtGe3-3	**C_{2v}**	**2.477**	**1.329**	**7.308**	**1.011**	**6.297**	**2.427**	**2.629**
PtGe3-5	C_s	2.392	1.068	7.336	1.159	6.177	2.461	2.675
PtGe3-4	C_{3v}	2.367	0.603	6.982	1.465	5.517	2.657	2.657
PtGe4-5	**C_{2v}**	**2.703**	**1.393**	**7.451**	**1.224**	**6.227**	**2.615**	**2.757**
PtGe4-13	C_s	2.555	0.944	7.235	1.548	5.689	2.561	2.498
PtGe4-15	C_s	2.466	0.389	6.869	1.756	5.113	2.444	2.644
PtGe5-7	**C_s**	**2.802**	**1.326**	**7.519**	**1.431**	**6.088**	**2.833**	**3.001**
PtGe5-13	C_1	2.752	1.104	7.141	1.459	5.682	2.705	2.728
PtGe5-12	C_s	2.678	0.852	7.025	1.670	5.355	2.634	2.658
PtGe6-4	**C_{5v}**	**2.902**	**1.049**	**7.440**	**1.982**	**5.458**	**2.741**	**2.740**
PtGe6-7	C_s	2.895	1.284	7.314	1.658	5.656	2.723	2.683
PtGe6-5	C_s	2.883	1.669	7.301	1.296	6.005	2.777	2.599
PtGe6-25	C_{2v}	2.864	1.335	7.204	1.418	5.786	2.769	2.778
PtGe7-15	**C_s**	**2.9596**	**1.574**	**7.242**	**1.456**	**5.787**	**2.772**	**2.719**
PtGe7-3	C_{3v}	2.953	2.025	7.432	1.263	6.169	2.755	2.588
PtGe7-1	C_1	2.922	0.781	6.794	1.871	4.923	2.747	2.754
PtGe7-6	C_{2v}	2.912	1.425	7.344	1.688	5.656	2.762	2.515

PtGe8-25	**C_1**	**2.9598**	**0.958**	**7.067**	**2.067**	**5.000**	**2.795**	**2.656**
PtGe8-5	C_s	2.956	1.188	6.888	1.705	5.183	2.781	2.690
PtGe8-12	C_s	2.952	1.076	7.173	2.133	5.040	2.685	2.813
PtGe8-17	C_1	2.946	1.000	6.933	1.949	4.983	2.756	2.716
PtGe9-23	**C_1**	**3.014**	**1.395**	**7.046**	**1.795**	**5.252**	**2.769**	**2.648**
PtGe9-1	C_s	2.994	0.832	6.894	2.171	4.723	2.781	2.685
PtGe9-12	C_s	2.986	0.986	6.975	2.121	4.854	2.772	2.798
PtGe9-9	C_s	2.984	1.183	6.987	1.952	5.035	2.751	2.823
PtGe10-13	**C_1**	**3.064**	**1.753**	**7.243**	**1.640**	**5.603**	**2.795**	**2.605**
PtGe10-16	C_{3v}	3.045	1.322	7.067	1.975	5.092	2.765	2.576
PtGe10-3	C_s	3.041	0.599	6.887	2.523	4.364	2.726	2.782
PtGe10-7	C_1	3.040	1.543	7.147	1.853	5.294	2.800	2.611
PtGe11-13	**C_s**	**3.086**	**0.919**	**7.008**	**2.370**	**4.638**	**2.672**	**2.806**
PtGe11-22	C_{5v}	3.085	1.07001	6.988	2.190	4.799	2.785	2.750
PtGe11-1	C_{5v}	3.085	1.07121	6.989	2.190	4.799	2.797	2.750
PtGe11-9	C_{2v}	3.072	0.728	7.009	2.563	4.446	2.694	2.784
PtGe12-22	**S_4**	**3.169**	**0.9789**	**7.069**	**2.471**	**4.598**	**2.653**	**2.856**
PtGe12-24	C_1	3.114	1.354	6.895	1.953	4.943	2.864	2.795
PtGe12-13	C_s	3.102	0.913	6.810	2.338	4.472	2.657	2.795
PtGe12-1	C_s	3.096	0.158	6.160	2.574	3.587	2.612	2.902
PtGe13-7	**C_s**	**3.146**	**0.954**	**6.560**	**2.064**	**4.495**	**2.696**	**2.888**
PtGe13-5	C_1	3.138	0.609	6.610	2.477	4.133	2.770	2.855
PtGe13-4	C_{3v}	3.130	1.178	6.746	2.020	4.726	2.678	2.900
PtGe13-1	C_s	3.126	1.093	6.636	2.036	4.600	2.860	2.823
PtGe14-20	**C_1**	**3.176**	**0.857**	**6.519**	**2.247**	**4.272**	**2.664**	**2.947**
PtGe14-19	C_s	3.164	0.693	6.651	2.518	4.133	2.645	2.945
PtGe14-14	C_s	3.156	0.840	6.651	2.340	4.312	2.799	2.935
PtGe14-11	C_{4v}	3.144	0.728	6.648	2.396	4.252	2.775	2.883
PtGe15-18	**C_s**	**3.189**	**1.179**	**6.615**	**2.037**	**4.578**	**2.751**	**2.892**
PtGe15-6	C_s	3.167	1.073	6.788	2.299	4.489	2.745	2.900
PtGe15-21	C_1	3.153	0.997	6.508	2.182	4.326	2.766	2.937
PtGe15-1	C_1	3.148	0.756	6.691	2.580	4.111	2.704	2.934
PtGe16-1	**C_1**	**3.188**	**1.544**	**6.808**	**1.952**	**4.856**	**2.742**	**2.906**
PtGe16-19	C_1	3.146	1.065	6.673	2.281	4.391	2.793	2.909
PtGe16-8	C_{4v}	3.137	1.325	6.713	2.096	4.617	2.722	2.913
PtGe16-17	C_1	3.135	0.696	6.687	2.724	3.963	2.659	2.825
PtGe17-21	**C_1**	**3.151**	**1.145**	**6.571**	**2.235**	**4.337**	**2.800**	**2.956**
PtGe17-19	C_1	3.145	1.006	6.537	2.327	4.211	2.698	2.928
PtGe17-8	C_1	3.140	0.965	6.440	2.249	4.191	2.757	2.971
PtGe17-25	C_1	3.134	0.896	6.670	2.601	4.069	2.676	2.912
PtGe18-18	**C_1**	**3.159**	**1.178**	**6.612**	**2.276**	**4.336**	**2.764**	**2.919**
PtGe18-6	C_s	3.141	1.140	6.640	2.335	4.305	2.761	2.939
PtGe18-21	C_1	3.129	1.032	6.427	2.251	4.175	2.726	2.992
PtGe18-8	C_1	3.127	1.072	6.415	2.212	4.204	2.819	2.903
PtGe19-12	**C_1**	**3.134**	**0.543**	**6.240**	**2.638**	**3.602**	**2.816**	**2.917**
PtGe19-6	C_{3v}	3.131	0.953	6.407	2.357	4.050	2.710	2.935
PtGe19-21	C_1	3.118	0.675	6.334	2.610	3.725	2.744	2.909
PtGe19-22	C_1	3.117	0.845	6.353	2.436	3.917	2.778	2.911
PtGe20-25	**C_1**	**3.143**	**0.809**	**6.415**	**2.592**	**3.824**	**2.704**	**2.949**
PtGe20-1	C_1	3.128	0.884	6.491	2.574	3.917	2.758	2.932
PtGe20-23	C_1	3.125	1.042	6.580	2.482	4.098	2.780	2.940
PtGe20-11	C_1	3.119	0.926	6.391	2.447	3.943	2.830	2.837

3.3.2.6 Density of states and the Kohn-Sham orbitals

Using the shame described earlier implemented in the Gaussian software, density of states (DOS) of $PdGe_{16}$ was figure out as well as the Kohn-Sham orbitals. We can distinguish the character of the orbitals which the organization in shell structure as well as the pooling of electrons contributes to the high stability of the cluster. The electronic structure shows a shell filling with the following sequence: $1S^2$ $1P^6$ $1D^{10}$ $1F^{14}$ $2D^{10}$ $2S^2$ $2P^6$ $1G^{18}$ $1H^6$. Same properties were found for $PtGe_{16}$ as well.

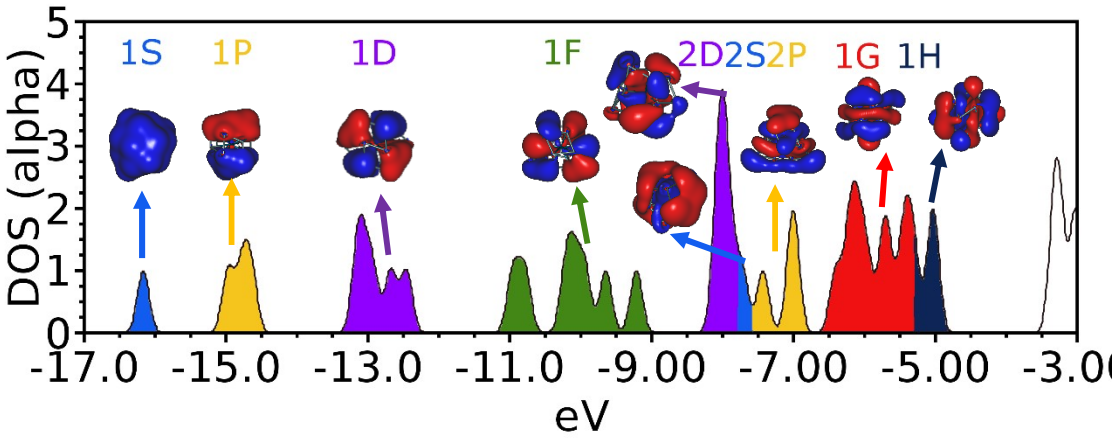

Fig (3.10): Density of states (DOS) of $PdGe_{16}$ for alpha spin electrons. For each band, the Kohn-Sham orbitals are plotted. The electronic structure shows a shell filling with the following sequence: $1S^2$ $1P^6$ $1D^{10}$ $1F^{14}$ $2D^{10}$ $2S^2$ $2P^6$ $1G^{18}$ $1H^6$.

3.3.2.7 Absorption spectra of $PdGe_{10}$ and $PdGe_{16}$ clusters

Moreover, the UV-Visible absorption spectra of both cage-like and surface-bond structure is presented in figure 3.11, for $PdGe_n$ n=10 and 16. Spectra are calculated with both PBE and ωB97x density-functional. The calculated absorption spectra shown in the Figure (3.11), give the oscillator strength as a function of the excitation energy together with a curve obtained by a Lorentz broadening with a full width at half-maximum (fwhm) of 0.08 eV. The main purpose was to discriminate the endohedral from exohedral structure, but we found that the absorption was few dependent on the position of the metal atom.

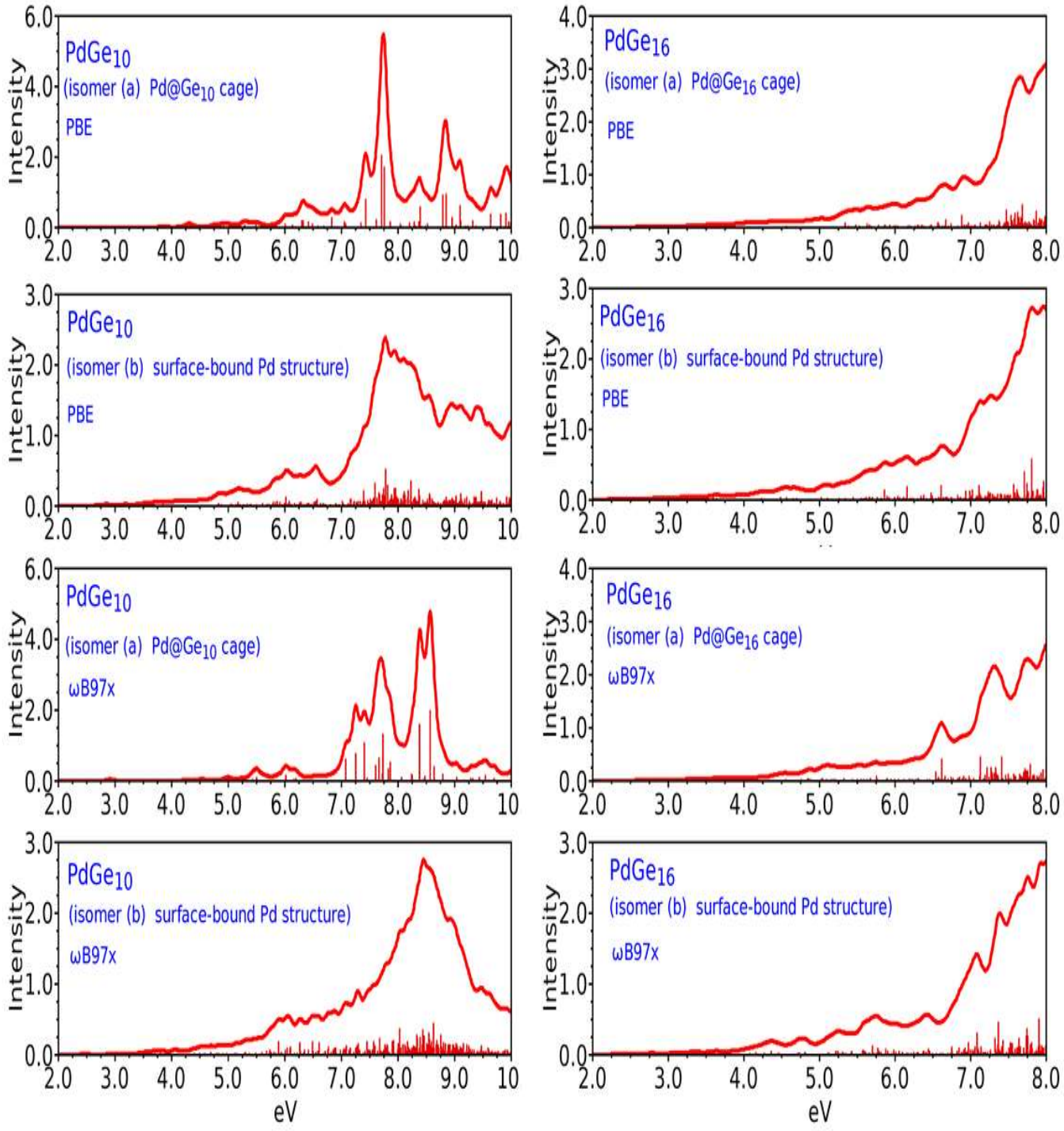

Fig (3.11): Absorption spectra of $PdGe_{10}$ and $PdGe_{16}$ clusters calculated for the two low-lying isomers: isomer (a) the lowest-energy isomer is a cage-like structure, and isomer (b) the lowest-energy isomer with a surface-bound Pd structure. Spectra are calculated with both PBE and ωB97x density-functional. The calculated absorption spectra shown in the Figure give the oscillator strength as a function of the excitation energy together with a curve obtained by a Lorentz broadening with a full width at half-maximum (fwhm) of 0.08 eV.

3.3.2.8 Atomic charge and electron configuration of Pd and Pt atoms

Using natural population analysis we made the electronic configuration and the atomic charge of Pd and Pt metal atoms (see table III.3). As the metal atoms goes from exohedral to endohedral position the relative atomic charge is clearly affected. It goes from about -0.5 to -2.5 au. The main reason which makes the atomic charge increases was the behavior of the metal atom which get more bonding to Ge atoms, which every captured electron was mainly associated to 5p or 6p electron configuration for Pd and Pt respectively.

Table (III.3): Atomic charge (in a.u., |e|) and electron configuration on the metal atom from the natural population analysis.

Cluster	$q_{Pd/Pt}$	Electron configuration on Pd/Pt atom
PdGe	-0.44	$5s^{1.02}\ 4d^{9.40}\ 5p^{0.02}$
$PdGe_{10}$ a (endohedral structure)	-2.76	$5s^{0.39}\ 4d^{9.63}\ 5p^{2.72}$
$PdGe_{10}$ b (exohedral structure)	-0.09	$5s^{0.34}\ 4d^{9.57}\ 5p^{0.20}$
$PdGe_{11}$ a	-2.31	$5s^{0.37}\ 4d^{9.56}\ 5p^{2.21}$
$PdGe_{12}$ a	-1.83	$5s^{0.36}\ 4d^{9.48}\ 5p^{1.98}$
$PdGe_{13}$ a	-1.75	$5s^{0.37}\ 4d^{9.51}\ 5p^{1.86}$
$PdGe_{14}$ a	-1.65	$5s^{0.37}\ 4d^{9.49}\ 5p^{1.78}$
$PdGe_{15}$ a	-1.49	$5s^{0.37}\ 4d^{9.49}\ 5p^{1.61}$
$PdGe_{16}$ a(endohedral structure)	-1.68	$5s^{0.37}\ 4d^{9.56}\ 5p^{1.74}$
$PdGe_{16}$ b (exohedral structure)	-0.48	$5s^{0.34}\ 4d^{9.56}\ 5p^{0.61}$
$PdGe_{17}$ a	-1.62	$5s^{0.37}\ 4d^{9.55}\ 5p^{1.68}$
$PdGe_{18}$ a	-1.57	$5s^{0.38}\ 4d^{9.57}\ 5p^{1.61}$
PtGe	-0.62	$6s^{1.34}\ 5d^{9.25}\ 6p^{0.03}$
$PtGe_{10}$ a	-0.35	$6s^{0.66}\ 5d^{9.42}\ 6p^{0.28}$
$PtGe_{11}$ a	-2.05	$6s^{0.63}\ 5d^{9.50}\ 6p^{2.04}$
$PtGe_{12}$ a	-2.05	$6s^{0.63}\ 5d^{9.47}\ 6p^{1.95}$
$PtGe_{13}$ a	-1.90	$6s^{0.65}\ 5d^{9.47}\ 6p^{1.78}$
$PtGe_{14}$ a	-1.74	$6s^{0.64}\ 5d^{9.47}\ 6p^{1.63}$
$PtGe_{15}$ a	-1.57	$6s^{0.63}\ 5d^{9.49}\ 6p^{1.44}$
$PtGe_{16}$ a	-1.75	$6s^{0.65}\ 5d^{9.56}\ 6p^{1.55}$
$PtGe_{17}$ a	-1.68	$6s^{0.61}\ 5d^{9.56}\ 6p^{1.51}$
$PtGe_{18}$ a	-1.69	$6s^{0.64}\ 5d^{9.57}\ 6p^{1.47}$

3.4 Discussion

Our results highlight a transition from exohedral to endohedral structures of $PdGe_n$ and PtGen occurring at n = 10 and 11 respectively. This structural modification strongly affects the electronic properties. The atomic charges on metal atoms have been estimated through a natural population analysis (NPA) [119]. When Pd is located on a surface site, its atomic charge is relatively low (between −0.5 and −0.1 a.u.), but when the M atom move to an endohedral position to be encapsulated inside the germanium, its charge strongly increases to about −1.6 a.u. or more (Table III.3). Similarly, the atomic charge on Pt in $PtGe_n$ goes from about −0.4 to about −1.7 a.u. for the exohedral and endohedral structures respectively. The additional electrons captured by the metal atom in cage-like structure are mainly associated to 5p or 6p electron configurations. The large atomic charge indicates that the metal interacts with several Ge atoms, thus playing a stabilizing role of the Ge_n cage.

The transition from exohedral to endohedral structure has been already observed at n = 12 in the case of $AgGe_n$ and $AuGe_n$ [72], at n = 10 for $CuGe_n$ [72, 81], VGe_n [73,106], WGe_n [84], $NbGe_n$ and $TaGe_n$ [120], and at n = 9 for $NiGe_n$ [83,88]. The encapsulated transition metal eliminates the dangling bonds of germanium atoms. In the present work, the cage-like structures enhance the binding energy, in particular for n = 12–16.

Interestingly, $PdGe_{16}$ and $PtGe_{16}$ present a relatively high stability. They have the highest stability from both the binding energy (Fig 3.4) and the second-order energy difference (Fig 3.5). They also show a relatively high HOMO-LUMO gap (Fig 3.6), and a large chemical hardness (Fig 3.9). In Fig (3.10), we show the density of states (DOS) and the Kohn-Sham orbitals calculated at PBE/cc-pvtz level with the software Gaussian09 [114] in the case of $PdGe_{16}$. The 10 valence electrons of Pd, the 3s and 3p valence electrons of Ge exhibit a shell structure associated to the somewhat spherical structure. We can easily distinguish the character of the orbitals, though there are some little deviations from a perfect sphere due to explicit location of atoms and the Cs symmetry instead of K_h (the symmetry of the atom). The 74 valence electrons of the cluster are organized with the following occupations: $1S^2\ 1P^6\ 1D^{10}\ 1F^{14}\ 2D^{10}\ 2S^2\ 2P^6\ 1G^{18}\ 1H^6$. The number of electrons does not fit with shell closings numbers, but the pooling of electrons and the organization in shell contributes to the high stability of the cluster. Similar results are found for $PtGe_{16}$.

In experiment, the geometrical structure is most often inaccessible, and the discrimination between endohedral and exohedral structures is generally highlighted by a measurement of discriminated physical or chemical properties. For example, the expected relatively low reactivity of endohedral structures has been used to highlight the formation of metal-doped germanium or silicon cages [121]. Neukermans et al. [122] have used the mass spectroscopy and interpret the high abundance CuGe10 in terms of peculiarly stable dopant-encapsulated cage-like structures. More recently, several groups have used the photoelectron spectroscopy [79,106,123]. Here, we have calculated the UV–visible absorption spectra of both cage-like and surface-bound metal structures in order to discriminate endohedral and exohedral structures. Spectra are given in Fig (3.11) for PdG_{16} and $PdGe_{10}$. Unfortunately, they are found to be only few dependent on the position of the metal atom, while the density of states is much higher in the case of surface-bound metal due to a lower symmetry of the

structure. Spectra show a slowly increasing response in the visible and near UV domain, and a strong signal above 7 eV (above the ionization potential). This low dependency of the absorption spectra on the geometrical can be explained by the electronic arrangement which tends to favor the pooling of valence electrons and the organization in shells where electrons occupy orbitals fully delocalized over the whole volume of the cluster. The shells are clearly visible in the case of symmetric structures, like cage-like structures (Fig 3.10 for example), but are no easily identifiable in the case of geometries without any symmetry like exohedral structures. The pooling of electrons is likely to be somewhat independent of the details of the structure, and consequently the optical absorption as well.

Conclusions

We systematically carry out a first-principles DFT calculations of structural, energetic absorption spectra and electronic properties of MGe_n (M= Pd and Pt) quantum computations. The lowest-energy structures and some low-lying isomers have been identified for all germanium doped clusters. The growth pattern for MGe_n (M = Pd, Pt) shows that the M atom occupies a peripheral position for very small clusters ($n < 10$), while for $n \geq 10$ endohedral structures in which the germanium cage encapsulates the metal atom in shall structure are strongly favoured. As an explanation the rigidity of Ge_n framework toward the M atom doping is originated from the covalent character of Ge atom. The binding energy increases with the increasing cluster size for all MGe_n (M = Pd, Pt) clusters and the influence of M atoms on these clusters making them a little more stable compared to the corresponding pure germanium cluster. This stability is related to the pooling of valence electrons from both germanium and metal atoms. Our results show that measurements of optical absorption spectra are likely unable to discriminate the endohedral and exohedral structures. The HOMO−LUMO gaps of the doped clusters are presenting an overlapping behavior than those of the corresponding Ge_{n+1} cluster. The calculated binding energy, the second-order energy difference, the HOMO−LUMO gaps, vertical ionization potential, and chemical hardness manifest the large stability of the $PdGe_n$ and $PtGe_n$ clusters with specific sizes n = 10, 12, 16 and 18. Amongst, $PdGe_{16}$ and $PtGe_{16}$ are the most stable clusters. These clusters can be considered as a good candidate to be used as building blocks to make cluster assembled materials for eventual applications in the news nanotechnologies.

Chapter 4

Theoretical investigation of $IrGe_n$ Clusters

Chapter 4

Theoretical investigation of $IrGe_n$ Clusters

4.1 Introduction

Nowadays, the domain of nanotechnology has recognized a very fast development because of the large number of researchers interested in this fascinating science. Nanotechnology has inspired several areas namely technologies and information services, transportation and constructions, giving us many promises for a very healthy life and a greener world. Such technologies which study the infinitely small, faces very important challenges especially in the manufacturing process which are avoidable if theoretical studies are well defined. Clusters are nanomaterials range among atoms and bulk, their structural, electronic and optical properties are much related to their size. Germanium and transitional metals are widely used in electronics, optoelectronics and cancer treatment. Furthermore, many researchers in experimental and theoretical fields had interested in studying the ability of using them in different innovative ideas worth spreading in the worldwide.

The trend towards miniaturization in electronics, while increasing performance, has triggered interest in small nanoparticles [124]. The properties (electronic, optical, structural, etc.) of nanoparticles and nanoclusters strongly depend on size, shape, and chemical composition. In particular, they may change dramatically with the addition or substitution of one or few atoms in the cluster. Accordingly, clusters, used as building blocks, could offer great opportunities to develop self-assembly of nanocrystals and materials with tuned properties [124]. Especially, ultra-stable clusters, e.g, ligand-coated clusters or endohedrally doped cage clusters, are highly desired [125, 126, 127, 121].

Germanium is an important semiconductor material widely used in the electronics industry and for nano technology applications. At the nanoscale, small- and medium-sized germanium clusters have been extensively studied in both theoretical and experimental fields [13, 67, 101, 57, 65]. Also, much experimental and theoretical research on Ge_n clusters doped with different transition metals has been reported [126, 128, 129]. The presence of a foreign atom often leads to enhance the stability, as it saturates the dangling bonds, particularly in endohedral structures where the metal atom is encapsulated inside a germanium cage. Also, the metal induces significant changes in electronic and magnetic properties [130].

Among recent studies on metal-doped clusters, one can cite the works of Deng et al. [79, 106] where the structural and magnetic properties of $CoGe_n^-$ and $VGe_n^{-/0}$ (n = 2–12) clusters were investigated using anion photoelectron spectroscopy combined with density functional theory (DFT) calculations. The structural evolution was found to be much related to the electron transfer pattern and the minimization of the magnetic moments for most of these clusters. Several computational studies, mainly at DFT level, have investigated the geometries, stabilities, and electronic properties of $NiGe_n$ (n = 1–20) [98, 83, 107, 88, 96, 93]; WGe_n (n = 1–17) [84]; $ZnGe_n$ (n = 1–13) [102]; $CrGe_n$ (n < 30) [95-74]; $CoGe_n$ (n = 1–13) [93, 78]; $FeGe_n$ (n ≤ 16) [103, 91]; Mo_2- doped Ge_n (n = 9–15) [85]; $MnGe_n$ (n = 2–16) [94];

$TiGe_n$, $ZrGe_n$, and $HfGe_n$, ($n \leq 21$) [80, 110]; $RuGe_n$ ($n \leq 12$) [111]; VGe_n ($n < 20$) [73]; $NbGe_n$ and $TaGe_n$ ($n < 20$) [120]; $PdGe_n$ and $PtGe_n$ ($n \leq 20$) [131-132], and noble metal-doped Ge_n clusters [77, 81, 92, 72, 133]. A more extensive review can be found in Ref [126, 120]. These studies highlight the dependence of the growth patterns as well as magnetic and electronic properties on the nature of the doping metal. While doping with Cr, Fe, Co, and Mn seems to favor high-spin states, the magnetic moment is generally quenched for the other foreign atom. Most often, the doping atom contributes to strengthen the stability of the germanium framework and adopts an endohedral position when the number of atoms is enough to form a cage covering the metal atom. This is, e.g., the case for the vanadium atom, for which VGe_{14} shows a relatively high stability in an Oh symmetry cage-like geometry [73]. Similarly, $NbGe_{15}$ and $TaGe_{15}$ adopt a cage-like structure which present a high stability [120]. However, the energetics also depend on the metal, as the early transition metals seem to increase the stability of the germanium framework more strongly than noble metals do.

Iridium presents an unfill atomic 5d shell and is known to be low reactive. Ir-based alloys are widely used in industry. Recently, germanium- and iridiumbased bulk alloys were synthesized and characterized [134-135]. Superconductivity was reported for the compound TaIr2Ge2, which surprisingly displays a structure based on endohedral Ta@Ir7Ge4 clusters [134]. Also, small iridium–germanium complexes were synthetized in solution [136].

Here, we investigate the structural and electronic properties of IrGen clusters, for which, to the best of our knowledge, no previous study has been reported in the literature. Our purpose in this work is to investigate with ab initio DFT calculations the effect of one iridium atom on the structural and electronic properties of small germanium cage clusters and their evolution as a function of the size and shape. We hope that our work would be constructive to understand the properties and the growth behavior of IrGen clusters and will guide further theoretical and experimental investigations. This manuscript is organized as follows: the computational details are described in the "Computational methodology" section, the structural and energetic properties are presented in the "Results and discussion" section following by a discussion about the electronic and optical properties.

4.2 Computational Methodology

The spin-polarized DFT implemented in the SIESTA package [18] are used in all calculations performed in this work. Under the generalized gradient approximation formulated by Perdew, Burke, and Ernzerhof [112] (PBE), the exchange−correlation energy functional was described. In the case of norm-conserving Troullier−Martins nonlocal pseudo-potentials [45], a flexible basis set of localized numerical-type atomic orbitals were used together and Mesh Cut-Off of 150 Ry was taken and the Energy-Shift is taken equal to 50 meV. Furthermore, core electrons were replaced by nonlocal, norm-conserving pseudo-potentials factorized in the Kleinman− Bylander form [113]. We used $4f^{14}\ 5d^7\ 6s^2$configurations for Ir and $4s^2\ 4p^2$ for Ge. In this study the geometries were optimized without any symmetry constraints, and by solving the Kohn−Sham equations [30] the optimization of electronic structure was obtained, using self- consistent with a convergence criterion of 1×10^{-4} a.u. on

the energy and electron density. For Brillouin zone sampling we used the k = 0 (Γ) point approximation. We employed the double ζ (DZ) basis for Ge atoms and double ζ (DZP) basis with polarization function for iridium atom. In the optimization method, the volume of the system was kept constant, and a big super-cell of 40 Å was used to avoid interaction between the neighboring clusters. Structural optimizations were performed using conjugate gradient algorithm, and the convergence criterion on the Hellmann−Feynman forces imposed that the residual forces were less than 10^{-2} eV/Å. Several spin multiplicity states were tested. The Mulliken population analyses were done to obtain the atomic charge and the unpaired spin population. So as to find the global minimum structures of $IrGe_n$ clusters, firstly, we have used several optimized isomers of pure germanium clusters with size of 2–21 atoms [73]. Secondly, a great number of isomers doped $IrGe_{n+1}$ from 1-20 were considered. Further analysis of the electronic properties and molecular orbitals has been performed with the software Gaussian09 [114] using PBE and the Gaussian-type basis sets cc-pvtz for Ge and LanL2DZ for Ir. They include the electron population analysis, the plot of density of states, as well as the prediction of optical absorption spectra calculated in the framework of the Time-Dependent DFT (TDDFT). Despite all these works a complete exploration of geometrical configurations is most fundamental challenging and practical problems in clusters physical technology due to the existence of numerous possibilities.

The firmness of Ir doped germanium clusters can be inquired by the calculation of the binding energy, HOMO–LUMO gap, and the second-order energy difference. The binding energies per atom of $IrGe_n$ are defined by the following formula:

$$E_b(MGe_n)(eV/atom) = (n\,E(Ge) + E(M) - E(MGe_n)) / (n + 1) \quad (4.1)$$

Where E(Ge) is the total energy of free Ge atom, E(M) is the total energy of free M atom and $E(MGe_n)$ is the total energy of the MGe_n cluster. The HOMO–LUMO gap is calculated from the energy of the orbitals:

$$\Delta E\,(eV) = E\,(LUMO) - E\,(HOMO) \quad (4.2)$$

The second-order energy difference for the ground-state MGe_n clusters can be calculated by:

$$\Delta_2 E = E\,(MGe_{n+1}) + E\,(MGe_{n-1}) - 2\,E\,(MGe_{n2}) \quad (4.3)$$

Where E is the total energy of the most stable relaxed structure for each species. At the present level of calculation, the bond lengths of Ge_2 were found to be 2.450 Å, and it is in good agreement with the experimental results [115]. As that, in the case of Ir_2, the calculations showed a value of 2.353 Å, compared to the experimental value of 2.35 Å [137]. The binding energy per atom for Ge_2 was calculated to be 1.44 eV, which is in good agreement with the experimental (~1.35 eV) [116] data.

4.3 Results and discussion

The first goal in cluster atomistic simulation investigation is to determine the ground-state of our initial structures, which will allow us after that to unveil the other properties. As a beginning we looked into the doped germanium clusters and compare them to the relaxed pure clusters, and if there is any important or remarkable changes, we will try to figure out the origin of this evolution in order to understand the phenomena happening, so that, to bring the most outstanding improvement and why not to manage a useful way to be indented for.

4.3.1 Structural properties

Using the computational method described earlier basing on the pillars of quantum physics, the doped germanium clusters MGe_n in our calculations show a growth pattern in which the planar structures only appears in the very small clusters, while the tridimensional structures dominate from n + 1 = 4. Up to n + 1 = 21, prolate type structures compete with nearly spherical structures, and almost all atoms are located in surface. Many of the obtained best structures are in agreement with the previous theoretical studies of the literature. Our lowest-energy isomers are shown in Figure 1. For each size, data for most stable isomers are reported in bold character. The symmetry group, binding energy E_b (eV/atom), HOMO–LUMO gap ΔE (eV), the vertical ionization potential VIP (eV), the vertical electron affinity VEA (eV), the chemical hardness η (eV) and the average Ge–Ge and M–Ge bond lengths are summarized in Table 1 for all $IrGe_n$ clusters. First of all, the dimers MGe had a bond length of 2.256 Å. In the case of binding energy (per atom) a 1,778eV was found. For the trimer $IrGe_2$ cluster, the bond length was 2.410Å, and 2,368 eV for the binding energy. The triangular structure with C_{2v} (2mm) symmetry is found to be the lowest-energy structure. Low laying isomers of $IrGe_3$ have obtained and the structure had C3v (3mm) symmetry with 2.555Å bond length. The binding energy for this lowest-energy structure was 2,755eV. A tri-dimensions structure was assigned to $IrGe_4$ with a symmetry group of C_s (m), 2.655 Å was found for the bond length. The analyzing of binding energy per atom had given us 2,879 eV for the respective cluster. The bicapped tetrahedron structure with C_1 symmetry is found to be the lowest-energy structure for $IrGe_5$ with 2.627Å bond length, 2,985 eV for the binding energy per atom. For the $IrGe_6$ a geometry of a bicapped pentagonal with C_{5v} symmetry were found with 2.662 Å bond length along of 3,129 eV for the binding energy per atom. In the case of $IrGe_7$ cluster, he had the capped pentagonal bipyramid structure-like; C_s symmetry was shown to be the ground state structure. 2.739Å was the bond length and for the binding energy per atom a 3,136eV was presented. The lowest-energy structure of the $IrGe_8$ cluster was a oblate edge-capped pent bipyramid geometry with C_s symmetry. The bond length was 2.663 Å and for the binding energy per atom it's 3,177eV. In the case of $IrGe_9$ cluster, the lowest-energy structure can be viewed as a capped prismatic structures with C_2 symmetry and bond length of 2.728 Å while the binding energy was 3,221 eV for the respective cluster. The doped germanium clusters from n=10~20 atom show an encapsulated metal atom for the all low-lying isomers structure. For the $IrGe_{10}$ cluster, we see that the most stable isomer was a partially encapsulated metal atom in capped prismatic structures without any symmetry (C_1).

The bond length was 2.809 Å for the stable isomer where the binding energy per atom was 3,248 eV.

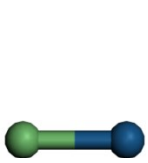

$IrGe_{1}$ C∞

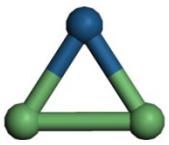

$IrGe_{2-3}$ C2v (mm2)
(-0 eV)

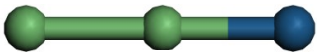

$IrGe_{2-2}$ C∞
(-0.492 eV)

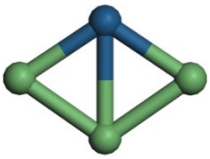

$IrGe_{3-3}$ C2v (mm2)
(-0 eV)

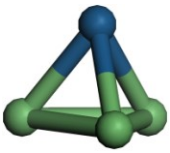

$IrGe_{3-4}$ C3v (3m)
(-0.08 eV)

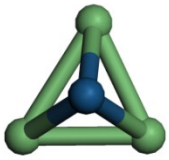

$IrGe_{3-5}$ Cs (m)
(-0.108 eV)

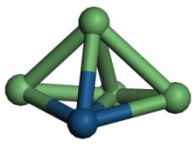

$IrGe_{4-2}$ Cs (m)
(-0 eV)

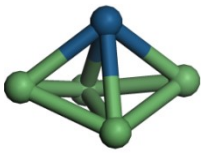

$IrGe_{4-1}$ C2v (mm2)
(-0.017 eV)

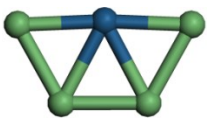

$IrGe_{4-3}$ (C2v (mm2)
(-0.14 eV)

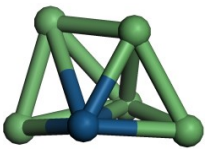

$IrGe_{5-17}$ C1
(-0 eV)

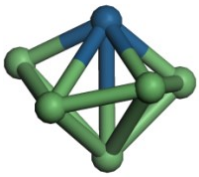

$IrGe_{5-1}$ C1
(-0.005 eV)

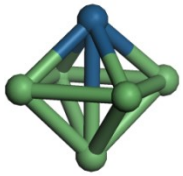

$IrGe_{5-4}$ C4v (4mm)
(-0.019 eV)

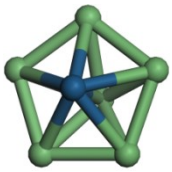

$IrGe_{6-19}$ C5v
(-0 eV)

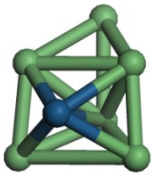

$IrGe_{6-11}$ Cs (m)
(-0.087 eV)

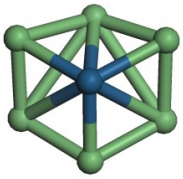

$IrGe_{6-2}$ Cs (m)
(-0.1 eV)

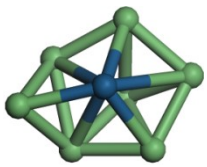

$IrGe_{7-14}$ Cs (m)
(-0 eV)

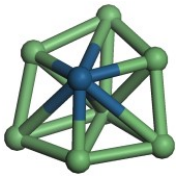

$IrGe_{7-3}$ C3v (3m)
(-0.029 eV)

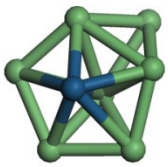

$IrGe_{7-1}$ Cs (m)
(-0.043 eV)

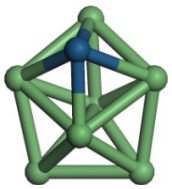

$IrGe_{7-5}$ Cs (m)
(-0.109 eV)

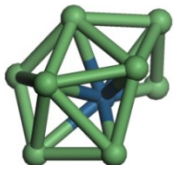

$IrGe_{8-20}$ Cs (m)
(-0 eV)

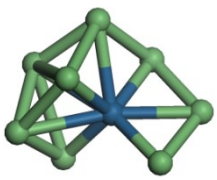

$IrGe_{8-16}$ C1
(-0.024 eV)

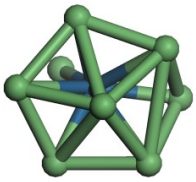

$IrGe_{8-3}$ Cs (m)
(-0.039 eV)

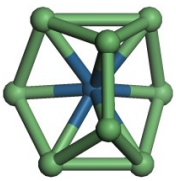

$IrGe_{8-12}$ Cs (m)
(-0.051 eV)

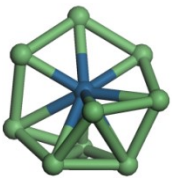

$IrGe_{9-24}$ C2
(-0 eV)

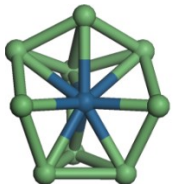

$IrGe_{9-12}$ Cs (m)
(-0.03 eV)

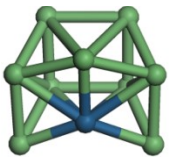

$IrGe_{9-9}$ Cs (m)
(-0.083 eV)

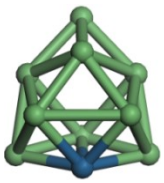

$IrGe_{9-26}$ Cs (m)
(-0.111 eV)

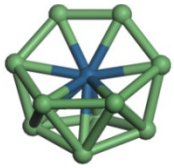

$IrGe_{10-5}$ C1
(-0 eV)

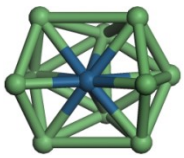

$IrGe_{10-2}$ C2v (mm2)
(-0.015 eV)

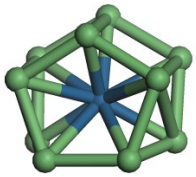

$IrGe_{10-3}$ Cs (m)
(-0.018 eV)

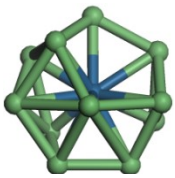

$IrGe_{11\text{-}9}$ C1
(-0 eV)

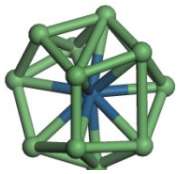

$IrGe_{11\text{-}4}$ C1
(-0.029 eV)

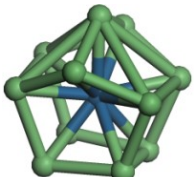

$IrGe_{11\text{-}1}$ C2
(-0.049 eV)

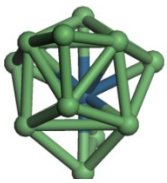

$IrGe_{11\text{-}25}$ Cs (m)
(-0.131 eV)

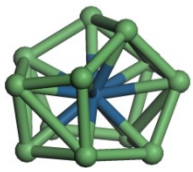

$IrGe_{12\text{-}7}$ C2
(-0 eV)

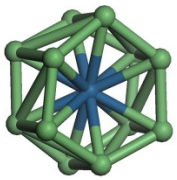

$IrGe_{12\text{-}1}$ Cs (m)
(-0.035 eV)

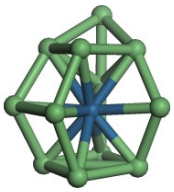

$IrGe_{12\text{-}13}$ C1
(-0.052 eV)

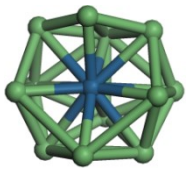

$IrGe_{12\text{-}16}$ Cs (m)
(-0.089 eV)

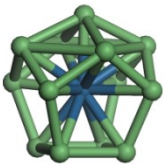

$IrGe_{13\text{-}11}$ C4v (4mm)
(-0 eV)

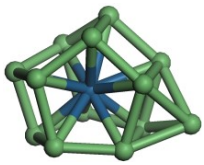

$IrGe_{13\text{-}7}$ Cs (m)
(-0.024 eV)

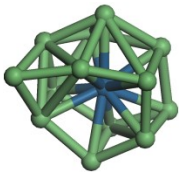

$IrGe_{13\text{-}1}$ C1
(-0.043 eV)

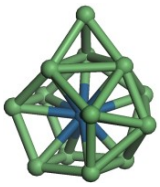

$IrGe_{13\text{-}10}$ Cs (m)
(-0.044 eV)

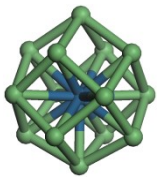

$IrGe_{14\text{-}11}$ C4v (4mm)
(-0 eV)

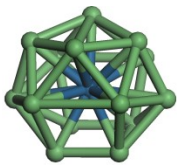

$IrGe_{14\text{-}14}$ C2v (mm2)
(-0.006 eV)

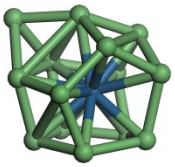

$IrGe_{14\text{-}19}$ Cs (m)
(-0.007 eV)

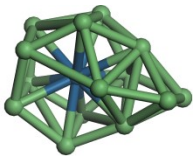

$IrGe_{14\text{-}17}$ C1
(-0.042 eV)

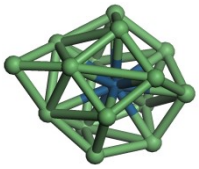

$IrGe_{15\text{-}18}$ Cs (m)
(-0 eV)

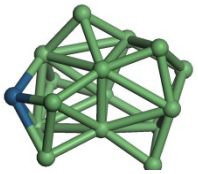

$IrGe_{15\text{-}19}$ C1
(-0.008 eV)

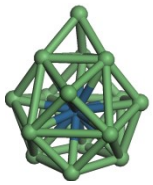

$IrGe_{15\text{-}6}$ Cs (m)
(-0.01 eV)

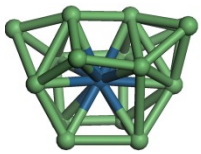

$IrGe_{15\text{-}25}$ C1
(-0.068 eV)

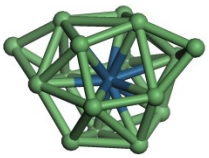

$IrGe_{16\text{-}8}$ C4v (4mm)
(-0 eV)

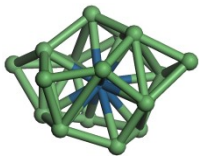

$IrGe_{16\text{-}2}$ Cs (m)
(-0.01 eV)

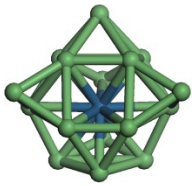

$IrGe_{16\text{-}3}$ C2
(-0.025 eV)

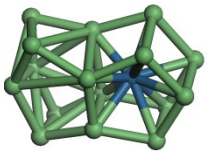

$IrGe_{16\text{-}17}$ C1
(-0.063 eV)

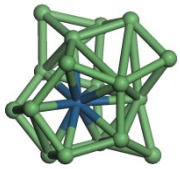

$IrGe_{17\text{-}22}$ C1
(-0 eV)

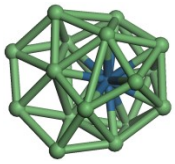

$IrGe_{17\text{-}8}$ C1
(-0.032 eV)

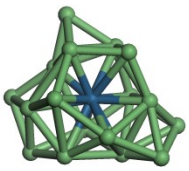

$IrGe_{17\text{-}25}$ C1
(-0.047 eV)

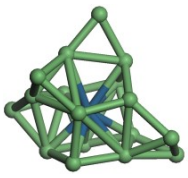

$IrGe_{17\text{-}21}$ C1
(-0.066 eV)

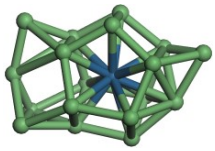

$IrGe_{18\text{-}2}$ Cs (m)
(-0 eV)

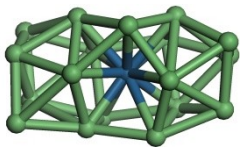

$IrGe_{18\text{-}8}$ Cs (m)
(-0.02 eV)

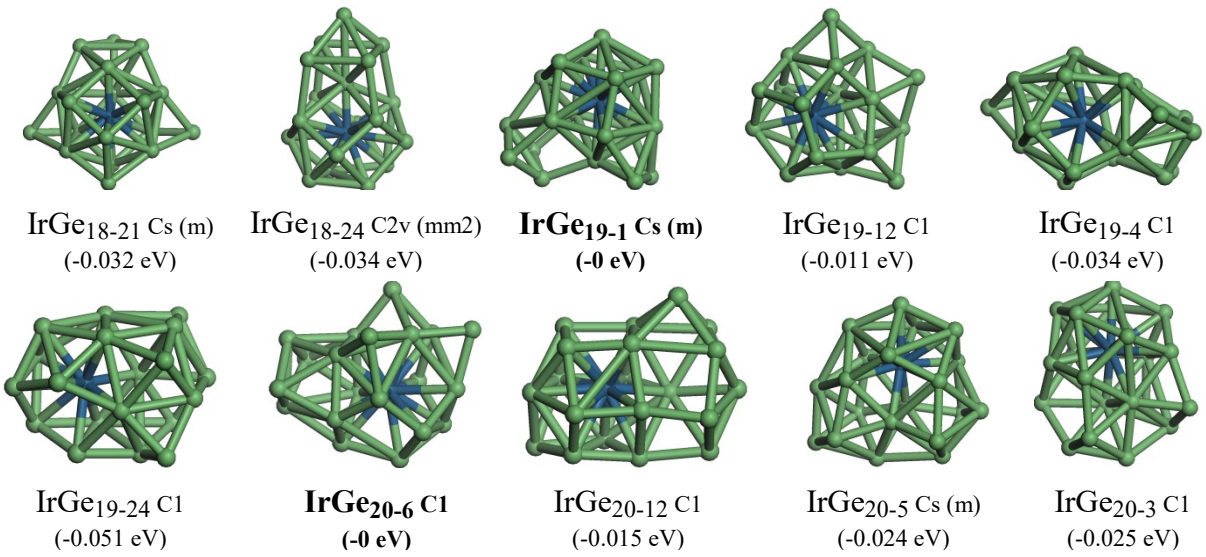

Fig (4.1): Low energy structures and their corresponding isomers for $IrGe_n$ (n=1-20) clusters

The $IrGe_{11}$ cluster presents a pentacapped tetragonal prism structure with a centered metal atom with C_1 symmetry. The stable isomer bond length was 2.796 Å which the binding energy was 3,307 eV. The stable structure for the doped germanium clusters was a capped pentagonal bipyramid for n = 12 size, with a symmetry group of C_2, present a bond length of 2.830Å and a binding energy per atom of 3,329 eV. Pentagonal-dodecahedron geometry was preferred to the most stable cluster in this study, $IrGe_{13}$ with symmetry of C_{4v} (4mm). The bond length for stable isomer and the binding energy respectively was 2.865 Å as well 3,347 eV. The shape of $IrGe_{14}$ cluster shows a rhombic dodecahedron structure with C_{4v} (4mm) symmetry. The bond length for the stable isomers was 2.872 Å when the binding energy for this lowest-energy structure was 3,322eV. Let's move on the next cluster, which is $IrGe_{15}$, he present an augmented tridiminished icosahedrons like-structure with an encapsulated metal atom in C_s symmetry. Moving into the bond length for the stable isomer we noticed 2.960 Å, while the binding energy per atom was 3,328 eV. For $IrGe_{16}$, a tricapped trigonal prism was obtained with C_{4v} (4mm) symmetry. Concerning the bond length structure and the binding energy per atom we mentioned 2.939Å with 3,305 eV. An irregular cage-like structure was found for $IrGe_{17}$, when the symmetry was absent (C_1). 2.869 Å was the bond length for stable isomer, while the respective binding energy was 3,277 eV. Thereafter, comes $IrGe_{18}$, he present a face-sharing pentagonal bipyramid structure with a C_s symmetry. By the same way, the bond length structure was 2.933Å, although the 3,269 eV have been mentioned for the respective binding energy. In the case of $IrGe_{19}$ a distorted square-antiprism structure was the one reached. The symmetry obtained for the cluster was C_s. In the subject of bond length structure and binding energy per atom, 2.904Å with 3,271 eV have been pulled, respectively. Face-sharing distorted tetra-capped pentagonal prism structures without any symmetry (C_1) was revealed for the last clusters isomers, $IrGe_{20}$. When the bond length for the stable isomers was 2.939 Å while the binding energy has been mentioned 3,254 eV.

Table (IV.1): Symmetry group, binding energy E_b(eV/atom), HOMO-LUMO gap ΔE (eV), vertical ionization potential VIP (eV), vertical electron affinity VEA (eV), chemical hardness η (eV) and average bond length $a_{Ge\text{-}Ge}$ (Å) and $a_{Ir\text{-}Ge}$(Å) for $IrGe_n$ clusters.

Size (n)	Sym.	Eb (eV/atom)	ΔE (eV)	VIP (eV)	VEA (eV)	η(eV)	$a_{Ge\text{-}Ge}$(Å)	$A_{Ir\text{-}Ge}$(Å)
IrGe1	**C_∞**	**1,778**	**0.705**	**6,546**	**0,441**	**6,105**	/	**2.256**
IrGe2-3	**C_{2v}**	**2,368**	**0.302**	**6,903**	**1,357**	**5,546**	**2.617**	**2.410**
IrGe2-2	C_∞	1,876	0.262	6,974	1,464	5,510	2.435	2.327
IrGe3-3	**C_{2v}**	**2,755**	**0.506**	**7,196**	**1,600**	**5,596**	**2.475**	**2.555**
IrGe3-4	C_{3v}	2,675	1.757	7,010	1,446	5,564	2.6921	2.5313
IrGe3-5	C_s	2,647	0.571	6,765	1,519	5,246	2.710	2.532
IrGe4-2	**C_s**	**2,879**	**0.452**	**6,938**	**1,707**	**5,231**	**2.682**	**2.655**
IrGe4-1	C_{2v}	2,862	0.146	6,984	1,993	4,991	2.628	2.653
IrGe4-3	C_{2v}	2,739	0.585	6,899	1,776	5,123	2.519	2.552
IrGe5-17	**C_1**	**2,985**	**0.254**	**6,558**	**1,730**	**4,827**	**2.742**	**2.577**
IrGe5-1	C_1	2,980	0.551	6,602	1,747	4,855	2.731	2.615
IrGe5-4	C_{4v}	2,966	0.498	7,049	2,242	4,807	2.742	2.577
IrGe6-19	**C_{5v}**	**3,129**	**0.875**	**7,075**	**2,341**	**4,734**	**2.708**	**2.662**
IrGe6-11	C_s	3,042	0.519	6,995	2,242	4,753	2.737	2.585
IrGe6-2	C_s	3,029	0.599	6,518	1,907	4,611	2.522	2.731
IrGe7-14	**C_s**	**3,136**	**0.572**	**6,600**	**2,197**	**4,403**	**2.741**	**2.739**
IrGe7-3	C_{3v}	3,107	0.669	6,514	2,217	4,297	2.744	2.589
IrGe7-1	C_s	3,093	0.558	6,579	2,108	4,471	2.734	2.696
IrGe7-5	C_s	3,027	0.564	6,759	2,209	4,550	2.804	2.616
IrGe8-20	**C_s**	**3,177**	**0.284**	**6,784**	**2,708**	**4,076**	**2.748**	**2.663**
IrGe8-16	C_1	3,153	0.731	6,708	2,603	4,104	2.682	2.726
IrGe8-3	C_s	3,138	0.275	6,718	2,671	4,048	2.713	2.730
IrGe8-12	C_s	3,126	0.661	6,871	2,700	4,172	2.697	2.644
IrGe9-24	**C_2**	**3,221**	**0.960**	**6,368**	**2,427**	**3,941**	**2.699**	**2.728**
IrGe9-12	C_s	3,191	0.483	6,914	2,823	4,091	2.691	2.726
IrGe9-9	C_s	3,146	0.534	6,698	2,614	4,084	2.742	2.749
IrGe9-26	C_s	3,110	0.574	6,525	2,396	4,129	2.755	2.640
IrGe10-5	**C_1**	**3,248**	**0.860**	**6,648**	**2,605**	**4,043**	**2.708**	**2.809**
IrGe10-2	C_{2v}	3,233	0.394	6,647	2,718	3,929	2.769	2.801
IrGe10-3	C_s	3,230	0.484	6,702	2,663	4,039	2.690	2.774
IrGe11-9	**C_1**	**3,307**	**0.762**	**6,619**	**2,777**	**3,842**	**2.746**	**2.796**
IrGe11-4	C_1	3,278	0.733	6,561	2,748	3,813	2.662	2.829
IrGe11-1	C_2	3,258	0.293	7,162	3,219	3,943	2.684	2.751
IrGe11-25	C_s	3,176	0.708	6,506	2,630	3,876	2.783	2.637
IrGe12-7	**C_2**	**3,329**	**0.349**	**7,068**	**3,233**	**3,835**	**2.619**	**2.830**
IrGe12-1	C_s	3,294	0.211	6,025	2,324	3,702	2.834	2.868
IrGe12-13	C_1	3,277	0.573	6,712	2,931	3,781	2.668	2.776
IrGe12-16	C_s	3,240	0.658	6,614	2,836	3,778	2.722	2.837
IrGe13-11	**C_{4v}**	**3,347**	**0.443**	**6,808**	**3,066**	**3,742**	**2.602**	**2.865**
IrGe13-7	C_s	3,323	0.685	6,507	2,838	3,669	2.660	2.850
IrGe13-1	C_1	3,304	0.786	6,377	2,685	3,692	2.702	2.826
IrGe13-10	C_s	3,303	0.606	6,573	2,917	3,656	2.759	2.821
IrGe14-11	**C_{4v}**	**3,322**	**0.495**	**6,098**	**2,325**	**3,773**	**2.669**	**2.872**
IrGe14-14	C_{2v}	3,316	0.608	6,300	2,637	3,663	2.767	2.939
IrGe14-19	C_s	3,315	0.385	6,495	2,952	3,542	2.614	2.918
IrGe14-17	C_1	3,280	0.564	6,544	2,974	3,570	2.736	2.836

IrGe15-18	**C_s**	**3,328**	**0.580**	**6,494**	**2,961**	**3,533**	**2.692**	**2.960**
IrGe15-19	C_1	3,320	0.488	6,107	2,690	3,417	2.744	2.593
IrGe15-6	C_s	3,318	0.713	6,218	2,653	3,565	2.722	2.925
IrGe15-25	C_1	3,260	0.662	6,283	2,858	3,425	2.719	2.864
IrGe16-8	**C_{4v}**	**3,305**	**0.472**	**5,901**	**2,531**	**3,370**	**2.767**	**2.939**
IrGe16-2	C_s	3,295	0.524	6,300	2,798	3,503	2.638	2.955
IrGe16-3	C_2	3,280	0.649	6,143	2,704	3,439	2.698	2.895
IrGe16-17	C_1	3,242	0.544	6,452	2,926	3,526	2.721	2.716
IrGe17-22	**C_1**	**3,277**	**0.677**	**6,519**	**2,944**	**3,575**	**2.662**	**2.869**
IrGe17-8	C_1	3,245	0.566	6,273	2,938	3,335	2.793	2.908
IrGe17-25	C_1	3,230	0.675	6,042	2,787	3,256	2.959	2.871
IrGe17-21	C_1	3,211	0.382	5,868	2,651	3,218	2.660	2.883
IrGe18-2	**C_s**	**3,269**	**0.499**	**6,021**	**2,809**	**3,212**	**2.693**	**2.933**
IrGe18-8	C_s	3,249	0.354	6,350	3,199	3,151	2.788	2.825
IrGe18-21	C_s	3,237	0.442	6,286	3,052	3,234	2.780	2.885
IrGe18-24	C_{2v}	3,235	0.321	6,645	3,293	3,352	2.806	2.890
IrGe19-1	**C_s**	**3,271**	**0.592**	**6,151**	**2,900**	**3,251**	**2.747**	**2.904**
IrGe19-12	C_1	3,260	0.349	6,218	3,047	3,171	2.709	2.919
IrGe19-4	C_1	3,237	0.568	6,026	2,851	3,175	2.712	2.913
IrGe19-24	C_1	3,220	0.779	6,176	2,992	3,184	2.789	2.831
IrGe20-6	**C_1**	**3,254**	**0.573**	**5,990**	**2,853**	**3,137**	**2.825**	**2.939**
IrGe20-12	C_1	3,239	0.586	6,133	2,939	3,194	2.782	2.913
IrGe20-5	C_s	3,230	0.392	5,834	2,666	3,167	2.814	2.793
IrGe20-3	C_1	3,229	0.559	6,146	2,883	3,262	2.777	2.935

4.3.2 Electronic properties

4.3.2.1 Binding energy

Figure 2 shows the evolution of the binding energy per atom (formula (4.1)) with the size n, for $IrGe_n$ and compared to that of Ge_n. The binding energy of $IrGe_n$ clusters gradually increases with n, rapidly for very small clusters up to n=6 and then the size dependence become very smooth from n= 7 to 13. Starting from n=14, the binding energy per atom decreases slowly from 3.347 eV for n=13 down to 3.254 eV for n=20.The curve of the average binding energy presents a local maximum value at n = 13 and 15, implying that these clusters are more stable than their neighbors. The binding energies of $IrGe_n$ clusters are always larger than the corresponding pure germanium clusters with the same size. These results indicate that the substitution of Ge by a Ir atom in $IrGe_n$ clusters leads to improve their stabilities which suggesting a higher Ir-Ge bond strength compared with the Ge-Ge bond one. Particularly, a strong improvement of the stability, comparatively to the corresponding pure Ge_{n+1}, is observed from n>8. This behavior is due to the absorption of the dangling bonds of the germanium cluster by the doping iridium atoms encapsulated inside of the Ge_n cage.

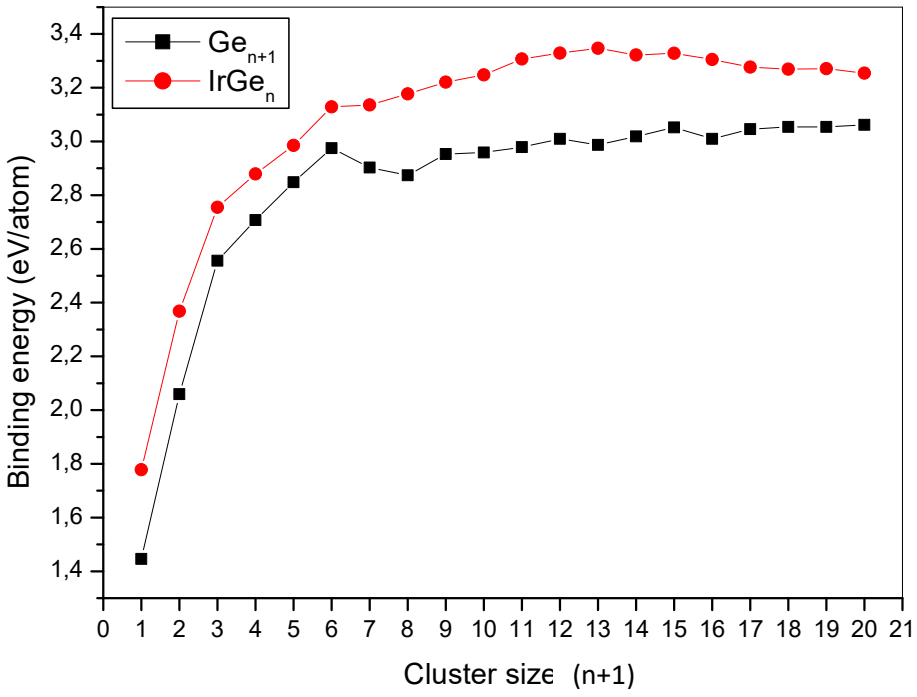

Fig (4.2): Binding energy (eV/atom) of the lowest energy structures of Ge_{n+1} [73] and $IrGe_n$ (n=1-20) clusters

4.3.2.2 Second-order energy difference

In cluster physics, the second-order difference in energy (Δ_2E) defined by the relation (4.3), can well reflect the relative stabilities of the corresponding clusters. It is generally compared with the relative abundances determined in mass spectroscopy experiments. The second-order difference of energy for the lowest-energy isomers of $IrGe_n$ clusters are shown in Figure 4.3 The pronounced positive values of Δ_2E are observed for n = 3, 6, 13 and 15, indicating that these clusters may have special stabilities more favorable than their neighbors.

4.3.2.3 HOMO–LUMO gaps

In the intention of having more information about the small clusters kinetic stability we investigated the energy difference between highest occupied molecular orbital (HOMO) and the lowest unoccupied molecular orbital (LUMO), which can also characterize the chemical activity of clusters. According to the literature, large HOMO−LUMO gap implies a low chemical activity and a high chemical stability, while the latter decreases as the HOMO−LUMO gap decreases. The size dependence of the HOMO-LUMO gap of $IrGe_n$ clusters is shown in figure 4.4, (using formula 4.2). We observe an oscillating behavior for both Ge_{n+1} and $IrGe_n$ clusters, with a pronounced decreasing tendency for pure $Ge_{n+1}$with the increasing size of clusters. The gaps of $IrGe_n$ clusters are generally much smaller than those for pure Ge_{n+1} clusters. Local maxima are found for n= 6, 9, 15 and 17, while the very small values observed for n= 2, 8 and 12, reminds a metallic character. Interestingly, all closed cage-like structures, i.e. n≥12, have a similar HOMO-LUMO gap (about 0.5 eV).

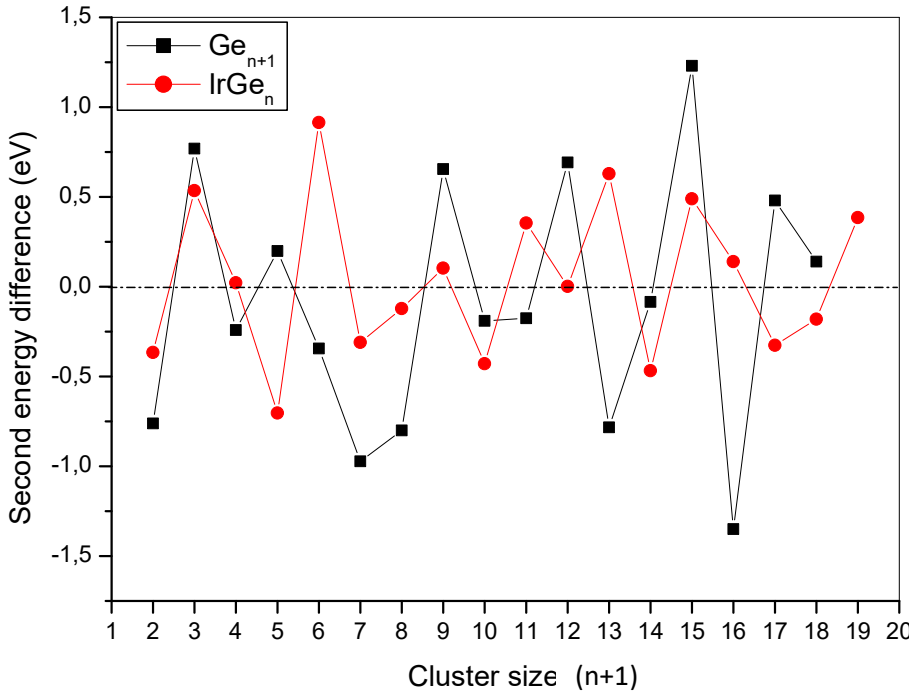

Fig (4.3): Second-order energy difference (eV) of the lowest energy structures of Ge_{n+1}[73] and $IrGe_n$ (n=1-20) clusters

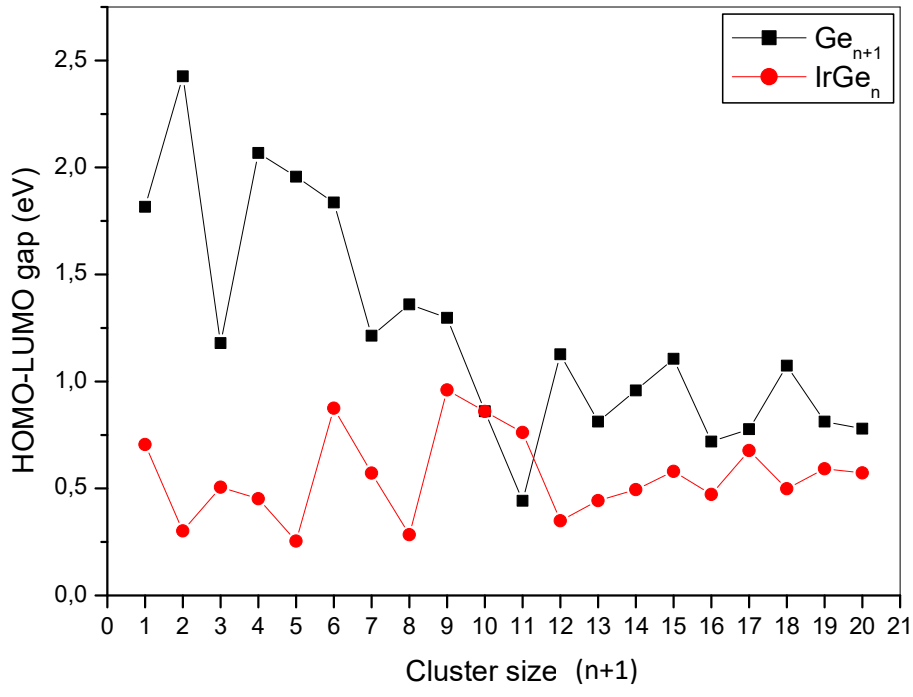

Fig (4.4): HOMO-LUMO gap (eV) of the lowest energy structures of Ge_{n+1}[73] and $IrGe_n$ (n=1-20) clusters

4.3.2.4 Vertical ionization potential, vertical electron affinity

The size dependence on vertical ionization potential (VIP) and vertical electron affinity (VEA) was displayed in Figures 4.5 and 4.6. They are two important parameters that can determine the chemical stability and the behavior of the small clusters. They are defined as following:

$$VIP = E\,(MGe_n)^+ - E\,(MGe_n) \quad (4.4)$$

$$VEA = E\,(MGe_n) - E\,(MGe_n)^- \quad (4.5)$$

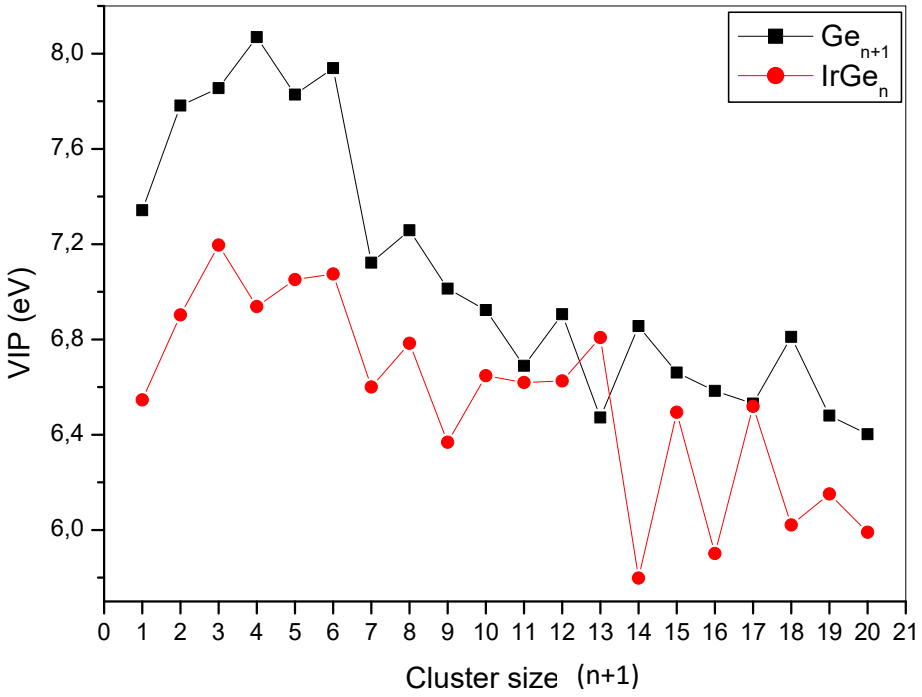

Fig (4.5): Vertical ionization potential VIP (eV) of the lowest energy structures of Ge_{n+1} [73] and $IrGe_n$ (n=1-20) clusters.

The VIP is defined by the energy difference between the cationic $E(MGe_n)^+$ and neutral clusters calculated at the equilibrium geometry of the neutral MGe_n cluster, the VEA is the energy difference between the neutral $E\,(MGe_n)$ and the anionic clusters calculated at the geometry of the neutral cluster. The size dependence of VIP shows an oscillating behavior with a global decreasing behavior with increasing size. Remarkable values are found for n = 3, 6, 13, 15 and 17, corresponding to the more pronounced local maxima. The VIP exhibits obvious odd-even oscillations from the size 13 to 20.The size dependence of VEA shows a non-monotone increasing from ~0.4 to ~3.0 eV. The largest values of VEA are generally observed for large clusters, indicating an increase of the chemical stability. Also, the values of VEA corresponding to $IrGe_6$, $IrGe_{13}$ and $IrGe_{15}$ clusters are larger than their neighbors indicating their special stability.

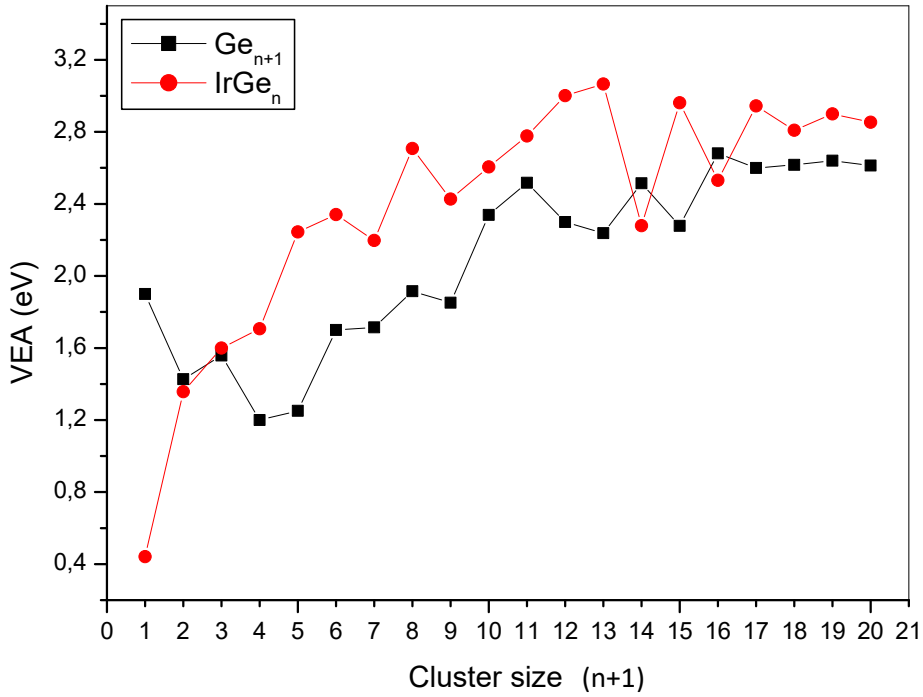

Fig (4.6): Vertical electron affinity VEA (eV) of the lowest energy structures of Ge_{n+1} [73] and $IrGe_n$ (n=1-20) clusters

This means that they are less able to acquire an electron. Another thing that we can deduce is the behavior of pure germanium for the both VIP and VEA that show an overlapping curve which states that these doping clusters had a weak feedback towards doped metal atoms.

4.3.2.5 Chemical hardness

For the latest parameter we investigate the difference between VIP and VEA in the following formula:

$$\eta = VIP - VEA \tag{4.6}$$

Through the principle of maximum Pearson hardness (MPH) [118-119], it has been established that chemical hardness given by $\eta = VIP - VEA$ is an important quantity which can be used to characterize the relative stability of small systems. The obtained results and their evolution as a function of the size for the most stable structures of $IrGe_n$ clusters are shown in Figure (07). Except for n = 7, 10, 16 when they present local maximum which means they are more stable than their neighboring clusters. Beyond the pure germanium clusters an overlapping behavior was noted.

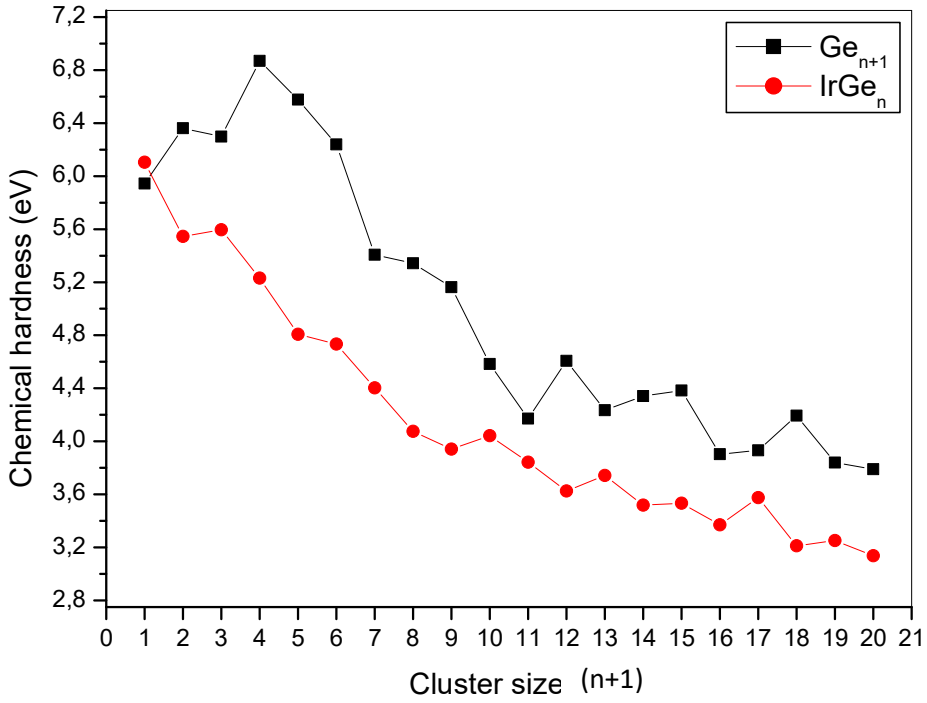

Fig (4.7): Chemical hardness η (eV) of the lowest energy structures of Ge_{n+1} [73] and $IrGe_n$ (n=1-20) clusters

4.3.2.6 Density of states and the Kohn-Sham orbitals

We also made an investigation on density of states (DOS) and the Kohn-Sham orbitals (K-H orbitals) using Gaussian09 calculated at PBE/cc-pvtz(Ge)/LanL2DZ(Ir) level, for $IrGe_{13}$ (see figure 4.8). Electronic shells can easily be identified, with their S, P, D, F, and G characters. We have found that the valance electrons from Ge and Ir leads to a shell structure where the orbitals are delocalized on the whole cluster. Hence, the 61 electrons fill the sequence $1S^2\ 1P^6\ 1D^{10}\ 1F^{14}\ 2S^2\ 2D^{10}\ 2P^6\ 1G^{11}$

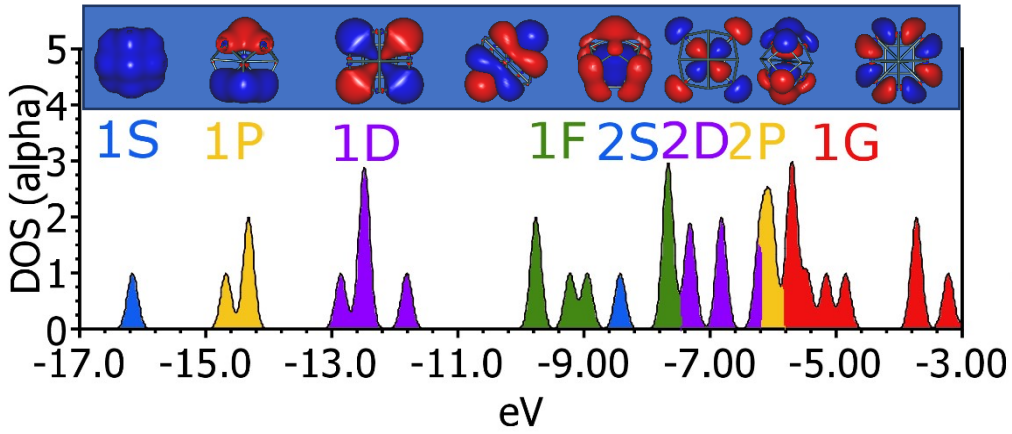

Fig (4.8): Density of states (DOS) of IrGe13 for alpha spin electrons. For each band, the Kohn-Sham orbitals are plotted. Plotted with the software Gabedit [138].

4.3.2.7 Absorption spectra of $PdGe_n$ and $PtGe_n$ clusters

To further characterize the clusters, we present in Figure 4.9 and 4.10 the optical absorption spectra of $IrGe_n$. Spectra are calculated by a TDDFT method. The calculated absorption spectra give the oscillator strength as a function of the excitation energy together with a curve obtained by a Lorentz broadening with a full width at half-maximum (fwhm) of 0.08 eV. Generally speaking, we found that a strong response was in the UV range of energy almost for all the low lying clusters, which correspond to transitions from d_{Ir} to s_{Ir} + p_{Ge} orbitals.

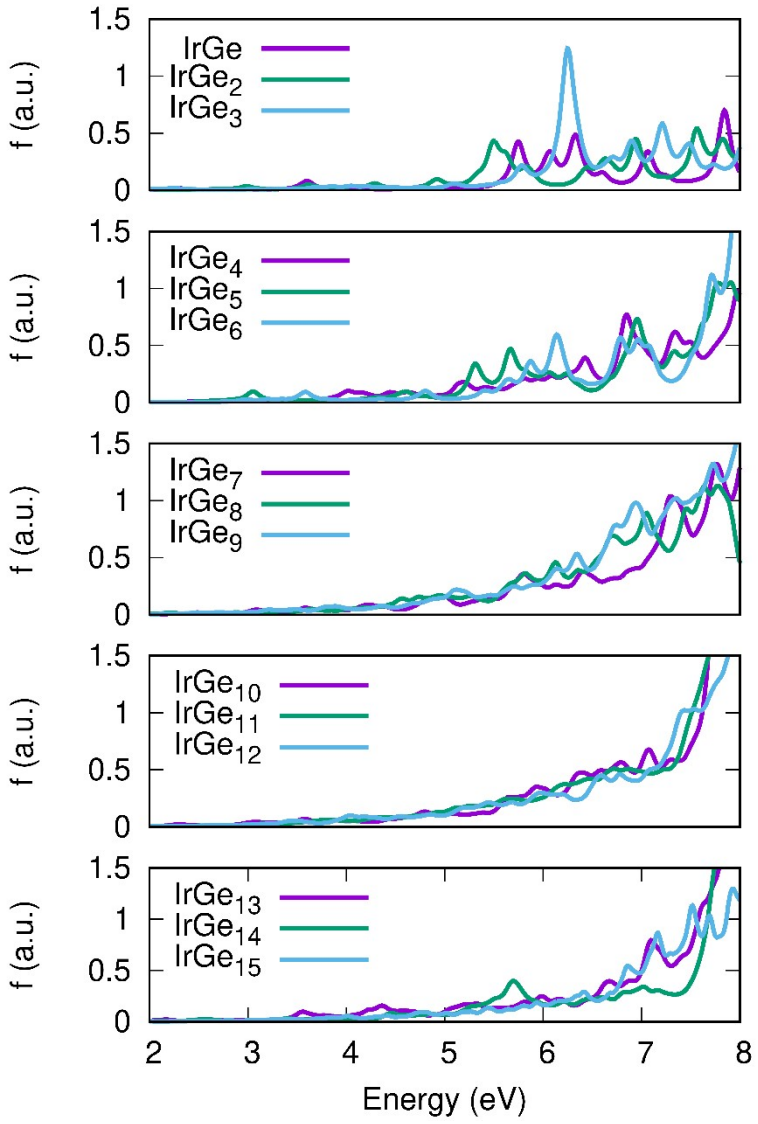

Fig (4. 9): Absorption spectra of $IrGe_n$ (n=1-15). More detailed spectra are available in Figure (4.10) for $IrGe_n$ (n=1-20).

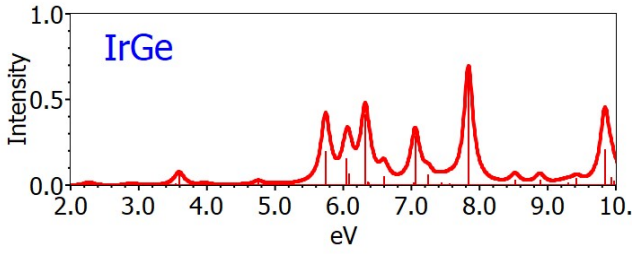
IrGe
Intensity
eV

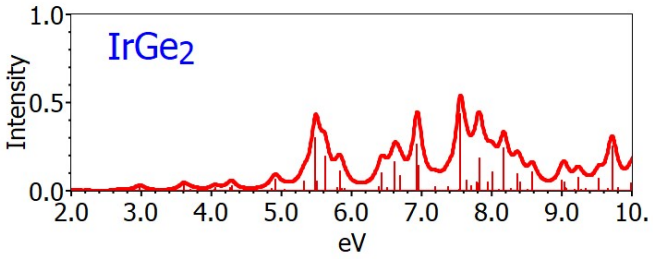
IrGe2
Intensity
eV

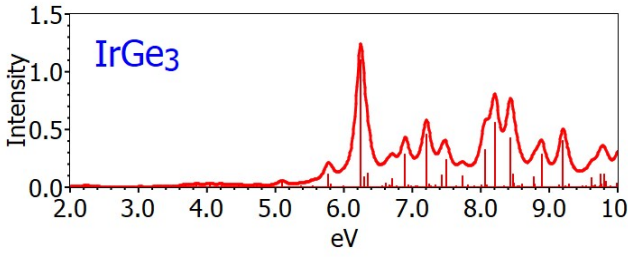
IrGe3
Intensity
eV

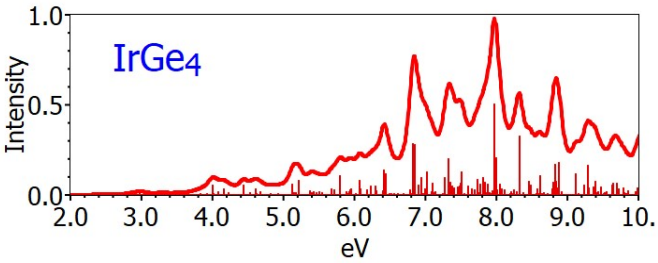
IrGe4
Intensity
eV

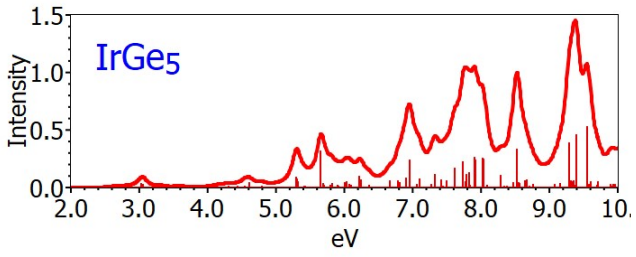
IrGe5
Intensity
eV

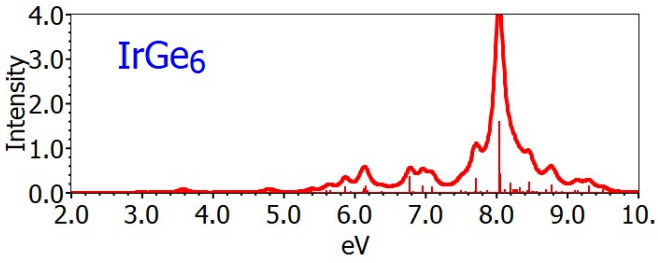
IrGe6
Intensity
eV

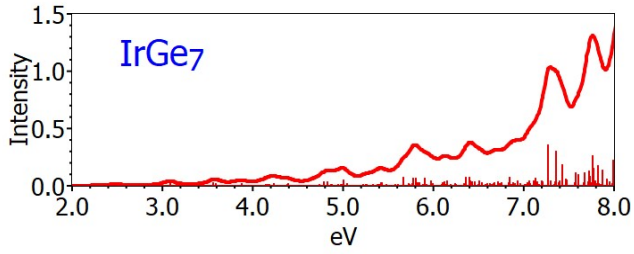
IrGe7
Intensity
eV

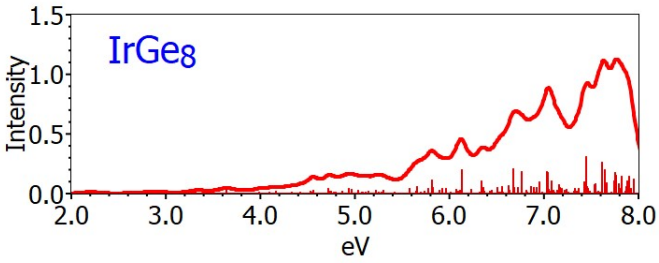
IrGe8
Intensity
eV

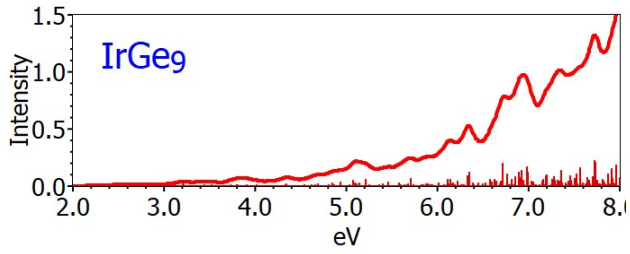
IrGe9
Intensity
eV

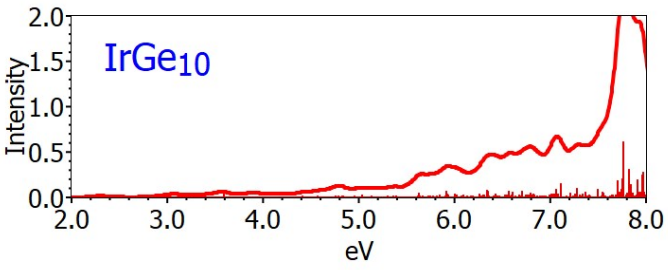
IrGe10
Intensity
eV

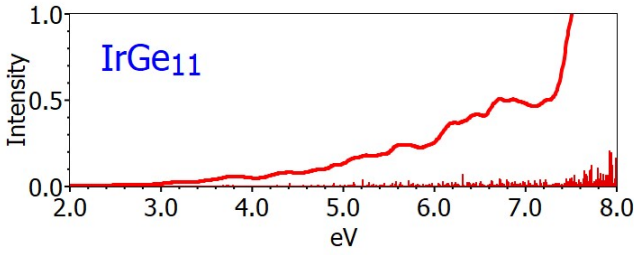
IrGe11
Intensity
eV

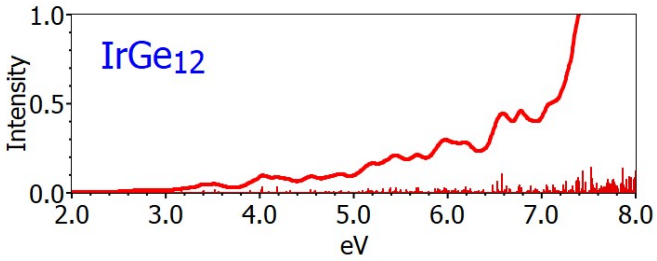
IrGe12
Intensity
eV

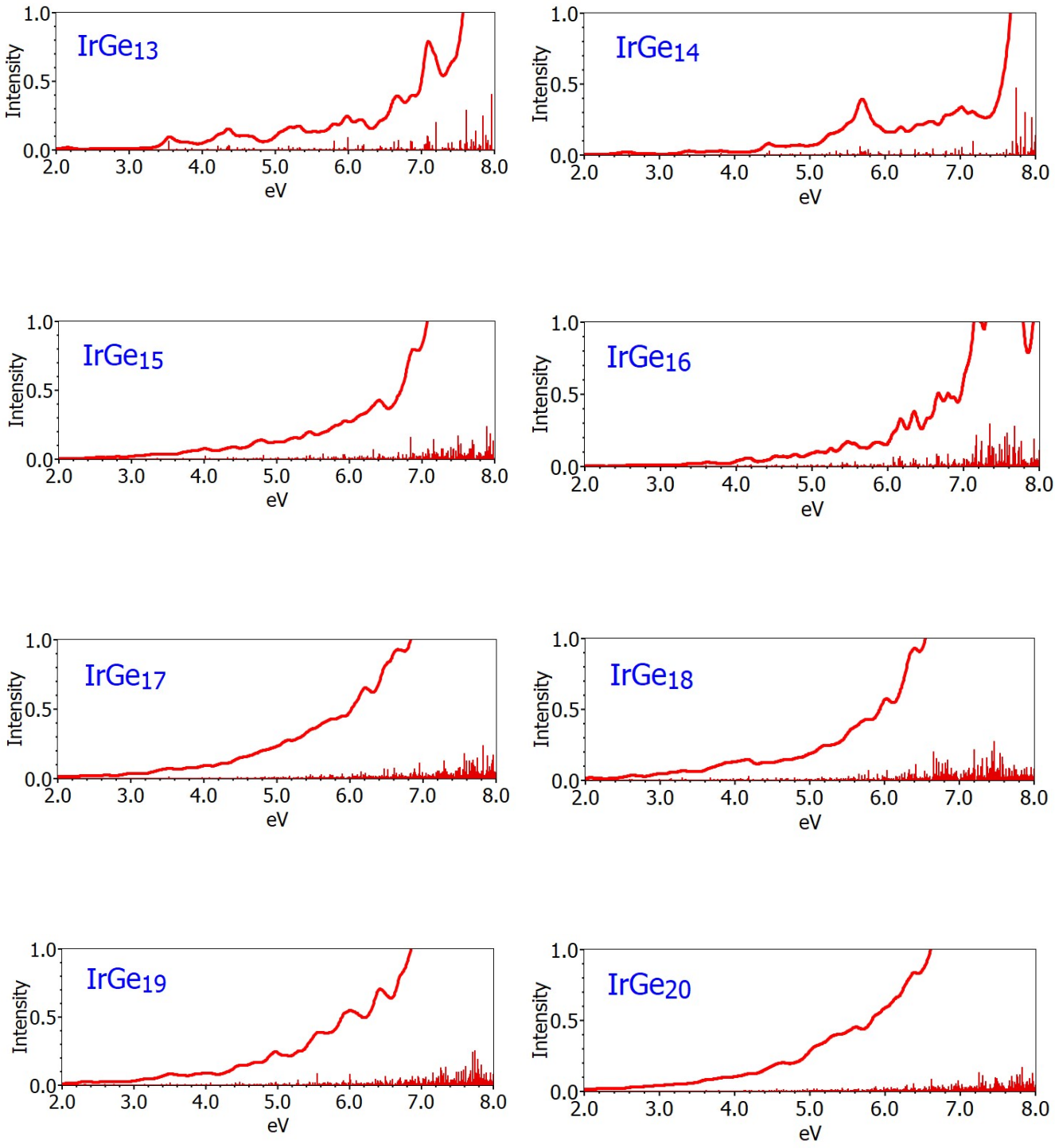

Fig (4. 10): Absorption spectra of $IrGe_n$. The calculated absorption spectra shown in the figure give the oscillator strength as a function of the excitation energy together with a curve obtained by a Lorentz broadening with a full width at half-maximum (fwhm) of 0.08 eV.

4.3.2.8 Atomic charge and electron configuration of Ir atom

Table (IV.2): Atomic charge q_{Ir} (in a.u., |e|) and electron configuration on Ir atom from the natural population analysis.

Cluster	q_{Ir}	Electron configuration on Ir
IrGe	-0.53	$6s^{1.46}\ 5d^{8.05}\ 6p^{0.04}$
$IrGe_2$	-0.72	$6s^{1.06}\ 5d^{8.54}\ 6p^{0.12}\ 7s^{0.01}$
$IrGe_3$	-0.66	$6s^{0.84}\ 5d^{8.54}\ 6p^{0.29}\ 7p^{0.01}$
$IrGe_4$	-0.61	$6s^{0.71}\ 5d^{8.64}\ 6p^{0.25}\ 7p^{0.01}$
$IrGe_5$	-0.81	$6s^{0.78}\ 5d^{8.63}\ 6p^{0.41}\ 7p^{0.01}$
$IrGe_6$	-0.88	$6s^{0.74}\ 5d^{8.62}\ 6p^{0.52}\ 7p^{0.02}$
$IrGe_7$	-1.06	$6s^{0.75}\ 5d^{8.68}\ 6p^{0.63}\ 7p^{0.01}$
$IrGe_8$	-2.10	$6s^{0.72}\ 5d^{8.91}\ 6p^{1.47}\ 6d^{0.01}$
$IrGe_9$	-2.44	$6s^{0.61}\ 5d^{9.04}\ 6p^{1.89}\ 7s^{0.01}\ 6d^{0.01}$
$IrGe_{10}$	-2.11	$6s^{0.62}\ 5d^{8.91}\ 6p^{1.58}\ 6d^{0.01}$
$IrGe_{11}$	-2.54	$6s^{0.61}\ 5d^{9.04}\ 6p^{1.89}\ 7s^{0.01}\ 6d^{0.01}$
$IrGe_{12}$	-2.59	$6s^{0.57}\ 5d^{9.03}\ 6p^{1.98}\ 7s^{0.01}\ 6d^{0.01}$
$IrGe_{13}$	-2.36	$6s^{0.58}\ 5d^{8.97}\ 6p^{1.80}\ 7s^{0.01}\ 6d^{0.01}$
$IrGe_{14}$	-2.59	$6s^{0.57}\ 5d^{9.11}\ 6p^{1.91}\ 7s^{0.01}$
$IrGe_{15}$	-2.18	$6s^{0.58}\ 5d^{9.01}\ 6p^{1.59}\ 7s^{0.01}$
$IrGe_{16}$	-2.33	$6s^{0.57}\ 5d^{9.10}\ 6p^{1.66}\ 7s^{0.01}$
$IrGe_{17}$	-2.26	$6s^{0.57}\ 5d^{9.03}\ 6p^{1.66}\ 6d^{0.01}$
$IrGe_{18}$	-2.07	$6s^{0.57}\ 5d^{9.02}\ 6p^{1.48}\ 7p^{0.01}$
$IrGe_{19}$	-2.33	$6s^{0.57}\ 5d^{9.13}\ 6p^{1.64}$
$IrGe_{20}$	-2.12	$6s^{0.57}\ 5d^{9.05}\ 6p^{1.51}\ 7p^{0.01}$

Atomic charge and electron configuration of Ir metal atom was investigated using natural population analysis. . As we can distinguish for small clusters the atomic charge is relatively low, but starting from n=8 the charge strongly increases to about -2.5 au. All this, was originated from each additional bonding with the Ge atoms in the endohedral structure. Each additional electron captured by the metal atom are mainly associated to 5d and 6p electron configuration.

4.4 Discussion

Our results highlight a transition from exohedral to endohedral structures occurring at n = 8-12. From n=8, Ir is located at an endohedral site, but the encapsulating cage of germanium is fully closed at n = 12. This structural modification strongly affects the electronic properties. The atomic charge and the electron configuration on the metal atom have been estimated through a natural population analysis [139] (Table IV.2). For smaller cluster, Ir is located on exohedral site, and its atomic charge is relatively low (between -0.5 and -1 |e|). But, starting from n = 8, the charge strongly increases to about -2.5 a.u. The transition at n = 8 appears clearly, as q_{Ir} increases from -1.06 to -2.10|e| for n = 7 and 8 respectively. Each additional bonding with Ge leads to an increase of the electronic charge on Ir. In the doublet state, the electron configuration of the isolated atom Ir is $6s^1 5d^8$. The additional electrons captured by the metal atom are mainly associated to 5d and 6p electron configurations. In cage-like structure, the gain on 6p becomes dominant. The large atomic charges indicate that the metal interacts with several Ge atoms, thus playing a stabilizing role of the Ge_n cage.

Among all $IrGe_n$ clusters, $IrGe_{13}$ presents a relatively high stability. It has the larger binding energy (Figure 4.2), a relatively high second-order energy difference (Figure 4.3), and relatively high values for VIP, EAV, and chemical hardness (Figures 4.5-4.7). Beside its atomic structure belongs the C_{4v} symmetry group. In Figure 4.8, we give the density of states (DOS) together with the Kohn-Sham orbitals calculated at PBE/cc-pvtz(Ge)/LanL2DZ(Ir) level. Electronic shells can easily be identified, with their S, P, D, F, and G character. Actually, the reorganization of the valence electrons from Ge and Ir atoms, i.e. $3s_{Ge}$, $3p_{Ge}$ and $5d_{Ir}$, $6s_{Ir}$ electrons, leads to a shell structure where orbitals are delocalized on the whole cluster. Hence, the 61 electrons fill the sequence $1S^2\ 1P^6\ 1D^{10}\ 1F^{14}\ 2S^2\ 2D^{10}\ 2P^6\ 1G^{11}$. Such a pooling of electrons has been already found for VGe_{14} [73], $CuGe_{10}$ [72], $PdGe_{16}$ [131].

To further characterize the clusters, we present in Figure 4.9 and Figure 4.10 the absorption spectra of $IrGe_n$. For the molecule IrGe, the first optical transition is found at 3.6 eV, it corresponds to the excitation from d_{Ir} to $s_{Ir} + p_{Ge}$ orbitals. Then, there is a transition at 4.75 eV with very low oscillator strength, and the absorption becomes intense from 5.7 eV. Most of excitations between 5 and 10 eV correspond to transitions from d_{Ir} to $s_{Ir} + p_{Ge}$orbitals as well. To our knowledge, no experimental and theoretical data is available. For all clusters, a strong response in found in the UV range of energy. When the number of Ge atoms and the number of Ir-Ge bonds increase, the density of states become much higher. Thus, the absorption spectra of endohedral structures show an increasing response in the UV. For

$IrGe_{13}$, a first optical excitation is calculated at 3.55 eV, which corresponds to the transitions from the shells 2P and 2D to the unfilled 1G shell. Between 4 and 5 eV, several excitations from the super shell 1G to 1H are observed. In a very recent work, we have showed that the absorption spectra of $PdGe_n$ and $PtGe_n$ are few dependent on the position of the metal atom (exo versus endohedral position), while the density of states is much higher in the case of surface-bound metal due to a lower symmetry of the structure. The low dependency of the absorption spectra on the geometrical structure can be explained by the electronic arrangement which tends to favor the pooling of valence electrons and the organization in shells where electrons occupy orbitals fully delocalized over the whole volume of the cluster. The pooling of electrons is likely to be somewhat independent of the details of the structure, and consequently the optical absorption as well.

Conclusions

We have performed a systematic investigation of the geometry and the electronic properties of the iridium-doped germanium clusters by using DFT calculations. The growth pattern shows that the iridium atom occupies a peripheral position for very small clusters ($n < 8$). For $n \geq 8$, Ir moves to the endohedral position and becomes highly coordinated. From $n = 12$, it is completely encapsulated by the germanium cage. The substitution of one Ge atom by one Ir atom enhances considerably the stability of the host cluster. The calculated binding energy, the second-order energy difference, the HOMO−LUMO gaps and vertical ionization potential and electron affinities manifest the large stability of the $IrGe_{6,13,15}$ clusters. The HOMO-LUMO gap calculations show that the chemical activity of $IrGe_n$ clusters is generally higher than that of the corresponding pure Ge_{n+1}clusters. The optical absorption spectra highlight a strong response in the UV domain.

4.5 Comparative study on germanium doped clusters

Big number of studies are available in the literature which made investigations on different metal substituted in germanium clusters as presented previously which analyzed several properties, the thing that show us the significant attention that have Ge-based materials garnered recently.

V				Cu
Nb	Ru	Rh	Pd	Ag
Ta		Ir	Pt	Au

The table above collects some of the transition metals which were used as doping agent in germanium clusters made by our group and will be our candidate in this comparative study. As it is clear we will examined the effect of the substitution of the Ge atoms by a transition atom situated in the same column in the periodic table (Z ↗). The most majority of these studies were made at the DFT level using the Perdew-Burke-Ernzerhof (PBE) exchange-correlation density functional [112] using GGA approximation, all packaged in Siesta simulation code [18]. As known, germanium atoms interact with each other through sp^3 hybridization, which assume that pure germanium clusters are not able to form cage structures; thus, the suggestion to be doped with transition atom or substituted by an atom like our case will be somehow very helpful in improving stability of making cages and tailor their properties to be used as building blocks for cluster-assembled materials.

Systematic study was made by substituting vanadium atom into germanium clusters (n=1-19) and compared to the germanium pure clusters [73]. The study enhances the large stability of the VGe_{14} cluster, which presents an O_h symmetry cage-like geometry and a peculiar electronic structure in which the valence electrons of V and Ge atoms are delocalized and exhibit a shell structure associated with the quasi-spherical geometry. Furthermore, an investigation on noble doped germanium clusters was realized [72], whereas results highlight the great stability of the $CuGe_{10}$ cluster in a D_{4d} structure. While that of $AgGe_{15}$ and $AuGe_{15}$ which also presenting a hollow cage high stability but are less stable comparing to $CuGe_{10}$ cluster.

In the same size and class range of transition doped clusters MGe_n (M= Nb and Ta) [120], endohedral structures in which the metal atom is encapsulated are favored for the most stable clusters namely, $NbGe_{15}$ and $TaGe_{15}$ which BE ($NbGe_n$) < BE ($TaGe_n$). In the case of Ru and Rh doped germanium clusters a good stability was obtained for $RuGe_{11}$, $RhGe_{12}$ and $RhGe_{14}$ [140]. Moreover, in this thesis we showed of the remarkable most stable clusters which was in the case of MGe_n (M=Pd,Pt) with n =10, 12, 16 and 18 [131] and n=13 in the case of Ir doped germanium, which presents a high-symmetry cage-like geometry and a peculiar electronic structure in which the valence electrons of Ir and Ge atoms are delocalized and exhibit a shell structure[141].

The figure (4.11) shows the binding energy of different metal doped germanium clusters, it is clear that the growth pattern gain stability for $n \leq 6$ and referring to nature of the

metal we have particular behavior. As n grow over 6 we see a slow rate until n =19. According to binding energy Ag and Au doped Ge_n atoms reveal a low stability among all other clusters, so for Ru, Ir and Ta doped germanium clusters they shows high stability comparing to the rest of clusters. Likewise, among all the clusters seeing here, $TaGe_{15}$ appeared to be the most stable one. Common characteristics in $TMGe_n$ can be drawn; almost the most stable germanium doped clusters present an endohedral cage-like structure which the metal atoms occupy the center of the cage. Electronically, a peculiar structure is noticed in which the valance electron of the metal and Ge atoms are delocalized and exhibit a shell structure.

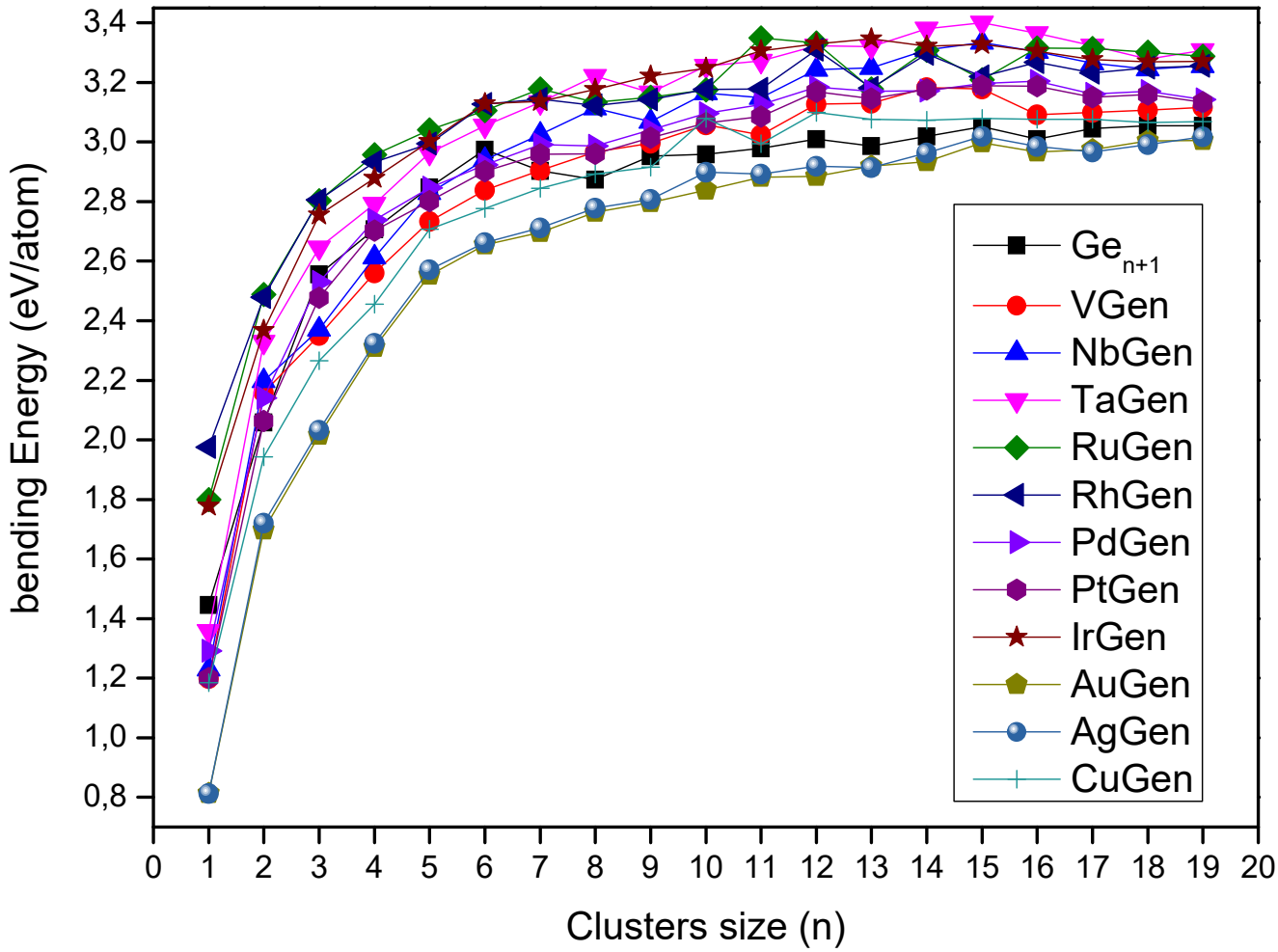

Fig (4. 11): Binding energy per atom (Eb) for the ground-sate isomers of Ge_n [73] and MGe_n (M=V [73], Nb, Ta [120], Ru, Rh [140], Pd, Pt [131], Ir [141], Au, Ag and Cu [72] and n=1-19)

In the case of the Homo-Lumo Gap we distinguish an oscillating behavior for the entire candidates, in which the electronic gap is oscillating between 0.15 eV and 2.45 eV which means between a near metallic and semiconductor behavior. Pronounced clusters with large gap are easy to be pulled, naming for $PdGe_n$ we have n= 5, 7, 9 and 16, and for $PtGe_n$ we have n= 1, 4, 7, 10 and 16. 1.5eV gap was gotten for VGe_{14}. In the near metallic nature of MGe_n clusters we can distinguish MGe_2 (with M= Cu, Au, Ag) and for MGe_5 we have M=Ir and Rh as well as $IrGe_8$, other clusters such as MGe_{12} (M= Ag, Ta, Cu), a gap of 0.15 eV was noticed for $NbGe_{13}$ which making him very easy to be exited. Moreover, MGe_{14} (M= Au and Ag), $AgGe_{16}$ and $NbGe_{18}$ shows low HOMO-LUMO Gap.

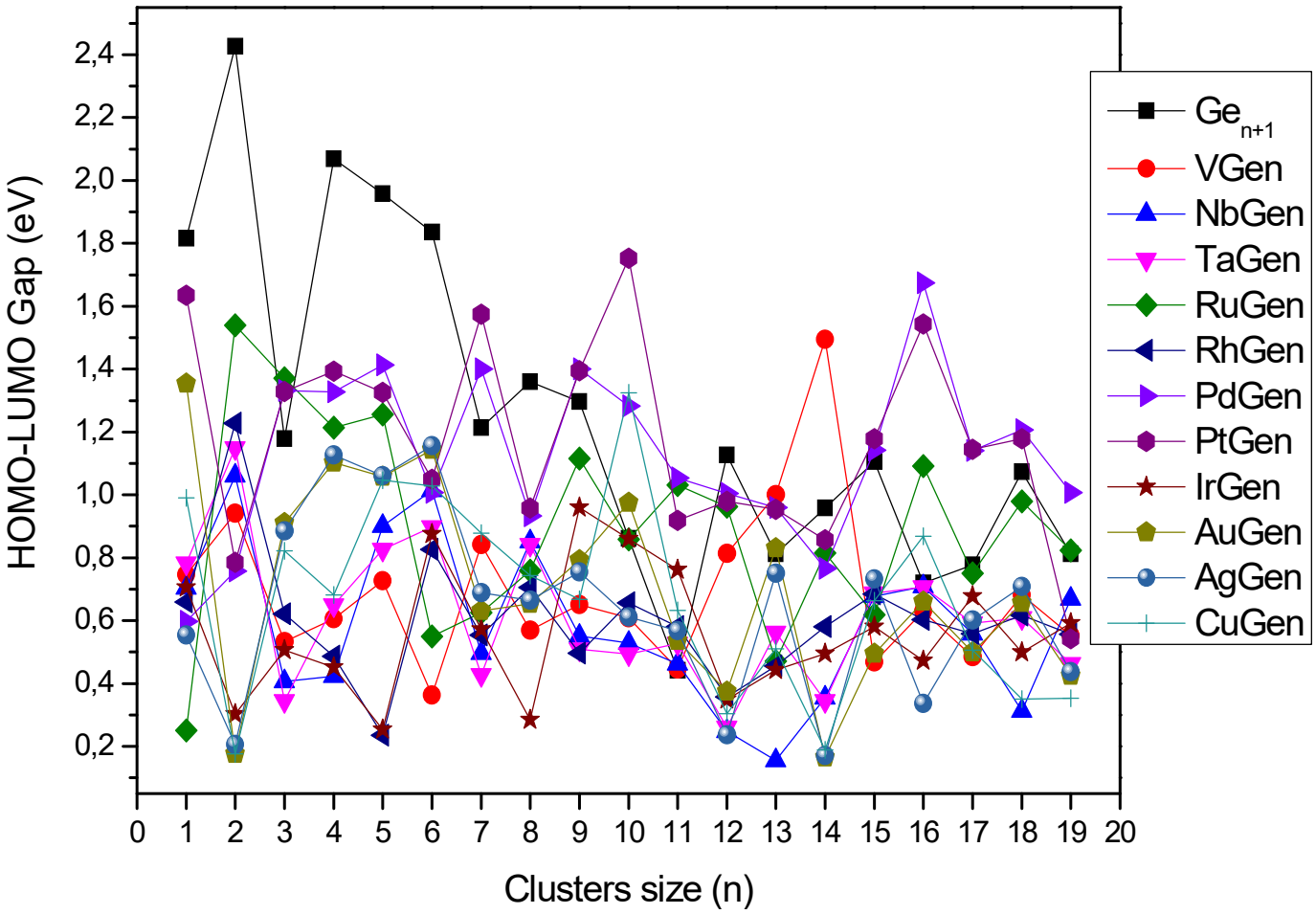

Fig (4. 12): HOMO-LUMO gaps (ΔE) for the ground-sate isomers of [73] and MGe_n (M=V [73], Nb, Ta [120], Ru, Rh [140], Pd, Pt [131], Ir [141], Au, Ag and Cu [72] and n=1-19) clusters.

Further in the literature, several investigations were made to study the effect of doping germanium clusters with different transition metal using various methods. Jin Wang and Ju-Guang Han [77] affirmed the high stability of $CuGe_{10}$ investigated theoretically at the UB3LYP level employing [142, 143] LanL2DZ basis sets, which is confirmed by the experimental measurement of the $CoGe^{10-}$isomer [116]. In another work and using the same approach, investigating Ni-doped germanium clusters [83] they found that the most stable cluster was for n=10. Furthermore, in a work which looked into cobalt doped germanium clusters where the exchange-correlation interaction was treated within the generalized gradient approximation (GGA) using PW91 functional [144], several properties of the Ge_nCo clusters was evaluated and find that the $Ge_{10}Co$ cluster show the strongest stability among these clusters [78], which agrees very well with the experimental results [145]. In an application of germanium clusters doped with dual transition metal for CO oxidation, Zhou et al [12] investigated for the first time M_2Ge_{12} (M=Cr, Mn, Fe, Co and Ni) and were proved to be a good candidate in CO oxidation catalysts on being rigid to segregation, stable in the reactions and exhibit a satisfied thermal stability. In another research paper, using linear combination of atomic orbital's where the exchange-correlation potential was incorporated by GGA proposed by Lee, Yang and Parr popularly known as B3LYP [143] using multiple bases sets. Different properties was studied on $MoGe_n$ clusters [146] which announce the $MoGe_{12}$ with hexagonal prism like structure to be the most stable isomer possesses strong aromatic character and predicted to be a good candidate Mo-based cluster assembled materials.

General conclusion and perspectives

General conclusion

In this thesis work we have presented a comprehensive investigation of the structural, electronic and optical properties of Pd, Pt and Ir atoms substituted in two-dimensional and three-dimensional structures of germanium clusters in range size of 2 to 21 atoms. Applying ab initio calculation methods with the use of DFT tool basing on different approximation under the use of SIESTA code, we described the physical and the chemical properties linked to such of semiconductor which include transition metals as impurities successfully.

In the case of Pd and Pt atoms in the MGe_n clusters a transition from exohedral to endohedral structures of $PdGe_n$ and $PtGe_n$ was remarked for n=10 and n=11, respectively, which leads to totally different electronic properties related to the variation in the structure. The atomic charges on metal atoms have been estimated through a natural population analysis (NPA). For instance, when the Pd atom move from a surface site to an endohedral position the atomic charge increases from −0.1 to −1.6 a.u., which in the case of Pt atom is about −0.4 to about −1.7 a.u. for the exohedral and endohedral structures, respectively. Further and as shown before the electrons captured are mainly associated to 5p or 6p electron configurations after interacting with several Ge atoms, which to say that the transition metal atom eliminates the dangling bonds of germanium atoms.

Interestingly, $PdGe_{16}$ and $PtGe_{16}$ present a relatively high stability. They have the highest stability from both the binding energy and the second-order energy difference. They also show a relatively high HOMO-LUMO gap, and a large chemical hardness. In the case of $PdGe_{16}$ a density of states (DOS) and the Kohn-Sham orbitals were calculated. Its spherical structure was an exhibition of a shell structure due to the 10 valence electrons of Pd and the 3s and 3p valence electrons of Ge. We also distinguished easily the character of the orbitals, though there are some little deviations from a perfect sphere due to explicit location of atoms and the Cs symmetry instead of K_h (the symmetry of the atom). The 74 valence electrons of the cluster are organized with the following occupations: $1S^2\ 1P^6\ 1D^{10}\ 1F^{14}\ 2D^{10}\ 2S^2\ 2P^6\ 1G^{18}\ 1H^6$. The number of electrons does not fit with shell closings numbers, but the pooling of electrons and the organization in shell contributes to the high stability of the cluster. Similar results are found for $PtGe_{16}$. As well and in order to discriminate endohedral and exohedral structures, we have calculated the UV–visible absorption spectra of both cage-like and surface-bound metal structures. Spectra are made for PdG_{16} and $PdGe_{10}$. Unfortunately, they are found to be only few dependent on the position of the metal atom, while the density of states is much higher in the case of surface-bound metal due to a lower symmetry of the structure. Spectra show a slowly increasing response in the visible and near UV domain, and a strong signal above.

In the sample of Ir atom substituted in Gen clusters with the same size range, we highlight a transition from exohedral to endohedral structures occurring at n = 8-12. From n=8, Ir is located at an endohedral site, but the encapsulating cage of germanium is fully closed at n = 12. And as it is shown previously, the electronic properties of the cluster are strongly affected by the structural modification. Thus, the atomic charge and the electron configuration on the metal atom have been estimated through a natural population analysis (NPA). For smaller cluster, Ir is located on exohedral site, and its atomic charge is relatively

low (between -0.5 and -1 |e|). But, starting from n = 8, the charge strongly increases to about -2.5 a.u. The transition at n = 8 appears clearly, as q_{Ir} increases from -1.06 to -2.10|e| for n = 7 and 8 respectively. Each additional bonding with Ge leads to an increase of the electronic charge on Ir. In the doublet state, the electron configuration of the isolated atom Ir is $6s^1 5d^8$. The additional electrons captured by the metal atom are mainly associated to 5d and 6p electron configurations. In cage-like structure, the gain on 6p becomes dominant. The large atomic charges indicate that the metal interacts with several Ge atoms, thus playing a stabilizing role of the Ge_n cage. Among all $IrGe_n$ clusters, $IrGe_{13}$ presents a relatively high stability. It has the larger binding energy, a relatively high second-order energy difference, and relatively high values for VIP, EAV, and chemical hardness. Beside its atomic structure belongs the C_{4v} symmetry group. Furthermore, we made the density of states (DOS) together with the Kohn-Sham orbitals calculated at PBE/cc-pvtz(Ge)/LanL2DZ(Ir) level. Electronic shells can easily be identified, with their S, P, D, F, and G character. Actually, the reorganization of the valence electrons from Ge and Ir atoms, i.e. $3s_{Ge}$, $3p_{Ge}$ and $5d_{Ir}$, $6s_{Ir}$ electrons, leads to a shell structure where orbitals are delocalized on the whole cluster. Hence, the 61 electrons fill the sequence $1S^2\ 1P^6\ 1D^{10}\ 1F^{14}\ 2S^2\ 2D^{10}\ 2P^6\ 1G^{11}$. To further characterize the clusters, we presented the absorption spectra of $IrGe_n$. For the molecule IrGe, the first optical transition is found at 3.6 eV, it corresponds to the excitation from d_{Ir} to $s_{Ir} + p_{Ge}$ orbitals. Then, there is a transition at 4.75 eV with very low oscillator strength, and the absorption becomes intense from 5.7 eV. Most of excitations between 5 and 10 eV correspond to transitions from d_{Ir} to $s_{Ir} + p_{Ge}$ orbitals as well. To our knowledge, no experimental and theoretical data is available. For all clusters, a strong response is found in the UV range of energy. When the number of Ge atoms and the number of Ir-Ge bonds increase, the density of states become much higher. Thus, the absorption spectra of endohedral structures show an increasing response in the UV. For $IrGe_{13}$, a first optical excitation is calculated at 3.55 eV, which corresponds to the transitions from the shells 2P and 2D to the unfilled 1G shell. Between 4 and 5 eV, several excitations from the super shell 1G to 1H are observed. And as we have showed in the absorption spectra of $PdGe_n$ and $PtGe_n$ that they are few dependent on the position of the metal atom (exo versus endohedral position), while the density of states is much higher in the case of surface-bound metal due to a lower symmetry of the structure. The low dependency of the absorption spectra on the geometrical structure can be explained by the electronic arrangement which tends to favor the pooling of valence electrons and the organization in shells where electrons occupy orbitals fully delocalized over the whole volume of the cluster. The pooling of electrons is likely to be somewhat independent of the details of the structure, and consequently the optical absorption as well.

Perspectives

Our main goal in the realization of this thesis was to have a look into the richness of germanium clusters properties and as well the modifications when substituting transition atoms into it. We tried to understand and explain the origin of the remarkable stability and varied like structures with the capability of such clusters to respond to an optical excitation with variant super shell excitation to predict eventual building blocks in purpose to use them as assembled units for nanomaterials. One of the perspectives is to make studies about the previous clusters or the most remarked one on the adsorption on different monolayer's

surfaces of chosen element or even compounds with specific uses in the nano-industry. Further investigation on the possible use of stable clusters of Pd, Pt and Ir doped germanium cage-like in opto-catalytic application and why not to use them on oxydo-reduction of nitric oxide (NO), and carbon monoxide (CO). At the attention to make an experimental work according to this class of matter and developing new areas of application.

References

References

[1] Jena, P. Clusters and Nanomaterials for Sustainable Energy. ACS Energy Letters, 428–429. (2020).

[2] Selvan S.T.; Narayanan K. Semiconducting Nanoparticles or Quantum Dots for Theranostics. In: Introduction to Nanotheranostics. SpringerBriefs in Applied Sciences and Technology. Springer, Singapore. (2016).

[3] Luo, J.; Bai, H.; Yang, P.; & Cai, J. One-pot aqueous synthesis of germanium-doped cadmium sulfide quantum dots as fluorescent probes for cell imaging. Materials Science in Semiconductor Processing, 34, 1–7. (2015).

[4] Muthuswamy, E.; Zhao, J.; Tabatabaei, K.; Amador, M. M.; Holmes, M. A.; Osterloh, F. E., & Kauzlarich, S. M.. Thiol-Capped Germanium Nanocrystals: Preparation and Evidence for Quantum Size Effects. Chemistry of Materials, 26(6), 2138–2146. (2014).

[5] Boote, B. W.; Men, L.; Andaraarachchi, H. P.; Bhattacharjee, U.; Petrich, J. W.; Vela, J.; & Smith, E. A.. Germanium–Tin/Cadmium Sulfide Core/Shell Nanocrystals with Enhanced Near-Infrared Photoluminescence. Chemistry of Materials, 29(14), 6012–6021. (2017).

[6] Philip Seidenberg, "From Germanium to Silicon, A History of Change in the Technology of the Semiconductors," in Facets: New Perspectivies on the History of Semiconductors, ed. Andrew Goldstein & William Aspray (New Brunswick: IEEE Center for the History of Electrical Engineering), 35-74. (1997).

[7] Sasan, K.; Lange, A.; Yee, T. D.; Dudukovic, N. A.; Nguyen, D. T.; Johnson, M. A.; … Dylla-Spears, R. J.. Additive manufacturing of optical quality germania–silica glasses. ACS Applied Materials & Interfaces. (2020).

[8] Teredesai, P. V.; Anderson, D. T.; Hauser, N.; Lantzky, K.; & Yarger, J. Infrared spectroscopy of germanium dioxide (GeO_2) glass at high pressure. Physics and Chemistry of Glasses, 46(4), 345-349. (2005).

[9] Paulus, U. A.; Wokaun, A.; Scherer, G. G.; Schmidt, T. J.; Stamenkovic, V.; Radmilovic, V.; Markovic, N. M; and Ross, P. N.. Oxygen Reduction on Carbon-Supported Pt-Ni and Pt-Co Alloy Catalysts. The Journal of Physical Chemistry B, 106(16) 4181-4191 (2002).

[10] Suo, Y. ; Zhuang, L. ; & Lu, J ;. First-Principles Considerations in the Design of Pd-Alloy Catalysts for Oxygen Reduction. Angewandte Chemie, 119(16), 2920–2922. (2007).

[11] Ham, H. C.; Manogaran, D.; Lee, K. H.; Kwon, K.; Jin, S.; You, D. J.; … Hwang, G. S;. Communication: Enhanced oxygen reduction reaction and its underlying mechanism in Pd-Ir-Co trimetallic alloys. The Journal of Chemical Physics, 139(20), 201104. (2013).

[12] Zhou, S.; Yang, X.; Shen, Y.; King, R. B.; & Zhao, J;. Dual transition metal doped germanium clusters for catalysis of CO oxidation. Journal of Alloys and Compounds. (2019).

[13] Bals, S.; Van Aert, S.; Romero, C. P.; Lauwaet, K.; Van Bael, M. J.; Schoeters, B.; … Van Tendeloo, G;. Atomic scale dynamics of ultra-small germanium clusters. Nature Communications, 3(1). (2012).

[14] Ely, T. O.; Pan, C.; Amiens, C.; Chaudret, B.; Dassenoy, F.; Lecante, P.; Casanove; M.-J.; Mosset, A.; Respaud, M.; and Broto, J.-M;. Nanoscale Bimetallic CoxPt1-x Particles Dispersed in Poly(vinylpyrrolidone): Synthesis from Organometallic Precursors and Characterization. The Journal of Physical Chemistry B, 104(4) 695-702 (2000).

[15] Castald, L. i; Giannakopoulos, K.; Travlos, A.; Niarchos, D.; Boukari, S. and Beaurepaire, E;. Superparamagnetic and ferromagnetic CoPt nanoparticles deposited on silicon dioxide. Journal of Physics: Conference Series, 10(1) 155 (2005).

[16] O'Connor, C. J.; Sims, J. A.; Kumbhar, A.; Kolesnichenko, V. L.; Zhou, W. L; and Wiemann, J. A;. Magnetic properties of FePtx/Au and CoPtx/Au core-shell nanoparticles. Journal of Magnetism and Magnetic Materials, 226(2) 1915-1917 (2001).

[17] Sun, X.; Jia, Z. Y.; Huang, Y. H.; Harrell, J. W.; Nikles, D. E.; Sun, K;. and Wang, L. M;. Synthesis and magnetic properties of CoPt nanoparticles. Journal of Applied Physics, 95(11) 6747{6749 (2004).

[18] Artacho, E. ; Cela, J. M. ; Gola, J. D. ; Garcia, A. ; Junquera, J. ; Ordejon, P. ; Sanchez-Portal, D; and Soler, J. M.; The SIESTA group, (1996-2016).

[19] Thomas, H, L. The Calculation of Atomic Fields. Mathematical Proceedings of the Cambridge Philosophical Society, 23, 542-548. (1927).

[20] Fermi, E. Eine statistische Methode zur Bestimmung einiger Eigenschaften des Atoms und ihre Anwendung auf die Theorie des periodischen Systems der Elemente. Z. Physik **48,** 73–79, (1928).

[21] Schrödinger, E. Quantisierung als Eigenwertproblem. Annalen Der Physik, 384(4), 361–376. (1926).

[22] Born, M.; & Oppenheimer, R ; Zur Quantentheorie der Molekeln. Annalen der Physik, 389, 457-484, (1927).

[23] Cramer, C. J.; "Essentials of Computational Chemistry Theories and Models‘' (England: John Wiley & Sons Ltd, 2004).

[24] Hartree, D. R; The Wave Mechanics of an Atom with a Non-Coulomb Central Field. Part I. Theory and Methods. Mathematical Proceedings of the Cambridge Philosophical Society, 24(01), 89, (1928).

[25] Samir Matar, Mono-electronic approach, Institute of condensed matter chemistry of Bordeaux (2004).

[26] Silk, M. G.; & Weight, J. P;. Ultrasonic transducers for nondestructive testing. NDT International, 18(4), 219–220. (1985).

[27]Fock, V. Naherungsmethode zur Losung des quantenmechanischen Mehrkorperproblems. Zeitschrift For Physik, 61(1-2), 126–148. (1930).

[28] Adel F. Al Alam. Modélisation au sein de la DFT des propriétés des structures électronique et magnétique et de liaison chimique des Hydrures d'Intermétalliques. Matériaux. Université Sciences et Technologies - Bordeaux I, Français. (2009).

[29] Slater, J. C. Note on the Effect of Pressure on the Curie Point of Iron-Nickel Alloys. Physical Review, 58(1), 54–56. (1940).

[30] Maylis Orio. Etude par la Théorie de la Fonctionnelle de la Densité des propriétés électroniques et magnétiques de complexes de fer. Application aux systèmes de types Catalase et Fer-Soufre. Autre. Université Joseph-Fourier - Grenoble I, Français. (2007).

[31] Dirac, P. A. M. Note-t-on Exchange Phenomena in the Thomas Atom. Mathematical Proceedings of the Cambridge Philosophical Society, 26 (03), 376. (1930).

[32] Hohenberg, P.; & Kohn, W. Inhomogeneous Electron Gas. Physical Review, 136(3B), B864–B871, (1964).

[33] Levy, M. Universal variational functionals of electron densities, first-order density matrices, and natural spin-orbitals and solution of the v-representability problem. Proceedings of the National Academy of Sciences, 76(12), 6062–6065, (1979).

[34] Levy, M. Electron densities in search of Hamiltonians. Physical Review A, 26(3), 1200–1208. (1982).

[35] Kohn, W.; Sham, L. J. Self-Consistent Equations Including Exchange and Correlation Effects. Phys. Rev., 140, 1133−1138. (1965).

[36] Martin. R. M.; Electronic Structure: Basic Theory and Practical Methods. Cambridge

University Press, 624, (2004).

[37] Dirac, P. A. M. Quantum Mechanics of Many-Electron Systems. Proceedings of the Royal Society A: Mathematical, Physical and Engineering Sciences, 123(792), 714–733. (1929).

[38] Vosko, S. H.; Wilk, L.; & Nusair, M. Accurate spin-dependent electron liquid correlation energies for local spin density calculations: a critical analysis. Canadian Journal of Physics, 58(8), 1200–1211. (1980).

[39] Ceperley, D.; and Alder, B.J.; The Low Density Phases of the Electron Gas, Journal de Physique C-7, 295 (1980).

[40] Van Leeuwen, R., & Baerends, E. J. Exchange-correlation potential with correct asymptotic behavior. Physical Review A, 49(4), 2421–2431. (1994).

[41] Perdew, J. P.; Chevary, J.A.; Vosko, S. H.; Jackson, K. A.; Pedreson, M. R.; Singh, D. J.; Fiolhais, C.; “Atoms, Molecules, Solid and Surfaces: Application of the generalized gradient approximation for exchange and correlation, Phys. Rev. B 46, 6671-6687, (1992).

[42] Rabilloud Franck. Etute théorique et expérimentale des agrégats de bromure d'argent. Physique Atomique [physics.atom-ph]. Université Paul Sabatier - Toulouse III, Français, (2000).

[43] Micaael Oliveira, Relativistic effets in the Optical response of law-dimensional functional theory framework, University of Coimbra, (2008).

[45] Richard, N;. Actinides and Rare Earths under pressure: pseudo-potential approach, Atomic Energy Commission, 22. Ile-de-France. (2002).

[46] Hamman, D. R.; Schulter, M.; and Chiang. Phys. Rev. Lelt 43:1494. (1979).

[47] Vanderbilt, D.; Soft self-consistent pseudopotentials in a generalized eigenvalue formalism. Physical Review B, 41(11), 7892–7895, (1990).

[48] Goedecker, S.; Teter, M.; and J. Hutter.; Phys. B, 54:1703. (1996).

[49] Hartwigsen, C.; Goedecker, S.; and Hutter, J.; Phys. Rev, B, 58:3641, (1998).

[50] Troullier, N.; Martins, J. L.; Efficient Pseudopotentials for PlaneWave Calculations. Phys. Rev. B: Condens. Matter Mater. Phys. 43, 1993−2006. (1991).

[51] Lennard-Jones, J. E.; The electronic structure of some diatomic molecules. Transactions of the Faraday Society, 25, 668. (1929).

[52] Debye, P.;"Näherungsformeln für die Zylinderfunktionen für große Werte des Arguments und unbeschränkt veränderliche Werte des Index", Mathematische Annalen, **67** (4): 535–558, (1909).

[53] Magnus R. Hestenes and Eduard Stiefel, Methods of Conjugate Gradients for Solving Linear Systems, Journal of Research of the National Bureau of Standards 49 (1952), 409–436.

[54] Troullier, N., & Martins, J. L. Efficient pseudopotentials for plane-wave calculations. Physical Review B, 43(3), 1993–2006. (1991).

[55] Burke, K.; and friends, the ABC of DFT http:/dft.uci.edu/materials/Book ABC DFT/gamma, 104. (2007).

[56] Yoo, S.; Zeng, X. C. Search for Global-Minimum Geometries of Medium-Sized Germanium Clusters. II. Motif-Based Low-Lying Clusters Ge21–Ge29. The Journal of Chemical Physics, 124 (18), 184309. (2006).

[57] Wang, L.; Zhao, J. Competition between Supercluster and Stuffed Cage Structures in Medium-Sized Gen (N=30–39) Clusters. The Journal of Chemical Physics, 128 (2), 024302. (2008).

[58] Wielgus, P.; Roszak, S.; Majumdar, D.; Saloni, J.; Leszczynski, J. Theoretical Studies on the Bonding and Thermodynamic Properties of GenSim (M+n=5) Clusters: The Precursors of Germanium/Silicon Nanomaterials. The Journal of Chemical Physics, 128 (14), 144305. (2008).

[59] King, R. B.; Silaghi-Dumitrescu, I.; Lupan, A. Density Functional Theory Study of Eight-Atom Germanium Clusters: Effect of Electron Count on Cluster Geometry. Dalton Transactions, No. 10, 1858. (2005).

[60] King, R. B.; Silaghi-Dumitrescu, I. Density Functional Theory Study of Nine-Atom Germanium Clusters: Effect of Electron Count on Cluster Geometry. Inorganic Chemistry, 42 (21), 6701–6708. (2003).

[61] Zhao, L.-Z.; Lu, W.-C.; Qin, W.; Wang, C. Z.; Ho, K. M. Comparison of the Growth Patterns of Si_n and Ge_n Clusters (n = 25−33). The Journal of Physical Chemistry A, 112 (26), 5815–5823. (2008).

[62] Islam, M. S.; Ray, A. K. Many-Body Perturbation Theory Applied to Small Germanium Clusters. Chemical Physics Letters, 153 (6), 496–502. (1988).

[63] Deutsch, P. W.; Curtiss, L. A. Electron Affinities of Germanium Anion Clusters, Ge_n^- (n=2±5). Chemical Physics Letters, 6. 344, 101-106. (2001).

[64] Deutsch, P.W.; Curtiss, L.A..; Blaudeau, j.p. Binding energies of germanium clusters, Ge_n (n = 2-5). Chemical Physics Letters, 270, 413-418. (1997).

[65] Zhao, L.-Z.; Lu, W.-C.; Qin, W.; Zang, Q.-J.; Wang, C. Z.; Ho, K. M. Fragmentation Behavior of Gen Clusters (2⩽n⩽33). Chemical Physics Letters, 455 (4–6), 225–231. (2008).

[66] Luo, H. B.; Li, X. B.; Zhang, Q. E.; Chen, M. D.; Cheng, Y.-K. A Density Functional Theory Study of Germanium Ge_{11} Clusters. Journal of Molecular Structure: THEOCHEM, 674 (1–3), 83–86. (2004).

[67] Li, B.-X.; Liang, F.-S.; Zhu, Y.; Xu, J.; Lai, G. Stable Structures of Neutral and Ionic Ge_n (N=11–19) Clusters. Journal of Molecular Structure: THEOCHEM, 756 (1–3), 19–24. (2005).

[68] King, R. B.; Silaghi-Dumitrescu, I.; Lupan, A. New Low Symmetry Low Energy Structures of 11-Atom Bare Germanium Clusters: A Density Functional Theory Study. Chemical Physics, 327 (2–3), 344–350. (2006).

[69] Li, B.-X.; Cao, P.-L.; Song, B.; Ye, Z.-Z. Electronic and Geometric Structures of Gen− and Gen+ (N=5–10) Clusters in Comparison with Corresponding Sin Ions. Physics Letters A, 307 (5–6), 318–325. (2003).

[70] Liang, F.-S.; Li, B.-X. Stable Structures of Ge_n Clusters. Physics Letters A, 328 (4–5), 407–413. (2004).

[71] ur Rehman, H.; Springborg, M.; Dong, Y. Structural and Electronic Properties of Si n, Ge n, and Si_nGe_n Clusters. The Journal of Physical Chemistry A, 115 (10), 2005–2015. (2011).

[72] Mahtout, S.; Siouani, C.; Safer, S; Rabilloud, F. Growth Behavior and Electronic Structure of Noble Metal-Doped Germanium Clusters. The Journal of Physical Chemistry A, 122 (2), 662–677. (2018).

[73] Siouani, C.; Mahtout, S.; Safer, S.; Rabilloud, F. Structure, Stability, and Electronic and Magnetic Properties of VGe_n (n = 1–19) Clusters. The Journal of Physical Chemistry A, 121 (18), 3540–3554. (2017).

[74] Mahtout, S.; Tariket, Y. Electronic and Magnetic Properties of $CrGe_n$ ($15 \leqslant n \leqslant 29$) Clusters: A DFT Study. Chemical Physics, 472, 270–277. (2016).

[75] Djaadi, S.; Eddine Aiadi, K.; Mahtout, S. First Principles Study of Structural, Electronic and Magnetic Properties of $SnGe_n$ (0,±1) (n= 1–17) Clusters. Journal of Semiconductors, 39 (4), 042001. (2018).

[76] Bulusu, S.; Yoo, S.; Zeng, X. C. Search for Global Minimum Geometries for Medium Sized Germanium Clusters: Ge12–Ge20. The Journal of Chemical Physics, 122 (16), 164305. (2005).

[77] Wang, J.; Han, J.-G. A Computational Investigation of Copper-Doped Germanium and Germanium Clusters by the Density-Functional Theory. The Journal of Chemical Physics, 123 (24), 244303. (2005).

[78] Jing, Q.; Tian, F.; Wang, Y. No Quenching of Magnetic Moment for the Ge_nCo (N=1–13) Clusters: First-Principles Calculations. The Journal of Chemical Physics, 128 (12), 124319. (2008).

[79] Deng, X.-J.; Kong, X.-Y.; Xu, X.-L.; Xu, H.-G.; Zheng, W.-J. Structural and Magnetic Properties of $CoGe_n^-$ (n =2-11) Clusters: Photoelectron Spectroscopy and Density Functional Calculations. ChemPhysChem, 15 (18), 3987–3993. (2014).

[80] Kumar, M.; Bhattacharyya, N.; Bandyopadhyay, D. Architecture, Electronic Structure and Stability of $TM@Ge_n$ (TM = Ti, Zr and Hf; n = 1-20) Clusters: A Density Functional Modeling. Journal of Molecular Modeling, 18 (1), 405–418. (2012).

[81] Bandyopadhyay, D. Architectures, Electronic Structures, and Stabilities of Cu-Doped Ge n Clusters: Density Functional Modeling. Journal of Molecular Modeling, 18 (8), 3887–3902. (2012).

[82] Singh, A. K.; Kumar, V.; Kawazoe, Y. Thorium Encapsulated Caged Clusters of Germanium: $Th@Ge_n$, n = 16, 18, and 20. The Journal of Physical Chemistry B, 109 (32), 15187–15189. (2005).

[83] Wang, J.; Han, J.-G. A Theoretical Study on Growth Patterns of Ni-Doped Germanium Clusters. The Journal of Physical Chemistry B, 110 (15), 7820–7827.(2006).

[84] Wang, J.; Han, J.-G. Geometries and Electronic Properties of the Tungsten-Doped Germanium Clusters: WGe_n (n = 1−17). The Journal of Physical Chemistry A, 110 (46), 12670–12677. (2006).

[85] Wang, J.; Han, J.-G. Geometries, Stabilities, and Vibrational Properties of Bimetallic Mo 2 -Doped Ge_n (n = 9−15) Clusters: A Density Functional Investigation. The Journal of Physical Chemistry A, 112 (14), 3224–3230. (2008).

[86] Gopakumar, G.; Ngan, V. T.; Lievens, P.; Nguyen, M. T. Electronic Structure of Germanium Monohydrides Ge_nH, n = 1−3. The Journal of Physical Chemistry A, 112 (47), 12187–12195. (2008).

[87] Zdetsis, A. D. Silicon−Bismuth and Germanium−Bismuth Clusters of High Stability. The Journal of Physical Chemistry A, 113 (44), 12079–12087. (2009).

[88] Bandyopadhyay, D.; Sen, P. Density Functional Investigation of Structure and Stability of Ge nand Ge_nNi (n = 1−20) Clusters: Validity of the Electron Counting Rule. The Journal of Physical Chemistry A, 114 (4), 1835–1842. (2010).

[89] Shi, S.; Liu, Y.; Zhang, C.; Deng, B.; Jiang, G. A Computational Investigation of Aluminum-Doped Germanium Clusters by Density Functional Theory Study. Computational and Theoretical Chemistry, 1054, 8–15. (2015).

[90] Kapila, N.; Garg, I.; Jindal, V. K.; Sharma, H. First Principle Investigation into Structural Growth and Magnetic Properties in Ge_nCr Clusters for n=1–13. Journal of Magnetism and Magnetic Materials, 324 (18), 2885–2893. (2012).

[91] Sosa-Hernández, E. M.; Alvarado-Leyva, P. G. Magnetic Properties of Stable Structures of Small Binary Clusters. Physica E: Low-dimensional Systems and Nanostructures, 42 (1), 17–21. (2009).

[92] Li, X.; Su, K.; Yang, X.; Song, L.; Yang, L. Size-Selective Effects in the Geometry and Electronic Property of Bimetallic Au–Ge Nanoclusters. Computational and Theoretical Chemistry, 1010, 32–37. (2013).

[93] Kapila, N.; Jindal, V. K.; Sharma, H. Structural, Electronic and Magnetic Properties of Mn, Co, Ni in Ge_n for (n=1–13). Physica B: Condensed Matter, 406 (24), 4612–4619. (2011).

[94] Zhao, W.-J.; Wang, Y.-X. Geometries, Stabilities, and Magnetic Properties of MnGen (N=2–16) Clusters: Density-Functional Theory Investigations. Journal of Molecular Structure: THEOCHEM, 901 (1–3), 18–23. (2009).

[95] Hou, X.-J.; Gopakumar, G.; Lievens, P.; Nguyen, M. T. Chromium-Doped Germanium Clusters $CrGe_n$ (n= 1−5): Geometry, Electronic Structure, and Topology of Chemical Bonding. The Journal of Physical Chemistry A, 111 (51), 13544–13553. (2007).

[96] Tang, C.; Liu, M.; Zhu, W.; Deng, K. Probing the Geometric, Optical, and Magnetic Properties of 3d Transition-Metal Endohedral Ge12M (M=Sc–Ni) Clusters. Computational and Theoretical Chemistry, 969 (1–3), 56–60. (2011).

[97] Han, J.-G. A Computational Study on Electronic Structures of Ge_nF and $Ge_nFŽn$ s 3–6/ Clusters by Density Functional Theory, 6. (2000).

[98] Lu, J.; Nagase, S. Metal-Doped Germanium Clusters MGens at the Sizes of N=12 and 10: Divergence of Growth Patterns from the MSi_n Clusters. Chemical Physics Letters, 372 (3–4), 394–398. (2003).

[99] Negishi, Y.; Kawamata, H.; Hayase, T.; Gomei, M.; Kishi, R.; Hayakawa, F.; Nakajima, A.; Kaya, K. Photoelectron Spectroscopy of Germanium-Fluorine Binary Cluster Anions: The HOMO-LUMO Gap Estimation of Gen Clusters. Chemical Physics Letters, 269 (3–4), 199–207. (1997).

[100] Han, J.-G.; Zhang, P.-F.; Li, Q.-X.; Gao, H.; Cao, G.-Y.; Sheng, L.-S.; Zhang, Y.-W. A Theoretical Investigation of GenSn (N=1–4) Clusters. Journal of Molecular Structure: THEOCHEM, 624 (1–3), 257–265. (2003).

[101] Ma, S.; Wang, G. Structures of Medium Size Germanium Clusters. Journal of Molecular Structure: THEOCHEM, 767 (1–3), 75–79. (2006).

[102] Wang, J.; Han, J.-G. The Growth Behaviors of the Zn-Doped Different Sized Germanium Clusters: A Density Functional Investigation. Chemical Physics, 342 (1–3), 253–259. (2007).

[103] Zhao, W.-J.; Wang, Y.-X. Geometries, Stabilities, and Electronic Properties of (n=9–16) Clusters: Density-Functional Theory Investigations. Chemical Physics, 352 (1–3), 291–296. (2008).

[104] Goswami, S.; Saha, S.; Yadav, R. K. Structural, Electronic and Vibrational Properties of Ge_xC_y (x+y=2–5) Nanoclusters: A B3LYP-DFT Study. Physica E: Low-dimensional Systems and Nanostructures, 74, 175–192. (2015).

[105] King, R. B.; Silaghi-Dumitrescu, I.; Uţă, M. M. Density Functional Theory Study of 10-Atom Germanium Clusters: Effect of Electron Count on Cluster Geometry. Inorganic Chemistry, 45 (13), 4974–4981. (2006).

[106] Deng, X.-J.; Kong, X.-Y.; Xu, H.-G.; Xu, X.-L.; Feng, G.; Zheng, W.-J. Photoelectron Spectroscopy and Density Functional Calculations of VGe n– (n = 3–12) Clusters. The Journal of Physical Chemistry C, 119 (20), 11048–11055. (2015).

[107] King, R. B.; Silaghi-Dumitrescu, I.; Uţă, M. M. Endohedral Nickel, Palladium, and Platinum Atoms in 10-Vertex Germanium Clusters: Competition between Bicapped Square Antiprismatic and Pentagonal Prismatic Structures. The Journal of Physical Chemistry A, 113 (3), 527–533. (2009).

[108] Ngan, V. T.; De Haeck, J.; Le, H. T.; Gopakumar, G.; Lievens, P.; Nguyen, M. T. Experimental Detection and Theoretical Characterization of Germanium-Doped Lithium Clusters Li_nGe (n = 1−7). The Journal of Physical Chemistry A, 113 (32), 9080–9091. (2009).

[109] Nagendran, S.; Sen, S. S.; Roesky, H. W.; Koley, D.; Grubmüller, H.; Pal, A.; Herbst-Irmer, R. RGe(I)Ge(I)R Compound (R = PhC(N t Bu) 2) with a Ge−Ge Single Bond and a Comparison with the Gauche Conformation of Hydrazine. Organometallics, 27 (21), 5459–5463. (2008).

[110] Jaiswal, S.; Kumar, V. Growth Behavior and Electronic Structure of Neutral and Anion $ZrGe_n$ (n = 1–21) Clusters. Computational and Theoretical Chemistry, 1075, 87–97. (2016).

[111] Jin, Y.; Tian, Y.; Kuang, X.; Lu, C.; Cabellos, J. L.; Mondal, S.; Merino, G. Structural and Electronic Properties of Ruthenium-Doped Germanium Clusters. The Journal of Physical Chemistry C, 120 (15), 8399–8404. (2016).

[112] Perdew, J. P.; Burke, K.; Ernzerhof, M. Generalized Gradient Approximation Made Simple. Phys. Rev. Lett., 77, 3865−3868. (1996).

[113] Kleinman, L.; Bylander, D. M. Efficacious Form for Model Pseudopotentials. Phys. Rev. Lett., 48, 1425−1428. (1982).

[114] Frisch, M.J. et al., Gaussian09, Revision D.01, Gaussian Inc., Wallingford CT, (2013).

[115] Gadiyak GV, Morokov YN, Mukhachev AG, Chernov SV Electron density functional method for molecular system calculations. J Struct Chem 22:670–674. (1982).

[116] Kingcade JE, Nagarathna-Naik HM, Shim I, Gingerich KA Electronic structure and bonding of the molecule Ge_2 from allelectron ab initio calculations and equilibrium measurements. J Phys Chem 90:2830–2834. (1986).

[117] Parr. R. G, Yang. W, Density Functional Theory of atoms and Molecules, Oxford University Press: New York, (1989).

[118] Parr. R. G, Pearson. R. G, Absolute Hardness: Companion Parameter to Absolute Electronegativity. J. Am. Chem. Soc. 105, 7512-7516. (1983).

[119] Reed, A.E; Weinhold, F.Natural bond orbital analysis of near-Hartree–Fock water dimer.J. Chem. Phys. 78, 4066. (1983).

[120] Siouani, C.; Mahtout, S.; Safer, S.; Rabilloud, F. Structure, Stability, and electronic properties of niobium-germanium and tantalum-germanium clusters. J. Mol. Model. 25, 113. (2019).

[121] Sporea, C.; Rabilloud, F. Stability of alkali-encapsulated silicon cage clusters, J. Chem. Phys. 127, 164306. (2007).

[122] Neukermans, S.; Wang, X.; Veldeman, N.; Janssens, E.; Silverans, R. E.; Lievens, P. Mass spectrometric stability study of binary MS_n clusters (S = Si, Ge, Sn, Pn, and M = Cr, Mn, Cu, Zn). Int. J. Mass Spectrometry, 252, 145-150. (2006).

[123] Tran, V. T.; Tran, Q.T., Spin State Energetics of $VGe_n^{-/0}$ [n = 5-7] Clusters and New Assignments of the Anion Photoelectron Spectra. J. Comput. Chem., 39, 2103-2109. (2018).

[124] Calvo F, Nanoalloys: from fundamentals to emergent applications, 2nd edn. Elsevier ISBN: 9780128223888. (2020).

[125] Sattler KD, Handbook of nanophysics clusters and fullerenes. CRC, Boca Raton ISBN: 978-0-12-819847-6. (2017).

[126] Zhao J, Du Q, Zhou S, Kumar V Endohedrally doped cage clusters. Chem Rev 120:9021–9163. (2020).

[127] Kumar V, Kawazoe Y Metal-encapsulated fullerenelike and cubic caged clusters of silicon. Phys Rev Lett 87:045503. (2001).

[128] Kumar V, Kawazoe Y Metal-encapsulated caged clusters of germanium with large gaps and different growth behavior than silicon. Phys Rev Lett 88:235504 (2001).

[129] Kumar V, Kumar Singh A, Kawazoe Y Smallest magic caged clusters of Si, Ge, Sn, and Pb by encapsulation of transition metal atom. Nano Lett 4:677–681. (2004).

[130] Kumar V, Kawazoe Y Metal-doped magic clusters of Si, Ge, and Sn: the finding of a magnetic superatom. Appl Phys Lett 83:2677–2679. (2003).

[131] M. Lasmi, S. Mahtout, F. Rabilloud, The Effect of Palladium and Platinum Doping on the Structure, Stability and Optical Properties of Germanium clusters: DFT study of $PdGe_n$ and $PtGe_n$ (n=1-20) clusters, Computational and Theoretical Chemistry 1181 112830. (2020).

[132] Trivedi R, Mishra V Exploring the structural stability order and electronic properties of transition metal M@Ge12 (M = Co, Pd, Tc, and Zr) doped germanium cage clusters. A density functional simulation (2021). J Mol Struct 1226: 129371. (2020).

[133] Bandyopadhyay D Electronic structure and stability of anionic $AuGe_n$ (n = 1–20) clusters and assemblies: a density functional modelling. Struct Chem 30:955–963. (2019).

[134] L. C. Srivichitranond, E. M. Seibel, W. Xie, Z. Sobczak, T. Klimczuk, R.J. Cav, Superconductivity in a new intermetallic structure type based on endohedral $Ta@Ir_7Ge_4$ clusters¸ Phys. Rev. B. 95 174521. (2017).

[135] M. Szlawska, A. Gribanov, S. Gribanova, D. Kaczorowski, Ferromagnetic Kondo lattice Ce_2IrGe_3, Intermetallics93 106-112. (2018).

[136] R. D. Adams, E. Trufan, Iridium-germanium and –tin carbonyl complexes, Organometallics, 29 4346-4353. (2010).

[137] J.L. Jules, J.R. Lombardi, Transition Metal Dimer Internuclear Distances from Measured Force Constants. J. Phys. Chem. A 107 1268-1273. (2003).

[138] A. R.Allouche, A Graphical user interface for computational chemistry software, J. Comput. Chem.32 174-182. (2011).

[139] A. E. Reed, F. Weinhold, Natural bond orbital analysis of near-Hartree–Fock water dimer. J. Chem. Phys. 78 4066. (1983).

[140] Benaida, Meriem & Kamal Eddine, Aiadi & Mahtout, Sofiane & Bentouila, Omar & Djaadi, Soumaia & Harb, Moussab. DFT-based investigation of different properties for transition metal-doped germanium TMGen (TM = Ru, Rh; n = 1–20) clusters. Journal of Molecular Modeling. (2020).

[141] Lasmi, M., Mahtout, S. & Rabilloud, F. Growth behavior and electronic and optical properties of $IrGe_n$ (n = 1–20) clusters. J Nanopart Res **23,** 26 (2021).

[142] Becke, A. D. (1988). Density-functional exchange-energy approximation with correct asymptotic behavior. Physical Review A, 38(6), 3098–3100.

[143] C. Lee, W. Yang and R. G. Parr, Physical Review B, 1988, 37, 785; J. P. Perdew, Physical Review B, 54, 16533, 1996.

[144] Perdew, J. P., & Wang, Y.. Accurate and simple analytic representation of the electron-gas correlation energy. Physical Review B, 45(23), 13244–13249 , (1992) .

[145] X. Zhang, G. L. Li, and Z. Gao, Rapid Commun. Mass Spectrom. **15**, 1573 2001.

[146] Trivedi, R., Dhaka, K., & Bandyopadhyay, D. Study of electronic properties, stabilities and magnetic quenching of molybdenum-doped germanium clusters: a density functional investigation. RSC Adv., 4(110), 64825–64834, (2014).

Abstract

Structural, electronic and optical properties of germanium clusters doped with palladium, platinum and Iridium atoms MGe_n (M= Pd, Pt and Ir , n=1–20) are investigated in the framework of the density functional theory. From n≥10 for Pd or 11for Pt or n≥12 for Ir, the cage like structures where the doping atom is totally encapsulated inside a Ge_n cage are favored. Relative stabilities of different MGe_n clusters have been analyzed from the average binding energies, second energy differences, HOMO–LUMO gap, and the vertical ionization potential and electronic affinity. Our results show that the clusters of MGe_n (M= Pd, Pt) with n=10, 12, 16 and 18 exhibit relative high stability, in which for Ir we highlight the great stability of $IrGe_{13}$ which presents a high-symmetry cage-like geometry and a peculiar electronic structure in which the valence electrons of Ir and Ge atoms are delocalized and exhibit a shell structure. Optical absorption spectra are predicted to be unable to discriminate the endohedral and exohedral structures.

Resumé

Les propriétés structurales, électroniques et optiques des clusters de germanium dopés avec des atomes de palladium, de platine et d'iridium MGe_n (M = Pd, Pt et Ir, n = 1–20) sont étudiées dans le cadre de la théorie de la fonctionnel de densité. A partir de n ≥ 10 pour Pd ou 11 pour Pt ou n ≥ 12 pour Ir, les structures en forme de cage où l'atome dopant est totalement encapsulé à l'intérieur d'une cage Ge_n sont favorisées. Les stabilités relatives de différents groupes de MGe_n ont été analysées à partir des énergies de liaison moyennes, des différences d'énergie secondaire, de l'écart HOMO – LUMO et du potentiel d'ionisation verticale et de l'affinité électronique. Nos résultats montrent que les clusters de MGe_n (M = Pd, Pt) avec n = 10, 12, 16 et 18 présentent des stabilités relatives élevées. Dans le cas de Ir, nous soulignons la grande stabilité d'$IrGe_{13}$ qui présente une haute symétrie en forme de cage géométrie et une structure électronique particulière dans laquelle les électrons de valence des atomes Ir et Ge sont délocalisés et présentent une structure de coque. Les spectres d'absorption optique ne permettent pas de distinguer les structures endohédriques et exohédriques.

ملخص

تمت دراسة الخواص التركيبية والإلكترونية والبصرية لمجموعات الجرمانيوم المدعمة بواسطة ذرات البلاديوم والبلاتين والإيريديوم (MGe_n (M = Pd وPt وIr، n = 1-20 في إطار نظرية الكثافة الوظيفية. من n≥10 لـ Pd و n≥11 لـ Pt أو n≥12 لـ Ir ، تفضل الهياكل مثل القفص حيث يتم تغليف الذرة المدعة بالكامل داخل قفص من Ge_n. تم تحليل الثابتات النسبية لمجموعات MGe_n المختلفة من متوسط طاقات الربط ، واختلافات الطاقة من الدرجة الثانية ، وفجوة HOMO-LUMO ، وإمكانات التأين الرأسي والتقارب الإلكتروني. تظهر نتائجنا أن مجموعات $PdGe_n$ و $PtGe_n$ مع n = 10 و 12 و 16 و 18 تُظهر ثباتًا عاليًا نسبيًا، حيث نسلط الضوء بالنسبة لحالة ال Ir على الاستقرار الكبير لـ $IrGe_{13}$ الذي يقدم قفصًا عالي التماثل يشبه الكرة هندسيا وهيكل إلكتروني فريد يتم فيه فصل إلكترونات التكافؤ لذرات Ir وGe حيث يعرض بنية غلافية. من المتوقع أن تكون أطياف الامتصاص البصري غير قادرة على التمييز بين الهياكل الداخلية والخارجية.

Agzul

Nexdemtazrawt i wayla n tsekka taliketrunit d usekdan i wegraw n jirmaniyum s ubelkam n bladinyum, blatinyum akked iridyum MGen (M=Pd, Pt, Ir, n=1-20) degukatay n tezri n tanezzi tawurant seg n ≥ 12 i Ir, tisekkiwin yesɛan talɣa n ukatayneɣ abelkam yesɣaɣen ɣument akk zedaxel n ukatay Gensnirfent. Arkad n yigrawen yimgaraden n MGe selḍent s wafud n wassaɣ alemmas, ifuden yemgaraden isnayen n uceqqiq HOMO- LUMO, s tawil n ubeddel s tbeddi d uqerreb aliktruni tbanen-d igmaḍ belli MGe_n (M=Pd, Pt) d n=10, 12, 16, 18 tbeyyinen-d arkad d ameqqran cwiṭ, iban-d s telqay. Deg tegnit n Ir iban-d urkad d ameqqran i $IrGe_{13}$ itebyyin-d azamul anĝi s talɣa n ukatay amenzag d tsekka taliktrunit anda izarumayen n umsawi n yibelkimen Ir d Ge bedlen yerna beynen-d tasekka n yiqcer. Aylalen n useblaɛ asekdan ur aɣtaĝan ara ad nsemgired tisekkiwin n zdaxel d berra.